2015

# INSIGHTS INTO THE RELATIONSHIP BETWEEN MIXING DURATION AND VOLCANIC EXPLOSIVITY INDEX (VEI): PACAYA AND FUEGO VOLCANOES, GUATEMALA

Nicola Mari
*Michigan Technological University*, nmari@mtu.edu

# INSIGHTS INTO THE RELATIONSHIP BETWEEN MIXING DURATION AND VOLCANIC EXPLOSIVITY INDEX (VEI): PACAYA AND FUEGO VOLCANOES, GUATEMALA

By

Nicola Mari

A THESIS

Submitted in partial fulfillment of the requirements for the degree of

MASTER OF SCIENCE

In Geology

MICHIGAN TECHNOLOGICAL UNIVERSITY

2015

This thesis has been approved in partial fulfillment of the requirements for the Degree of MASTER OF SCIENCE in Geology.

Department of Geological and Mining Engineering and Sciences

Thesis Advisor: *William I. Rose*

Committee Member: *Chad D. Deering*

Committee Member: *Gregory P. Waite*

Committee Member: *Alessandro Tibaldi*

Department Chair: *John S. Gierke*

# Table of Contents

Page

# List of Figures

Page

# List of Tables

Page

# Acknowledgements

First of all, I would to thank the INVOGE program of Double Master's Degree between USA and Italy, and the program coordinator Dr. Alessandro Tibaldi (University of Milano-Bicocca), this program has opened me the way to discover a new reality and given me the opportunity to improve my skills in scientific research.

I would to express my gratitude at many people of Michigan Technological University: my advisor, Dr. William Rose (MTU), for his great teachings, his funds for my research, and his suggestions of scientific journalism; Dr. Chad Deering (MTU), for his critical approach on my data; Dr. Greg Waite (MTU), for the great opportunity of the field work in Guatemala on Pacaya volcano, where I collected some of the samples used in this study.

A lot of people helped me with sample preparation and image acquisition, in particular I would to thank: Dr. Robert Barron for his extreme patience during the preparation of the thin sections; Owen Mills and Jessica Walitalo, for their help with SEM-EDS microanalyses.

I can't forget to thank my previous advisor and co-advisor from University of Urbino, Dr. Michele Mattioli and Dr. Alberto Renzulli.

Ironically, I also have to thank a volcano, Eyjafjallajökull volcano (Iceland), that because of the big eruption in 2010 cancelled my air flight (from Calabria to Milano) changing the destiny of my life.

I would to thank my family, Mamma, Papà, and my two sisters. Without them I would never do nothing that I have done. I have also to thank all my relatives, both from Italy and Los Angeles.

I have to thank all my friends from Italy, in particular from Calabria, Urbino, Milano and villages outside; friends from USA; and many others friends that I have known during my adventure around the World.

# Abstract

This study investigates whether the timing of magma mixing phenomena could be related to explosivity and style of volcanic activity. Lava flow and tephra samples, derived from observed, energetically-diverse eruptions, from Pacaya and Fuego volcanoes (Guatemala), were studied, the Volcanic Explosivity Index (VEI) was used as an indicator of eruption intensity. Polarized light microscopy and Scanning Electron Microscopy (SEM) techniques were used for textural and geochemical measurements. Results are interpreted as evolution of mixing through changes in textures of plagioclase and olivine crystals. These suggest that boxy-cellular plagioclase (high frequency in VEI 0 samples) is associated with brief mixing residence time prior to the eruption, while sieve and spongy textures in plagioclase (high frequency in VEI 1-2 samples) reflect heating by recharge events with a hotter melt, and reflect longer time in the magma chamber prior to the eruption. CSD data lead to a model to explain the increase in explosivity. Crystal size distributions with a significative step that derive from a single mixing event correlates with low intensity eruptions (VEI 0-1) because convection is hindered by the dissolution of the microcrysts, while multiple or prolonged events of mixing gives a more linear curve resulting in a high content of phenocrysts that make convection difficult, increasing the explosive potential (VEI 2). Besides, CSDs analysis show how the residence time in the shallow magma chamber increase from VEI 0 to VEI 2 samples. As a result, this study could assert that the number of mixing events that determine the final CSDs shape, and the magma mixing-to-eruption duration is proportional to the explosivity of the volcanic event.

# 1 - Introduction

## 1.1 - Postulate of research

Eruption explosivity dynamics are a target of volcanic research (Sparks & Aspinall, 2004; Newhall, 2000) and observations including magma mixing in particular have illuminated modifications in eruptive style (Sparks & Sigurdsson, 1977; Kremers *et al*, 2012).

Mixing of magmas can involve two end-members and result in blending and mingling. Blending is homogeneous mixing to form a chemically and physically intermediate magma. Mingling is a heterogeneous mixture, with some portions of the two end-member magmas and incomplete mixing, with spatially different parts of each magma still present. The extent of mixing depends on the physical and thermal properties of both magmas, especially density and viscosity (Bardintzeff, 1992; Laumonier *et al*., 2014).

In this work we investigate whether microscopic evidence and chemical-physical parameters for magma mixing can be used to explain variations in explosivity at volcanoes which exhibit variable activity without variation in magma composition. Mixing can transfer heat from a hot magma to a cooler one (Tsuchiyama, 1985), this can increase convection and vesiculation in the magma chamber and possibly break a brittle surface carapace, leading to explosive eruption (Sparks & Sigurdsson, 1977). The extent of magma mixing and heat exchange (Ruprecht & Bachmann, 2010), where mixing can transfer heat homogeneously into the cooler magma decreasing viscosity (resulting in less explosive eruption). Or alternatively a mafic melt might not reduce the viscosity of the silicic magma, but instead increase pressure (generating more explosive eruption). Can mixing evidence be related to eruption intensity at a specific volcano? How can this be related to eruptive heating, viscosity and crystallinity? In this research two basaltic volcanoes were selected, each with variable eruptive style and intensity, to see if ejecta and lava flows show mixing effects with similar and correlative variability.

The Volcanic Explosivity Index (VEI), devised by Newhall and Self (1982), is used as an indicator of intensity and selected samples of variable VEI, both lava flow and tephra, from Fuego and Pacaya volcanoes in Guatemala for analysis. Polarized light microscopy, Scanning Electron Microscopy (SEM), secondary electron images, energy dispersive x-ray analyses (EDS), CSDs and thermodynamic models are used to examine the relationship between mixing/mingling and VEI.

# 1.2 – Volcanism of Pacaya and Fuego

## 1.2.1 – Geodynamic setting

Fuego (~3700 m elevation) and Pacaya (~2500 m) are two of Central America's most regularly active volcanoes, located only 31 kilometers apart, along the volcanic front of Central America formed by subduction of the Cocos Plate beneath the Caribbean Plate (Carr *et al*., 1984). Geochemical and mineralogical data of lava and pyroclastic rocks of the volcanic front are calc-alkaline in composition, typical of subduction zones. Variation plots follow trends of high-Al basalts and basaltic andesites to dacite (Carr *et al*., 1982) and there are at large volumes of rhyolitic pumice at Atitlán and several other back arc centers (Rose *et al*., 1987). Although the volcanic front is marked by andesitic vents, the Fuego and Pacaya samples studied here are basalt and basaltic andesite.

## 1.2.2 – Pacaya volcano

Pacaya volcano (Fig. 1.1; Eggers, 1971) is located 30 km S of Guatemala City, on the rim of Amatitlán caldera (Wunderman & Rose, 1984). The volcanological complex of Pacaya is characterized by several volcanic cones including Cerro Grande, Cerro Chino, Pacaya Viejo, Pacaya, and Cerro Chiquito (Eggers, 1971). The Mackenney cone of Pacaya volcano is situated at the southern part of this volcanological complex and this feature was built up since 1961 enkarging the west side of Pacaya (Rose *et al*., 2013, see especially fig. 2, p. 3).

The Pacaya Complex has likely formed over many millennia and may consist of a series of active and quiescent eruptive periods (Kitamura & Matias, 1995; Eggers, 1972). In this study we investigate samples from an active period between 1961 and 2015 (Rose *et al*. 2013). The composition of magma erupted during this period is monotonous hi-Al basalt to basaltic andesite, with a substantial crystal content marked mainly by plagioclase and olivine (Bardintzeff & Deniel, 1992; Rose *et al*. 2013). The activity style ranged from effusive lava flows with tiny ashy explosions to energetic fire fountaining events with convective columns up to 20 km high (VEI from 0 to 3), and continuous degassing activity.

Fig. 1.1 - Pacaya volcano, active vents. It is possible to see the great eruptive fracture in the central part.

Like its mineralogy, the geochemistry of Pacaya lavas is monotonous without remarkable geochemical differences, but the eruptive style changes. If chemical composition remains the same, but the erupted materials show textural signs of mixing, this is consistent with a possible mixing control of eruptive style.

## 1.2.3 – Fuego volcano

Fuego Volcano (Fig. 1.2; Carr *et al*., 2002) is a stratovolcano built on the southern flank of the Fuego-Acatenango volcanological complex. It may be about 17 ka in age, the latest in a N-S series of vents which are older toward the N, away from the subduction zone. Its activity is marked by clustering of eruptions (Martin & Rose 1981), and evidence for magma mixing (Berlo *et al*., 2012). Trace-element data are consistent with fractionation from two chemically different magma bodies (Chesner & Rose, 1984). Samples studied here are all erupted in the last few decades, as Fuego has had subplinian activity interspersed with years of relative calm and much smaller events (Lyons *et al*., 2010), overall ranging from VEI 1 to 4.

Fig. 1.2 - Fuego volcano, active vent, during a typical explosion generated from the upper crater.

In general, the bulk magma chemical composition is in the range of 48-53 wt % $SiO_2$, while crystal content is marked by plagioclase, olivine, augite, and magnetite that derives from fractionation of the high-$Al_2O_3$ basalts. Melt inclusion analyses shows a general range of $H_2O$ content that varies from 2.1 wt % to 6.1 wt % (Sissons & Layne, 1993; Roggensack, 2001; Wade *et al*., 2008; Lloyd *et al*., 2014). Increasing in volatile content seems to be related to a change in the eruptive style (Lyons *et al*., 2010).

# 2 – Sample selection

Ten samples of lava and tephra from Pacaya volcano and three samples of tephra from Fuego volcano were used for this work. Five samples of Pacaya lava were collected by Otoniel Matías (2009) and Conway (1994), during 1972-2000. Three thin sections of tephra (scoria) from Pacaya were made in the Sample Preparation Laboratory of the Michigan Technological University, from samples collected by M.J. Carr and Enrique Molina, on 24 April 1985. Three thin sections of tephra from Fuego collected by Sam Bonis, in October 1974 were made in the same laboratory. Two thin sections were used from scoria collected by the author in January 2015.

Samples were chosen to represent different known degrees of explosivity (Fig. 2.1, Tab. 2.1), to test whether post eruption sampling can detect different eruptive energy and eruptive style in samples. The VEI was estimated from activity-observations/descriptions as a measure of energy. Studied samples include two samples of lava flow with VEI = 0 from Pacaya (1972 eruption); five samples of scoria with VEI = 1 from Pacaya (24 april 1985 eruption and 2014 eruption); three samples of lava flows with VEI = 2 from Pacaya (2000 eruption); and three samples of tephra with VEI = 4 from Fuego (October 17, 1974 eruption).

Fig. 2.1 – On the left, image showing an example of VEI 2 eruption at Pacaya volcano. It is possible to notice the high lava fountains and the ballistic trajectory of the pyroclasts; on the right, image showing an example of a very energetic and explosive eruption at Fuego volcano.

Tab. 2.1 – Table showing the volcano, sampling date, VEI and the description of the eruption for each selected sample.

| Sample | Volcano | Collector | Sample date | VEI | Description of the eruption |
|---|---|---|---|---|---|
| PA-19, PA-3 | Pacaya | Otoniel Matías and Conway | 1972 | 0 | Lava flows with fine ashes emission |
| PA-44, PA-45, PA-46 | Pacaya | M.J. Carr and Enrique Molina | 1985 | 1 | Lava flows and small strombolian explosions with lava fountains ejected 20 m high |
| PA-47, PA-49 | Pacaya | Nicola Mari | 2015 | 1 | Lava flows and strombolian explosions, lava fountains 500 m high |
| PA-27, PA-30, PA-14 | Pacaya | Otoniel Matías | 2000 | 2 | Lava fountains in Hawaiian style with pyroclasts ejected 800 m high |
| VF-74-130a,b,c | Fuego | Sam Bonis | 1974 | 4 | Energetic vertical explosive eruption column that reached the stratosphere, with blocks and generation of pyroclastic flows |

Details of the eruptive events are described in the Smithsonian GVN Website (http://www.volcano.si.edu/), Rose *et al*. (1978), Matías Gomez (2009), Rose *et al*. (2013) and Rose, WI (pers communication, 2015).

VEI assessments of the associated samples come from field descriptions of the activity of the volcano. Field notes associated with the sample collectors were also used.

PA-19 and PA-3, are from an effusive event on October 17, 1972. It was associated with very weak explosions, with releases of fine ashes which convected to levels of only a few tens of meters. This event was assigned VEI of 0.

Three Pacaya scoria samples PA-44, PA-45, and PA-46, occurred on April 24, 1985. The eruption was more energetic than PA-19, with lava flows and small strombolian explosions, also characterized by gas thrusts leading to 20 m high lava fountains every 7 minutes. The VEI of this event was assigned 1.The sample bag contained this field note: "Basaltic scoria from Pacaya volcano (Guatemala). *Mostly glass with small phenocrysts of plagioclase, olivine and pyroxene. Collected by M.J. Carr and Enrique Molina on 24 April 1985 (...) Scoria currently being producted looked essentially the same, but I decided not to attempt a real hot sample. Pele's hair was abundant, but did not survive the trip down the mountain*".

Two scoria (PA-47 and PA-49) are from the 2 March 2014 eruption of Pacaya. This eruption was characterized by gas thrust strombolian lava fountains that reached 500 meters high. The convecting ash plume reached 2.4 km high, but the explosions were small (assigned VEI 1).

Three lava flow samples (PA-27, PA-30, and PA-14), are from the 2000 paroxysmal eruption (peak intensity Jan 15 2000) at Pacaya. This eruption was characterized by 800 m gas thrust pyroclasts and lava mountain, with convective heights of several kilometers. It built a 50 m high cone around its vent. This was the largest event that occurred at Pacaya between 1961 and 2009 (Rose *et al*., 2013). This event is classified as VEI = 2.

Fuego's activity is frequent and is generally more energetic than Pacaya, possibly because its higher stature (longer conduit) may inhibit weak eruptions from reaching the surface, but most of its activity rates a VEI of 1-2. The activity patterns at Fuego have been reported in many volcanological papers (see Martin & Rose (1981) and Rose *et al.* (2007) for summaries and overall bibliography). Three tephra samples (VF-74-130), resulted from the peak (Oct 17) of the October 1974 sub-plinian eruption at Fuego

volcano (Rose *et al*., 1978). These are basaltic scoria (diameters 2-4.5 cm) collected at Quisache, 8km NW of Fuego summit. The October 1974 eruption was marked by four different pulses lasting 4-17 hours each, and a total duration of 10 days. Vertical explosive eruption from the central crater that created a convective column that reached the stratosphere, generating pyroclastic flows. The total volume of pyroclastic material produced was around 0.2 $km^3$ of high $Al_2O_3$ basalt. Although winnowing occurred, initial magmas were apparently rich in plagioclase phenocrysts, while the magmas erupted next became poor in phenocrysts. The VEI of this eruption was equal to 4.

# 3 – Methodology

## 3.1 – Polarized light microscopy

Thin sections and optical microscopy in plane-polarized light were used to document and quantify magma mixing features evidenced by disequilibrium textures.

In plagioclase crystals we found: *sieve plagioclase*, a coarse dissolution texture located at the center of the crystal representing the remnant of an interconnection of different channels (Nelson and Montana, 1992), *boxy-cellular plagioclase*, a dissolution texture located at the center characterized by "holes" pursuing a similar shape of the main crystal (Gibson et al., 2003), and *spongy-cellular plagioclase*, a crowned dissolution texture surrounding the center of the crystal formed by many small holes sometimes containing glassy material (Andersson and Eklund, 1994).

In olivine crystals we observed: *fractured olivine*, fractures related to increasing force as the eruptive explosivity increases (Swain & Atkinson, 1978), *resorption rims*, reaction features that generates and evolve at the rims (Claeson, 1998; Coombs and Gardner, 2004), and *sieve olivine*, a dissolution coarse texture (Anonymous, 1990) similar to that of sieve plagioclase.

The percentage of each disequilibrium texture calculated for each different VEI of the samples analyzed were presented in form of histogram, in order to assess whether variations resulted from differences in eruptive energy and style.

## 3.2 – SEM images acquisition and EDS analyses

The secondary electrons, generated by SEM, were used to obtain images (SEI) of different parts of the samples, while the chemical microanalysis was conducted measuring the energy and the distribution of the intensities of the X-rays generated by the electronic beam in the sample, by using Energy Dispersive Spectrometry (EDS). These analyses were made both in a selected area and at points of interests on the surface of the sample (microanalysis). In EDS, analyzed an area in order to obtain the general bulk composition of the sample surface and a point when the primary objective was the composition of a single mineral or part of mineral. X-ray elemental mapping was useful in cases of magma mingling, to show different phases of liquids.

In general, we conducted secondary electron images (SEI), EDS microanalyses, and X-ray elemental mapping of the most representative samples observed in plane-polarized light and considering differences in VEI. The sample selected are: PA-19, PA-

27, PA-44, PA-49, and VF-74-130a. All these samples were polished and coated, in order to be conductive.

Detailed studies are available of Fuego plagioclase which demonstrate very complex compositional zoning related to magma movement (Anderson, 1984). Because of obvious zoning SEI images were collected in both the central parts and the edges of many plagioclase microphenocrysts, to see chemical variations of elements as Na and Ca from the center to the rim, possibly detecting reverse zoning due to magma mixing phenomena (Shcherbakov *et al*., 2011).

## 3.3 – Image processing and CSD analysis

We conducted CSD analysis (Higgins, 2000; Vinet & Higgins, 2010; Brugger & Hammer, 2010) of samples representing different VEI conditions. To create an image of the entire thin section we took several microphotos (including edges) and made a mosaic of the sample. For measurements we used ImageJ, a free image processing software (based on Java script), developed at the National Institutes of Health (Rasband, 1997).

The scale is set by entering a value for the number of millimeters for a pixel scale factor. Polygons were drawn to include each phenocryst, crystal, and microcrystal of plagioclase, then the polygons were measured generating a best fit ellipse obtaining the area (crystal size) in $mm^2$ (Fig. 3.1 and 3.2). The measurement file was exported in other spreadsheet software for data analysis.

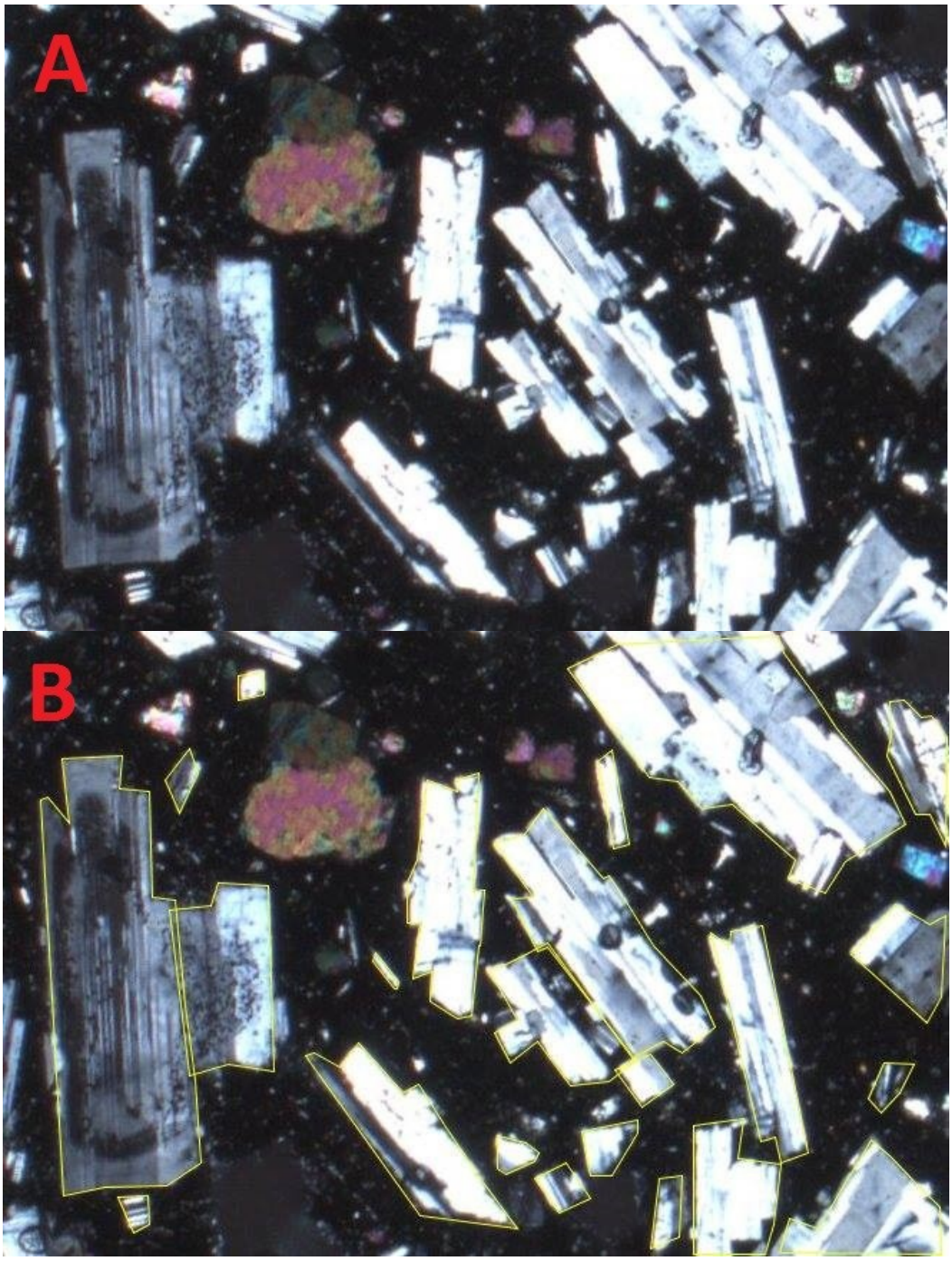


Fig. 3.1 – Methodology of CSD measurements. (A) A normal area of the thin section; (B) Inclusion in polygon for each crystal and microcrystal of plagioclase.

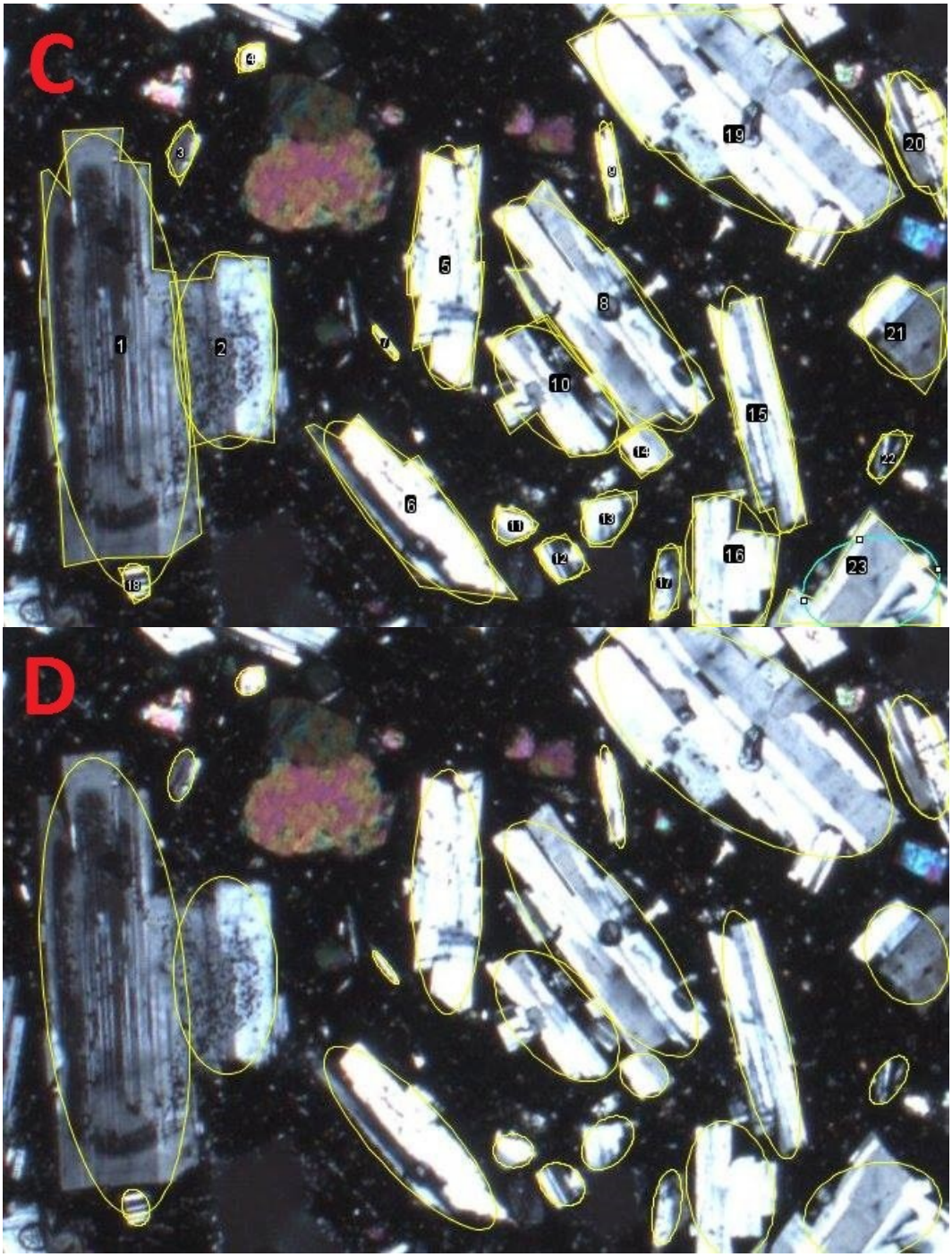


Fig. 3.2 – Methodology of CSD measurements. (C) Creation of a best fit ellipse for each polygon; (D) Cancellation of the previous polygons with only the remaining ellipses useful for measurements.

At the end of the process, a graph population density vs. crystal size was generated. In open magmatic systems there is a linear correlation between the natural

logarithm of the population density at size *L* and that size (Higgins, 2006; Marsh, 1998). Thus, for a single phase in the system:

$$n'_v(L) = n'_v(0)e^{\frac{-L}{G\tau}}$$

where $n'_v$(L) is the population density of the crystals for size *L*, $n'_v(0)$ is the final nucleation density, *G* is the growth rate and $\tau$ is the residence time. By finding the variation in slope of the two CSDs it is possible to estimate, relatively, the residence time of the crystals.

## 3.4 – Viscosity model

Estimates of the viscosity for each sample of differing VEI have been made, based on geochemical data. In order to incorporate the temperature dependence (η) of melt viscosity we used the Tammann-Vogel-Fulcher (TVF) equation (Giordano et al., 2008):

$$\text{Log } \eta = A + B/T(K) - C$$

where A is considered constant for all types of melts (A = -4.55±0.21), meaning that for a high-T all melts are at the same value of viscosity; B and C are related to compositional effects.

During the eruption the temperature and volatiles drop, thus we calculated viscosity for each intensity (VEI 0-4) for different values of temperatures and $H_2O$ wt %, in order to obtain a more accurate range of results.

Estimates for eruptive temperatures for Pacaya lavas vary in the range from ~1000°C to ~1100°C based on work by Bardintzeff & Deniel (1992); Bollasina *et al.* (2013); and Soldati *et al*. (2014). The pre-eruptive temperature for the VEI 4 eruption at Fuego was previously calculated in another study using a mineral equilibrium geothermometer and is ~ 1,050°C (Rose *et al*., 1978). The similarity between magma temperatures for Fuego and Pacaya is consistent with their very similar mineralogy and crystallinity.

The pre-eruptive $H_2O$ wt. % of Pacaya magma was inferred from melt inclusions (Walker *et al*., 2003), and could be about 2 wt. %, but because of a great variability in the gas emission rate (Rodriguez *et al*., 2004) we estimate from 0 to 5 $H_2O$ wt. %. Although analyses of melt inclusions from the 17 October 1974 eruption at Fuego (Lloyd *et al*., 2013) may have been a slightly higher in $H_2O$ than Pacaya, with a range from 1 to 4.4 wt. %, we estimate a range of 0 to 5 wt. % $H_2O$.

# 4 – Results

## 4.1 – Qualitative descriptions

### 4.1.1 – Sample characterization

Mineralogical paragenesis appears similar in all off the studied samples. Plagioclase, olivine, and magnetite phenocrysts occur in all these rocks. This mineralogy matches those previously reported for recent Pacaya and Fuego materials (Bardintzeff and Deniel, 1992; Cigala, 2013; Chesner and Rose, 1984; Roggensack, 2001; Rose et al., 1978). Plagioclase is much more abundant than olivine and magnetite is found as microlites only. Detailed modal data for each group of samples can be found below in Section 4.2.2.

The texture is seriate, with gradual variation from big to small phenocrysts. The groundmass is microcrystalline in almost all the samples, with the same mineralogy as the phenocrysts.

Both plagioclase and olivine are progressively more fractured (existing as broken crystals) as the VEI of the samples increase.

Polarized light microscopy reveals a variable disequilibrium features, mainly seen in plagioclase and olivine phenocrysts. Most of these disequilibrium textures are consistent with magma mixing phenomena: sieve plagioclase, inversely zoned plagioclase, boxy-cellular plagioclase, spongy-cellular plagioclase, embayed olivine, giant resorption rims in olivine, skeletal olivine, sieve olivine, and other minor textures.

In SEI images edges and rims of the crystals depict modifications and resorptions due to disequilibrium between the crystals and surrounding melt. The morphology of the edge varies from sharp to smooth. Many holes were noticed in the minerals - typically at the center - and are sometimes filled by inclusions of glassy material. The groundmass varies from cryptocrystalline to holocrystalline.

### 4.1.2 – Disequilibrium textures in VEI 0

In the samples PA-19 and PA-3 from 1972, reflecting VEI 0 eruption, plagioclase are mostly boxy-cellular and less commonly sieved plagioclase, without resorption rims (Fig. 4.1). Olivine crystals show weak signs of disequilibrium (Fig. 4.2). Plagioclase

phenocrysts, in SEI images, have resorbed edges (Fig. 4.3) and clusters of microcrysts surrounding the main crystal.

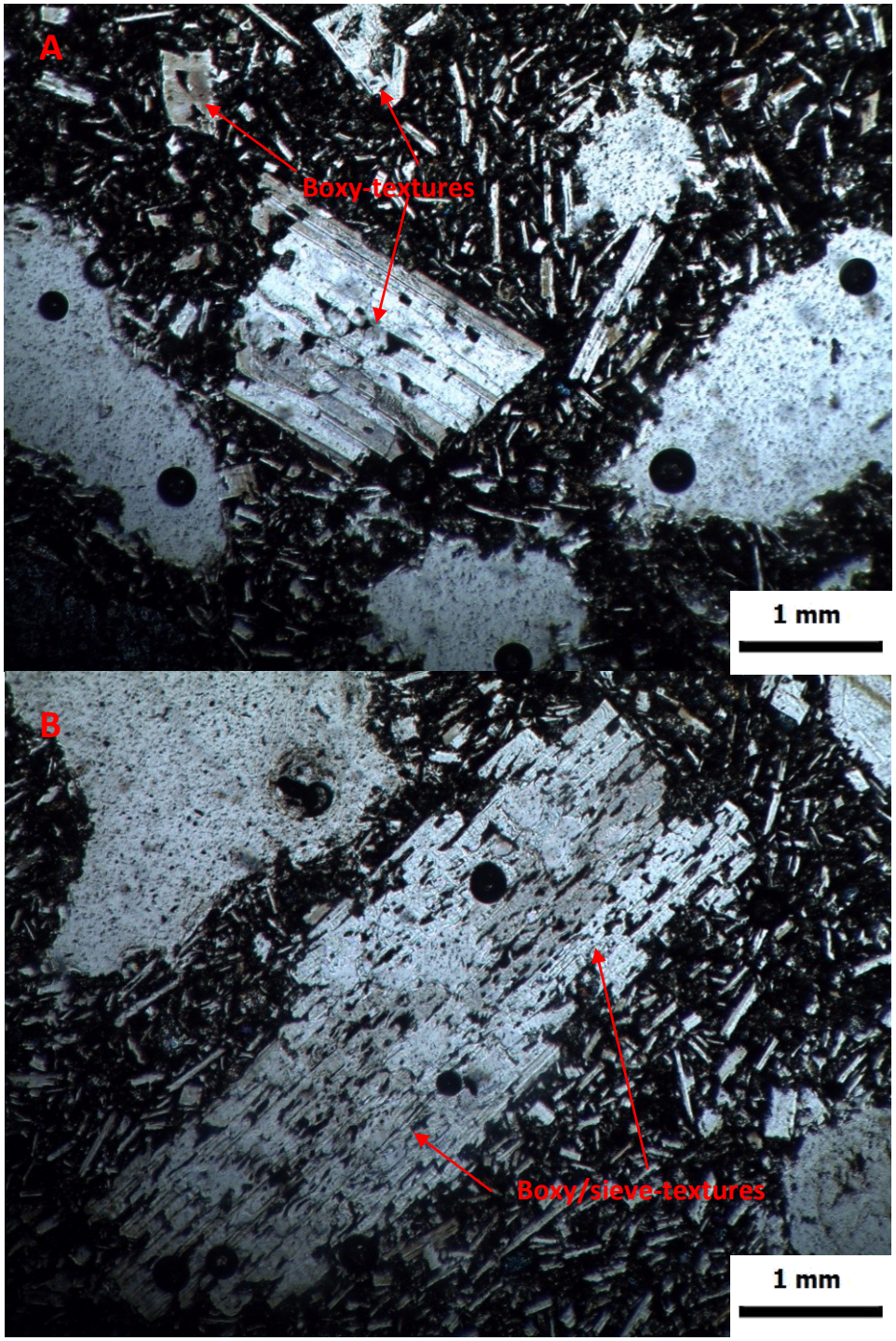


Fig. 4.1 – (A) Microphotograph of sample PA-19 (N//), at 2.5x: particular of boxy-cellular plagioclase, characterized by semi-rectangular holes distributed in the central part, following the pre-existent plane of

parallel striations; (B) Microphotograph of sample PA-19 (N//), at 2.5x: great example of a boxy/sieve plagioclase crystal, characterized by disequilibrium textures mainly distributed in the central part.

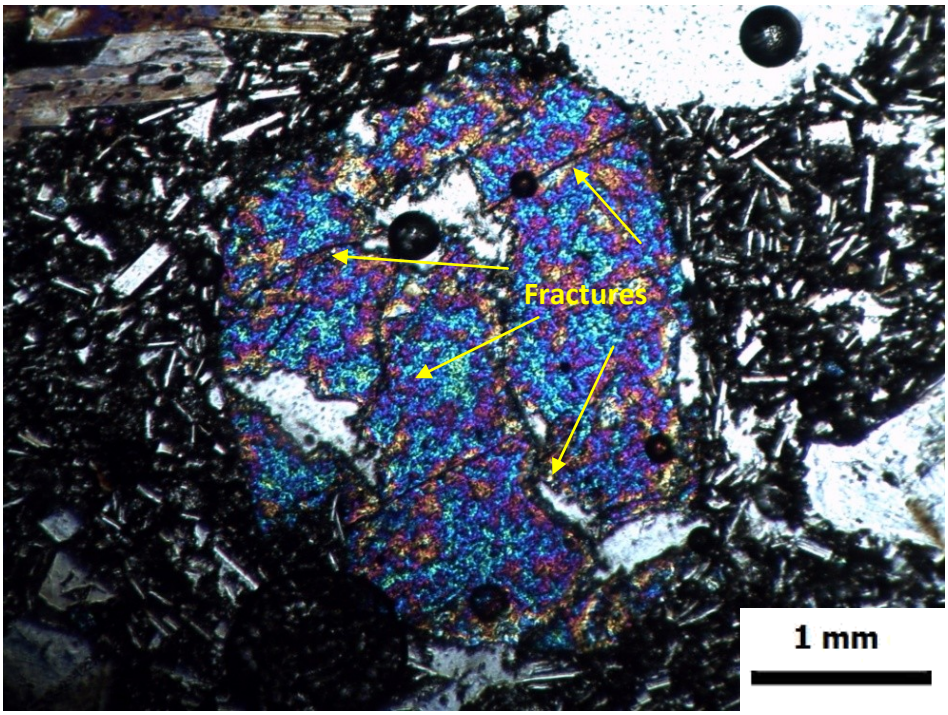


Fig. 4.2 - Microphotograph of sample PA-19 (NX), at 2.5x: typical of an olivine crystal characterized by decompression cracks, which are visible as fractures.

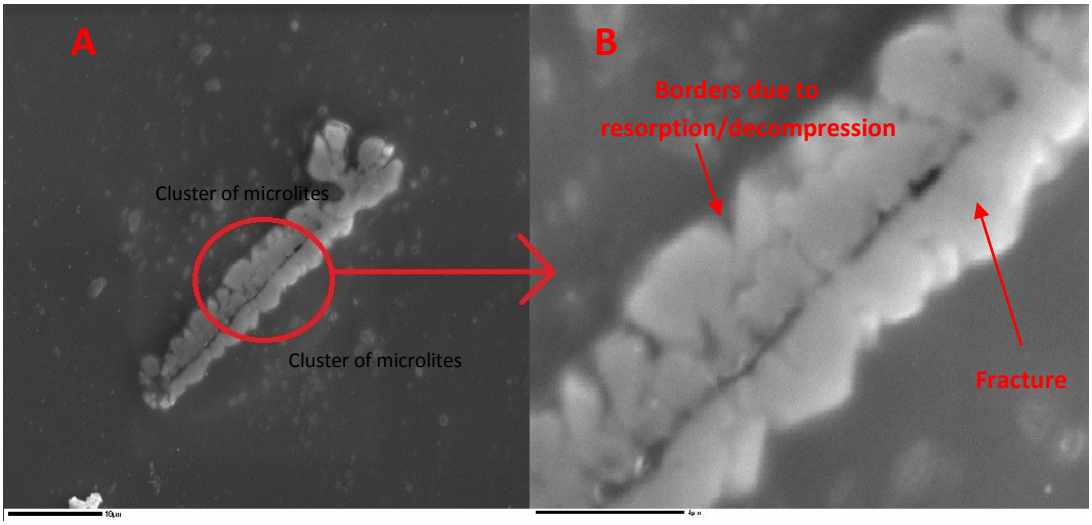

Fig. 4.3 – Crystal of plagioclase in the central part of the thin section PA-19: (A) SEI image that shows a semi-euhedral crystal of plagioclase with all the borders characterized by resorption phenomena and/or texture due to decompression. It is possible to notice a fracture on the center and clusters of microcrystals that surround the main crystal; (B) Magnified SEI image of the red signed zone.

## 4.1.3 – Disequilibrium textures in VEI 1

Five samples from VEI 1 eruptions contain plagioclase crystals with boxy-cellular and sieve textures or a hybrid between these two. They have weak resorption rims and zonation is not clearly visible (Fig. 4.4). A large crystal of plagioclase (1.7 cm), in sample PA-49, has a sieve texture at its center (Fig. 4.5). All samples are full of twinned plagioclase. Olivine has thin rims, which can be delineated by the presence of abundant glassy inclusions. Fractures in olivine (that sometimes appear as small holes) are also better developed here than the VEI 0 sample of the same volcano (Fig. 4.6). Intergrowths of plagioclase and olivine are twinned and appear in almost all these samples. Panoramic SEI images of this sample contain two distinct types of melts that coexist in the same thin section area (Fig. 4.7): where glass exhibits distinct dark and light colors in transmitted light. Larger crystals are found in the light colored glass. These two glasses are interpreted as recording the process of magma mingling and/or auto magma mingling (Mari, 2013) in a pre-eruptive phase. To obtain chemical information about these glasses, EDS microanalyses and an X-ray map were obtained (Fig. 4.8). These semi-quantitative results show higher concentrations of Si, Al, and Ca in the lighter glass. This is consistent with light glass being affected by more extensive olivine crystallization, which would raise the Al and Ca in the silicate melt.

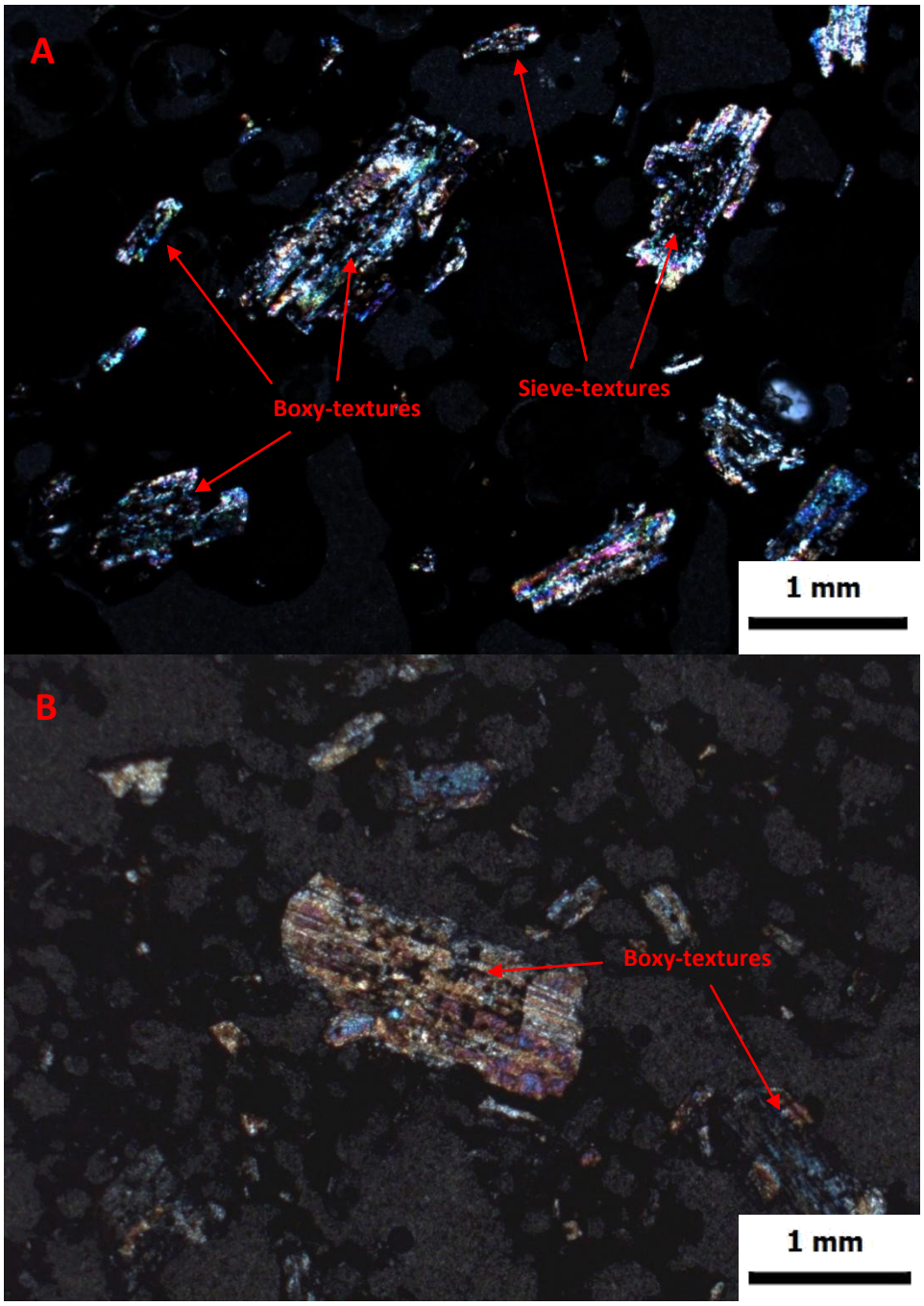


Fig. 4.4 – (A) Microphotograph of sample PA-44 (NX), at 2.5x: crystals of sieve and boxy-cellular plagioclase; (B) Microphotograph of sample PA-49 (NX), at 2.5x: particular of a boxy-cellular plagioclase.

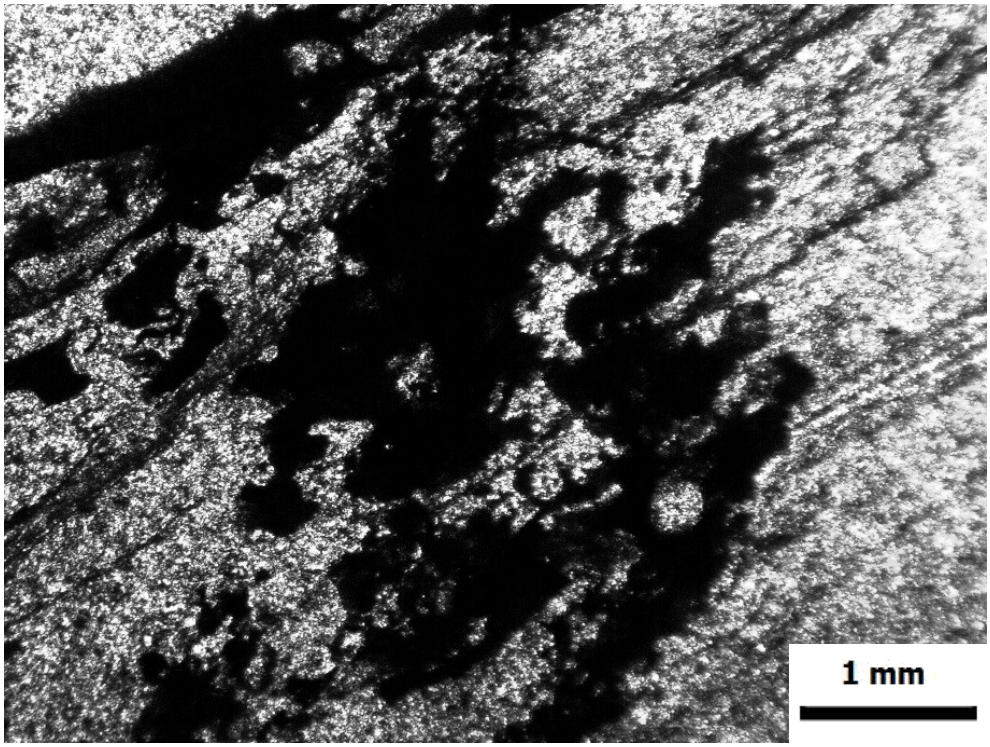


Fig. 4.5 - Microphotograph of sample PA-49 (N//), at 2.5x: sieve-texture located at the center of a big phenocryst of plagioclase.

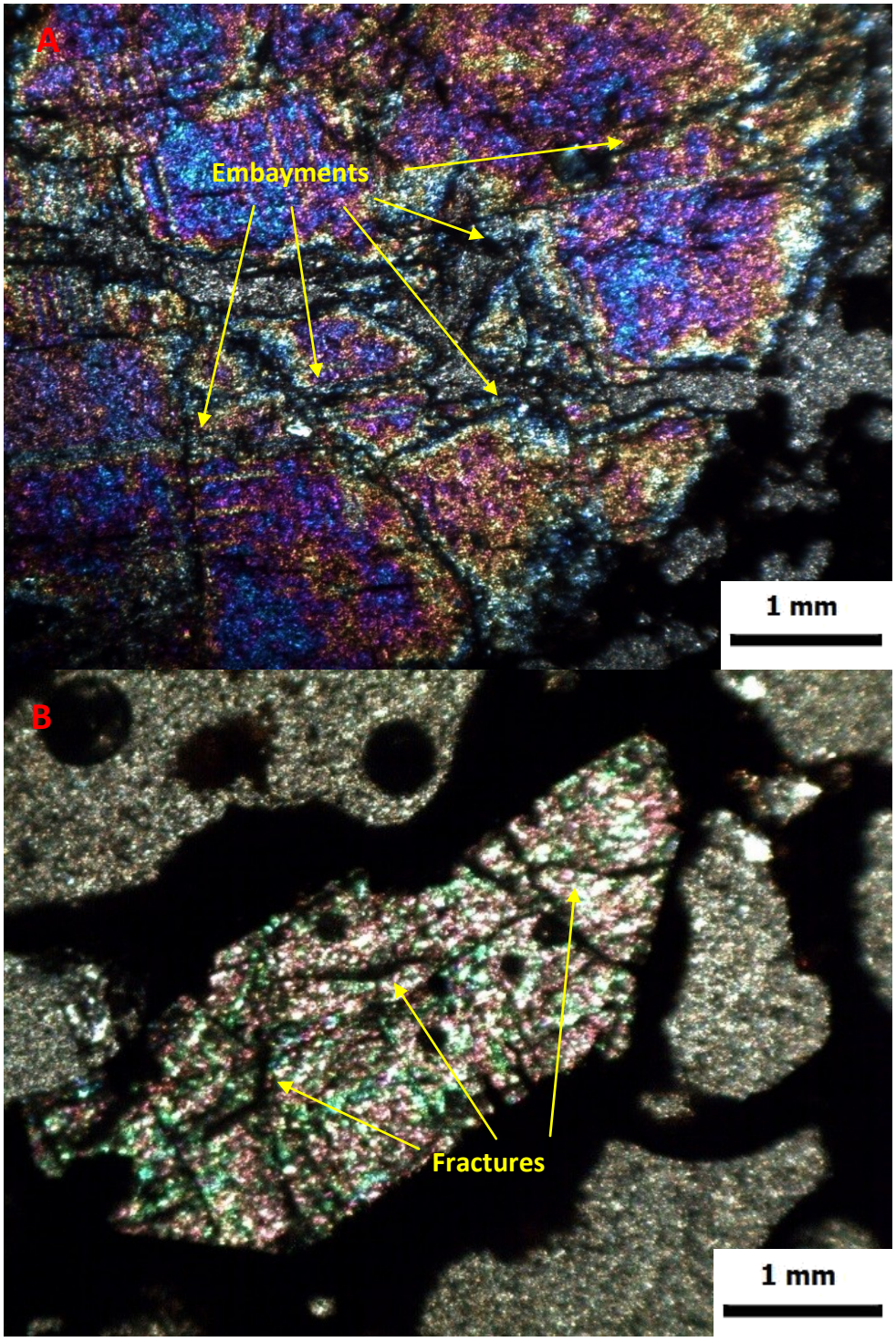


Fig. 4.6 – (A) Microphotograph of sample PA-44 (NX), at 2.5x: giant crystal (6 mm) of olivine with fractures, deeper than the thin section previously analyzed; (B) Microphotograph of sample PA-47 (NX), at 2.5x: example of embayed skeletal olivine.

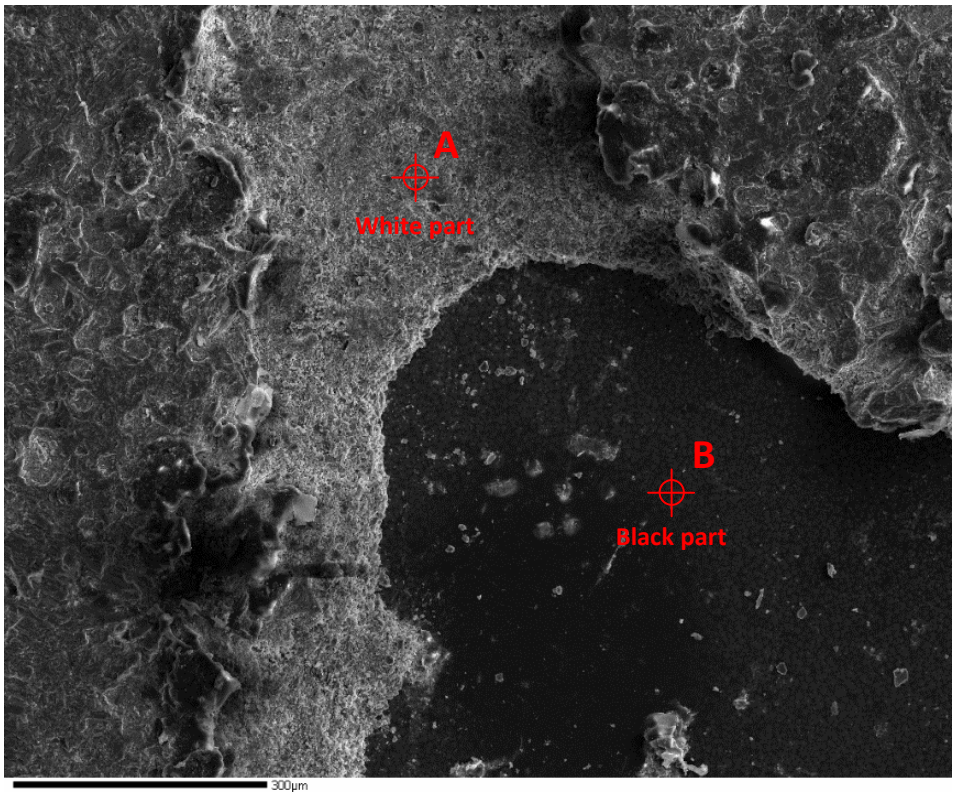


Fig. 4.7 - Panoramic of the sample PA-44 where it is possible to see two different parts of liquid: one more white (A) and one more black (B) in color. The white part is more enriched in crystals. Two EDS analyses were conducted in the two different areas (A and B).

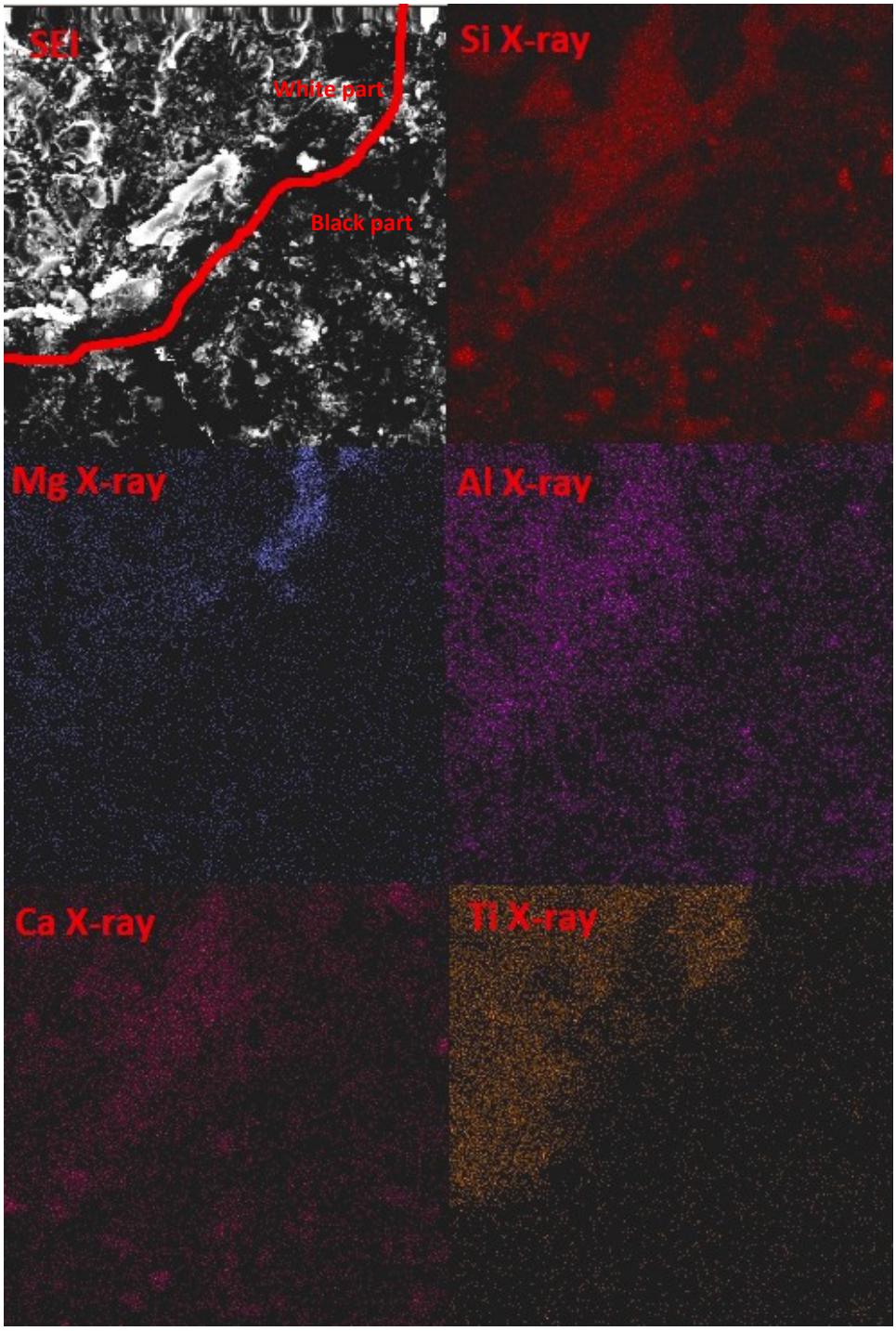


Fig. 4.8 - X-ray elemental map of an area of sample PA-44 where it is possible to see the boundary between two different types of liquids.

### 4.1.4 – Disequilibrium textures in VEI 2

Three samples from VEI 2 eruptions have more-evolved mixing textures in plagioclase than either VEI-0 or 1. Crystals are spongy-cellular, surrounded by thicker resorption rims (Fig. 4.9). Only a few cases of sieve-plagioclase are visible. Glassy inclusions are always noticeable, on the rims of the spongy-cellular plagioclase. The groundmass is heterogeneous in all the thin sections, showing evidence for mingling. Reverse zoning of plagioclase crystals is evident, something not observed in the samples from less energetic eruptions. Olivine crystals appear, in these three samples, broken, which could be induced by the high concentration of fractures of the crystal (Fig. 4.10). Reaction rims are well-developed and thicker than the samples analyzed from the VEI 1 eruptions. SEI images detect re-melted plagioclase edges and snowflake clusters on some sieve plagioclase (Fig. 4.11; see explanation by Berg, 1980). This could be related to phenomena of magma mixing and/or supercooling. Scanning electron microscopy and energy-dispersive spectroscopy microanalyses suggest that these snowflake clusters have major Si and minor Ca and Na (consistent with plagioclase composition).

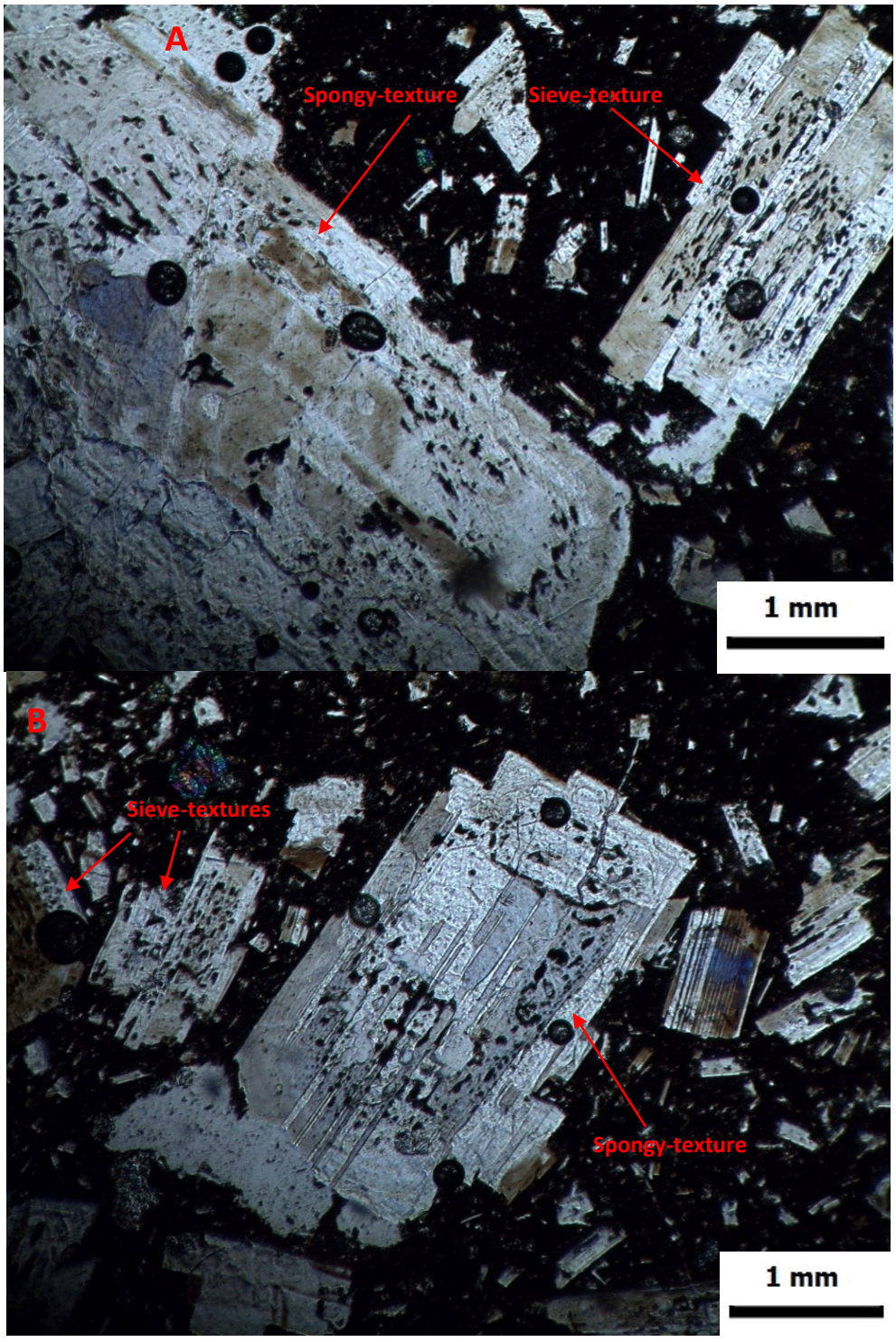


Fig. 4.9 – (A) Microphotograph of sample PA-27 (NX), at 2.5x: great example of the difference between two mixing textures in plagioclase, a giant spongy-cellular plagioclase (on the left) and a sieve-plagioclase (on the right). The difference is that the spongy-cellular plagioclase has disequilibrium signs on the borders, while the sieve-plagioclase has disequilibrium signs on the central part; (B) Microphotograph of sample

PA-27 (NX), at 2.5x: spectacular example of a spongy-cellular plagioclase. It is possible to notice the disequilibrium signs distributed on the "borders" as a crown morphology.

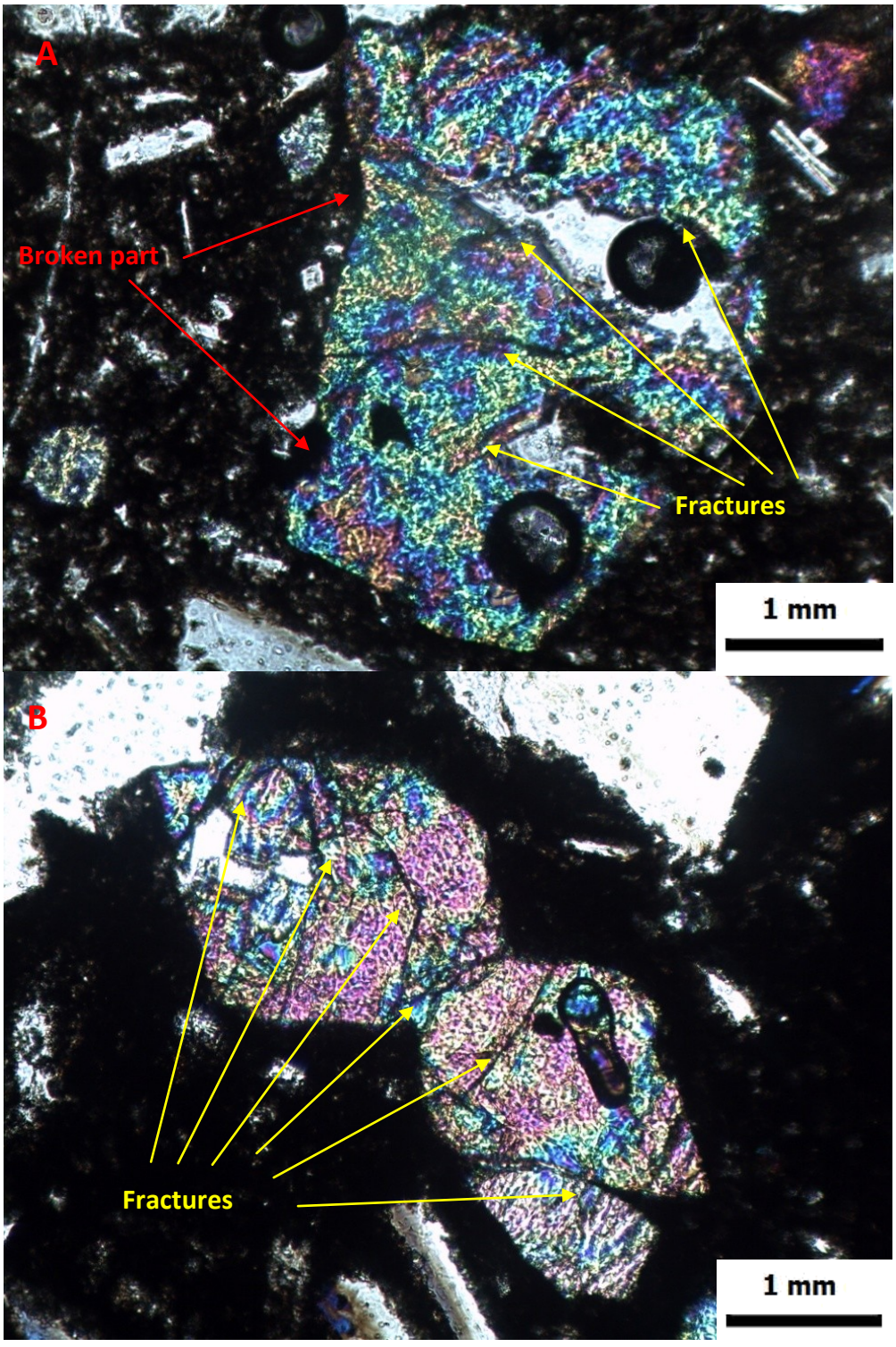


Fig. 4.10 – (A) Microphotograph of sample PA-27 (NX), at 10x: particular of a fractured olivine partially broken. Fractures are clearly visible; (B) Microphotograph of sample PA-14 (NX), at 10x: particular of a skeletal-olivine fractured.


Fig. 4.11 – Spectacular view of snowflake clusters of plagioclase. In particular, it is well noticeable how these snowflakes are generated directly from the main crystal, passing from small to large size.

## 4.1.5 – Disequilibrium textures in VEI 4

VEI 4 samples contain a more sodic plagioclase, and show hybrid spongy-cellular and sieve textures. Some boxy-cellular plagioclase can also be found, in minor quantities (Fig. 4.12). Plagioclase is surrounded by large and wide re-melted edges. Olivine crystals are strongly spliced and broken in different parts. Sieve olivine texture is conspicuous, characterized by more numerous signs of disequilibrium distributed inside the phenocryst centers that were not observed in samples from the less energetic eruptions (Fig. 4.13). Fractures in olivine, and resorption rims, are very wide and showy. Two different types of glass are present in many areas of the samples, one darker, with a low to medium degree of crystallinity, and one lighter in color, largely crystallized and containing the majority of phenocrysts. By using SEM-EDS microanalyses, the dark glass has a very low content of Si, and a relatively medium content of Na and K, while the light glass has a very high content in Si and low content in Fe. X-ray mapping clarifies the difference in composition within the two liquids (Fig. 4.14). These data reflect a magma mingling phenomenon with acid and basic melts. Mingling in this eruption is in accord with a previous work about Fuego volcano (Berlo *et al*. 2012).

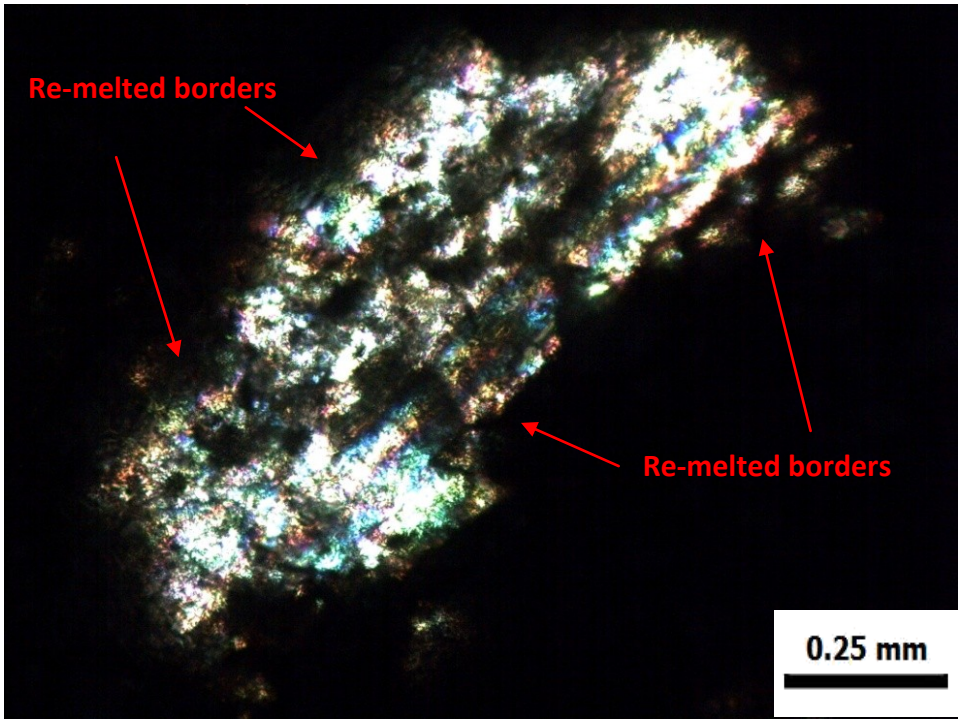


Fig. 4.12 - Microphotograph of sample VF-74-130 (NX), at 10x: particular of a plagioclase crystal with very wide and large re-melted borders.

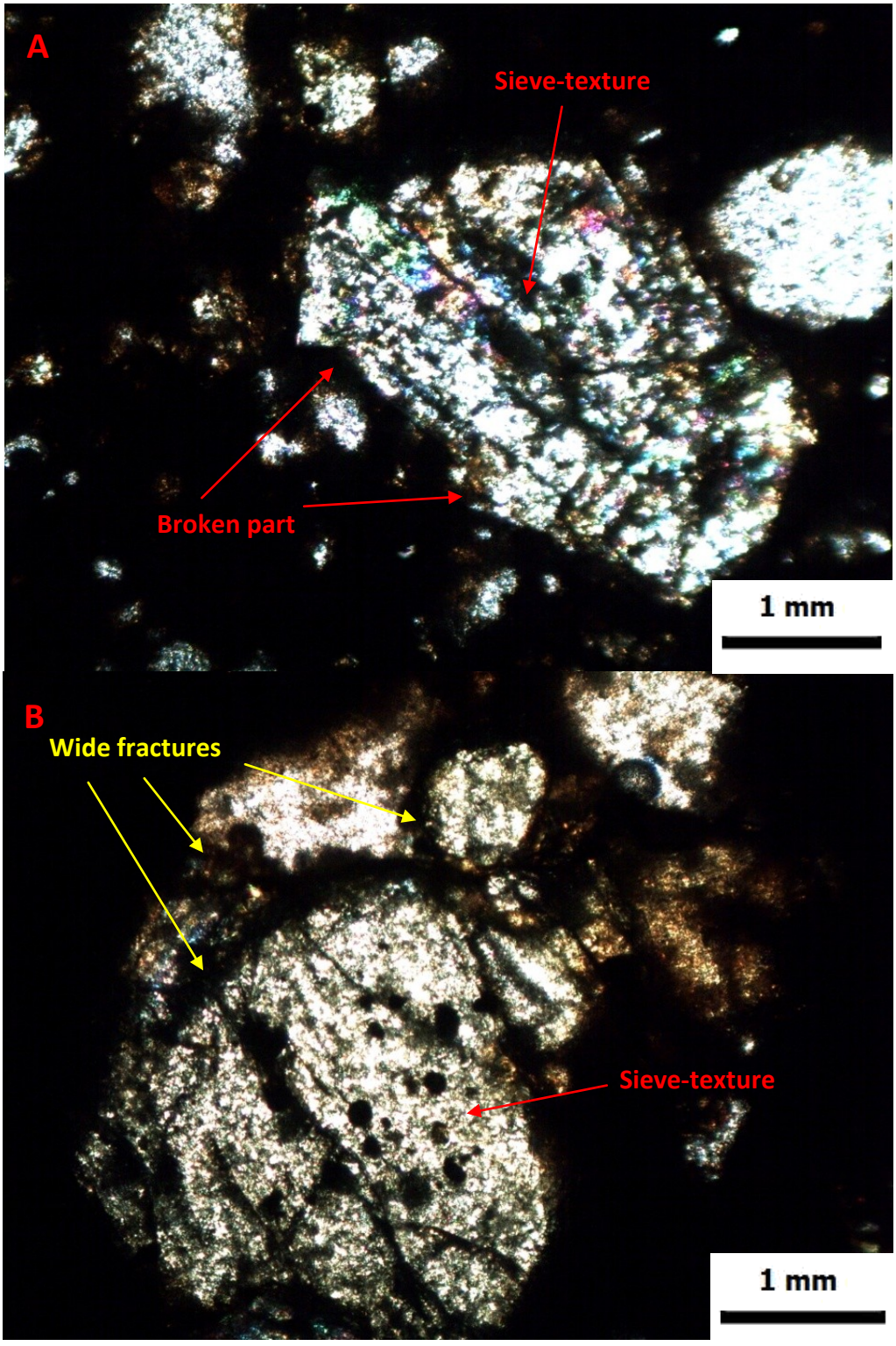


Fig. 4.13 – (A) Microphotograph of sample VF-74-130a (NX), at 2.5x: example of a sieve olivine (with a large resorption rim), characterized by disequilibrium signs that increase from the borders to the centre; (B)

Microphotograph of sample VF-74-130c (NX), at 2.5x: great example of a fractured sieve olivine phenocryst, characterized by many disequilibrium signs at the centre.

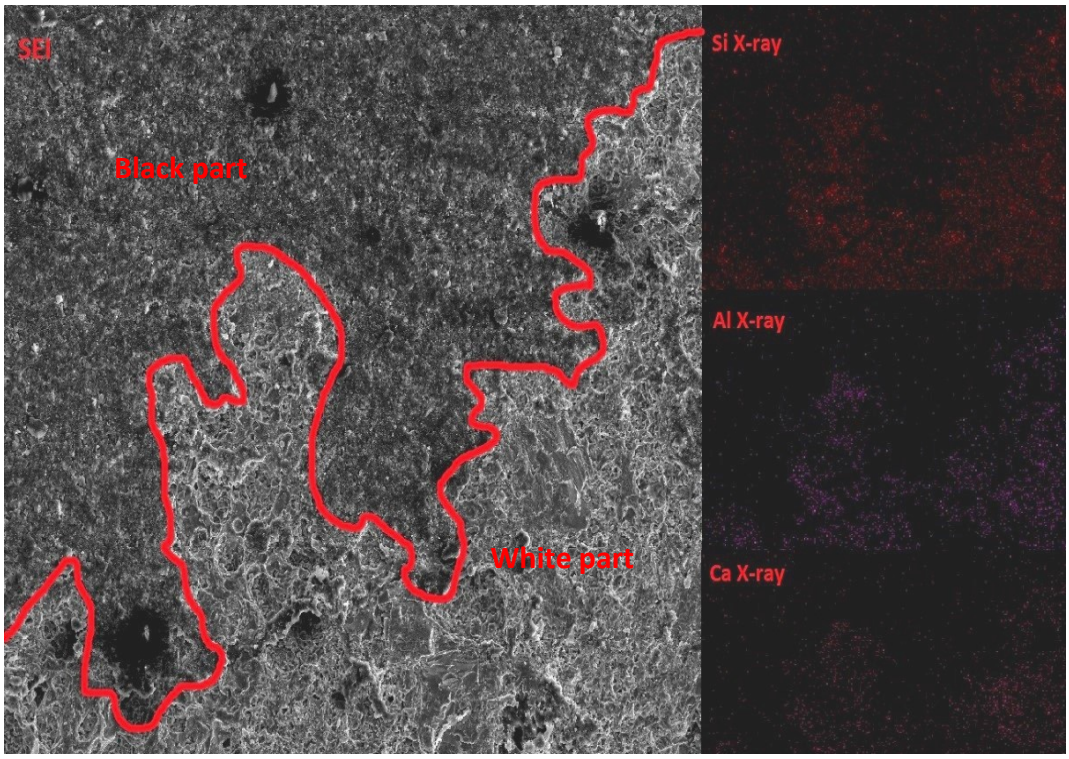


Fig. 4.14 – SEI image (on the left) where the two liquids (black and white part) are mingled in interdigitation. On the right, three types of X-ray elemental maps conducted on this image (Si, Al, and Ca).

# 4.2 – Quantitative analysis

## 4.2.1 – Geochemistry

Major element chemical compositions, obtained from XRF bulk-rock analyses, are presented in Table 4.1 and plotted in Fig. 4.15. Studied samples are basalts and basaltic andesite (Fig. 4.15). If samples are classified by the KWare MAGMA software: they show a trachybasaltic and tholeiitic basalt compositions (Table 4.2).

Table 4.1 – Geochemical data of the samples, from previous works, analyzed using XRF with element distribution in wt %. Sources: (1) Matias-Vogel, 2009; (2) Bardintzeff and Deniel, 1992; (3) Morgan et al., 2013; (4) Roggensack, 2001.

| Wt% Oxide | PA-19 (1) | PA-27 (1) | PA-44 (2) | PA-49 (3) | VF-74 (4) |
|---|---|---|---|---|---|
| $SiO_2$ | 51.16 | 51.13 | 50.07 | 49.27 | 53.65 |
| $TiO_2$ | 1.11 | 1.11 | 1.14 | 1.17 | 1.17 |
| $Al_2O_3$ | 19.56 | 20.75 | 19.22 | 18.96 | 17.22 |
| $Fe_2O_3$ | 9.15 | 8.52 | 9.78 | 9.78 | 9.67 |
| MnO | 0.17 | 0.15 | 0.05 | 0.18 | 0.13 |
| CaO | 9.74 | 10.47 | 9.73 | 9.96 | 8.67 |
| MgO | 4.61 | 3.28 | 4.53 | 4.90 | 3.55 |
| $Na_2O$ | 3.45 | 3.49 | 3.66 | 3.52 | 4.82 |
| $K_2O$ | 0.78 | 0.80 | 0.87 | 0.76 | 0.86 |
| $P_2O_5$ | 0.23 | 0.24 | 0.30 | 0.26 | 0.26 |
| Total | 99.96 | 99.94 | 99.35 | 98.76 | 100 |

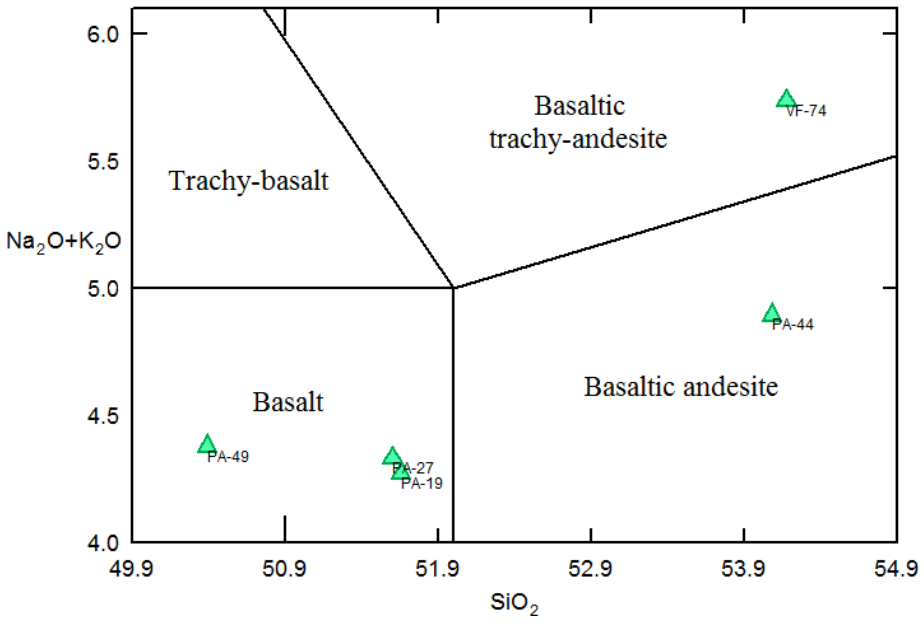


Fig. 4.15 – TAS diagram of the samples (green triangles) analyzed using XRF. PA-19, PA-27, and PA-49 are classifiable as relatively much evolved basalts; PA-44 is a basaltic andesite; VF-74 is a basaltic trachy-andesite (LaBas et al., 1986).

Table 4.2 – IUGS and Shand rock classification of each of the previous samples, obtained from IgPet software (Wohletz, 2002) .

| Sample | IUGS classification | Shand Classification |
|---|---|---|
| PA-19 | Latite-Basalt (Trachybasalt) | Metaluminous Silica saturated |
| PA-27 | Latite-Basalt (Trachybasalt) | Metaluminous Silica saturated |
| PA-44 | Latite-Andesite (Basaltic trachyandesite) | Metaluminous Silica saturated |
| PA-49 | Tholeitic basalt | Metaluminous Silica saturated |
| VF-74-130a | Tholeitic basalt | Metaluminous Silica saturated |

## 4.2.2 – Modal data

Petrographic and modal data (Fig. 4.16) are similar in all studied rocks and also resemble rock studied from the same periods by other authors [Appendix D, from Eggers (1972), Bardintzeff & Deniel (1992), Rose *et al*. (2013), Cigala (2013), and Berlo *et a*l. (2012)].

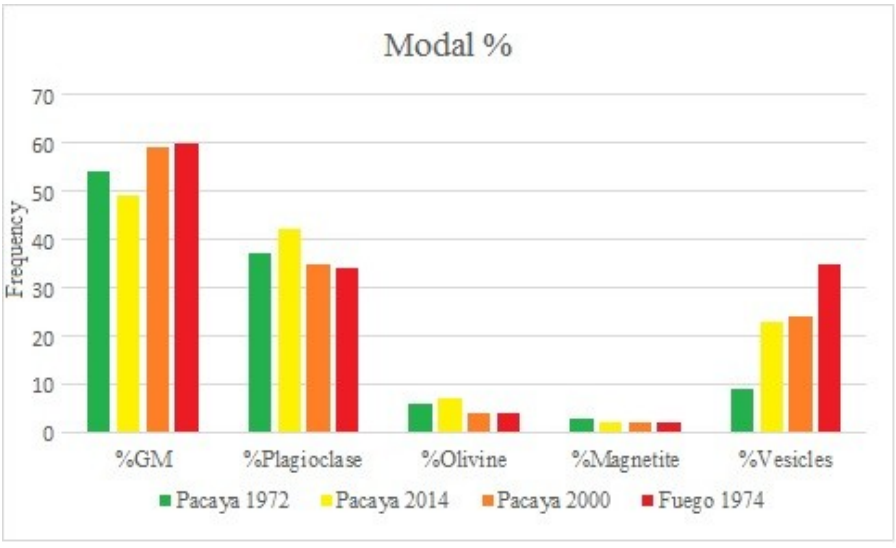


Fig. 4.16 – Modal and petrographic data for the samples studied in this work.

## 4.2.3 – Reverse zoning chemical data

In almost all the samples clear evidence of reverse zoning in plagioclase was observed, with an increase of Ca and decrease of Na from the center to the edge. We reported all chemical measurements both in core and rims of plagioclase phenocrysts, calculated for each sample analyzed using SEM-EDS, in Table 4.3.

Table 4.3 – Na and Ca core-to-rim chemical measurements calculated in plagioclase phenocrysts using SEM-EDS.

| Sample | Na Core | Ca core | Na rim | Ca rim |
|---|---|---|---|---|
| PA-19 | 14.91 | 9.88 | 10.60 | 17.50 |
| PA-27 | 13.93 | 3.87 | 11.97 | 10.81 |
| PA-44 | 4.01 | 9.27 | 3.39 | 9.75 |
| PA-49 | 0.50 | 20.27 | 0.55 | 23.80 |
| VF-74-130a | 0.92 | 2.27 | 2.87 | 1.67 |

## 4.2.4 – Disequilibrium textures vs. VEI

Counts of disequilibrium textures in samples with differing VEI are compiled in Table 4.4. The textural observations regarding disequilibrium state are generally more numerous as VEI increase (Fig. 4.17).

Table 4.4 – Average percentage of disequilibrium textures for each VEI analyzed.

| Disequilibrium textures | VEI 0 | VEI 1 | VEI 2 | VEI 4 |
|---|---|---|---|---|
| Sieve-plagioclase | 10 | 80 | 20 | 80 |
| Boxy-cellular plagioclase | 50 | 20 | 10 | 90 |
| Spongy-cellular plagioclase | 0 | 0 | 70 | 50 |
| Embayed olivine | 40 | 70 | 70 | 80 |
| Spliced olivine | 0 | 10 | 30 | 60 |
| Sieve-olivine | 0 | 0 | 0 | 80 |

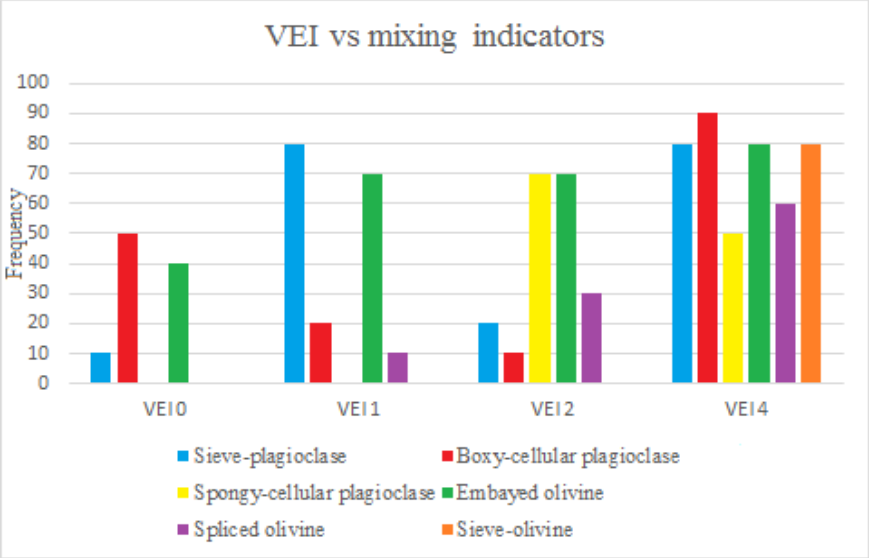


Fig. 4.17 – Distribution of mixing indicators in all the samples of different VEI.

## 4.2.5 – Plagioclase crystal size distributions (CSD)

Measurements of the long and short axes were made on 857 crystals of plagioclase for sample PA-27 (VEI 2), on 791 crystals of plagioclase for sample PA-14 (VEI 2), on 589 crystals of plagioclase for sample PA-44 (VEI 1), on 412 crystals of plagioclase for sample PA-45 (VEI 1), on 5,393 crystals of plagioclase for sample PA- 19 (VEI 0), and on 4,053 crystals of plagioclase for sample PA-3 (VEI 0), for crystal size distributions analysis. The latter three samples have more measurements because of the great quantity of microcrystals. The single slope for each sample can be found in Fig. 4.18, while Fig. 4.19 is comparative. Interpretations for each curve can be found in Section 5.2.

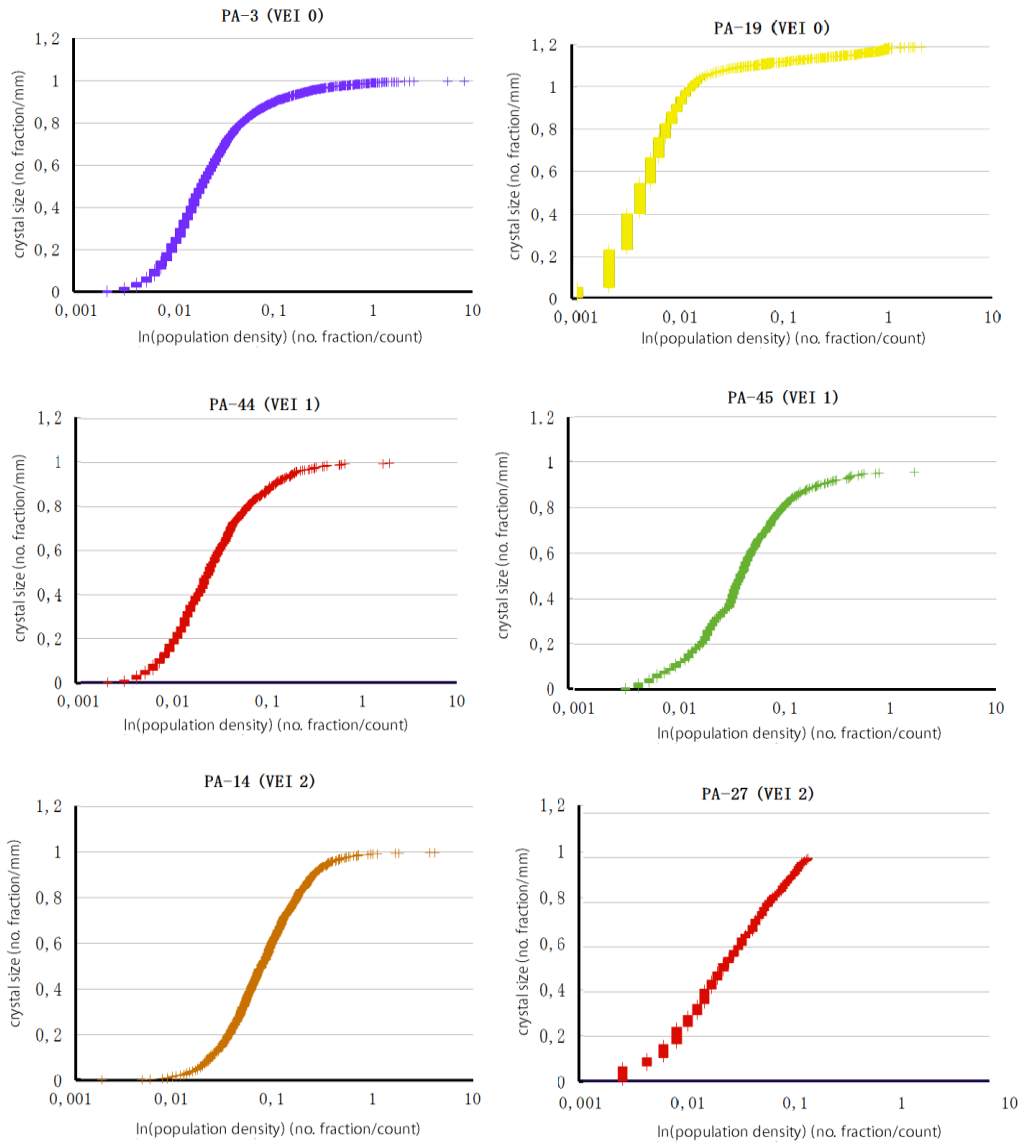


Fig. 4.18 – CSD for each sample analyzed. Measurements are presented in a graph crystal size vs. ln(population density).

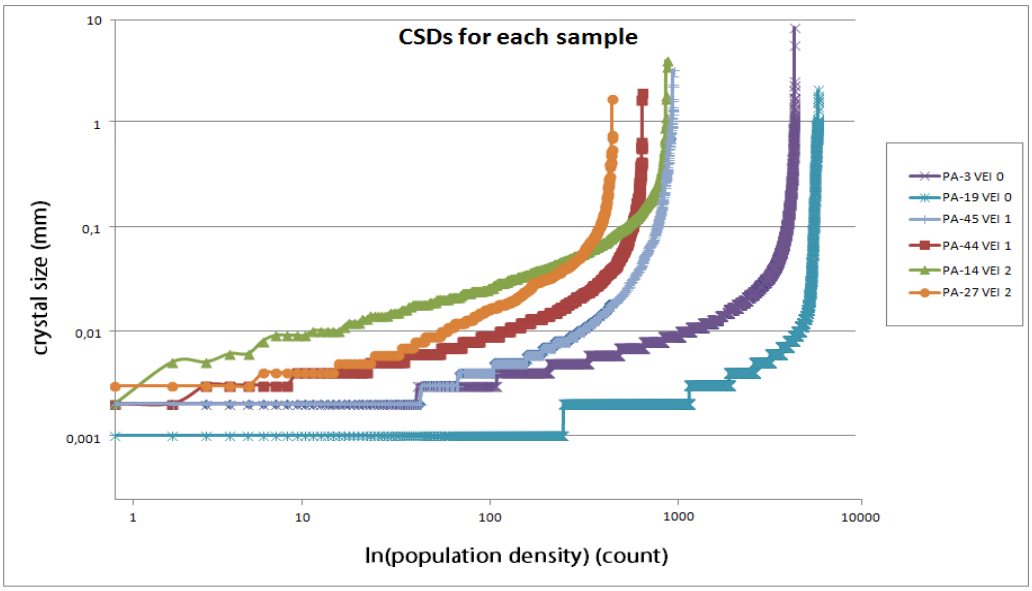


Fig. 4.19 - Comparative figure that shows relationship between all CSDs.

Broken crystals could affect the CSDs changing their shape, and possibly giving erroneous interpretations of the magmatic system. Consequently, during the process of drawing polygons each crystal would be examined individually to detect if it is a fragment (Higgins, 2006). Areas poor of broken microphenocrysts or phenocrysts are the best locations for more accurate analysis (Higgins and Roberge, 2003). Collecting data that include many broken crystal fragments could transform the shape of CSDs: the population of bigger crystals will be reduced and that of smaller crystals will be increased (Higgins, 2006). This will affect major the smaller crystals, overall if they are not so abundant in the rock.

## 4.2.6 – Viscosity data

According to the eruptive temperature data, we calculated viscosity for a range of temperatures between 1000°C and 1100°C for Pacaya and Fuego (Table 4.5).

Table 4.5 – Variation of viscosity for each VEI with increasing temperature at a constant $H_2O$ content of 2%.

| T[C] | T[K] | Log η VEI 0 | Log η VEI 1 | Log η VEI 2 | Log η VEI 4 |
|---|---|---|---|---|---|
| 1000 | 1273 | 2,23 | 2,11 | 2,35 | 3,98 |
| 1050 | 1323 | 1,85 | 1,73 | 1,96 | 3,44 |
| 1100 | 1373 | 1,51 | 1,39 | 1,62 | 2,96 |

The value of viscosity for each VEI varies with the content in $H_2O$, which can vary during an eruption. The trends show that increasing the $H_2O$ wt. % the viscosity decreases almost linearly (Fig. 4.20). Since this variation is very similar for each sample, we show here only how this occurs in sample PA-19 (VEI 0) and the other graphs can be found in Appendix F. Variation of viscosity related to the vesiculation index is shown in Fig. 4.21. Viscosity presented here is affected by the degree of crystallinity of the rock samples (41-51%), this means that real viscosity values are higher because of the medium-high content in phenocrysts (Sato, 2005; Marsh, 1981).

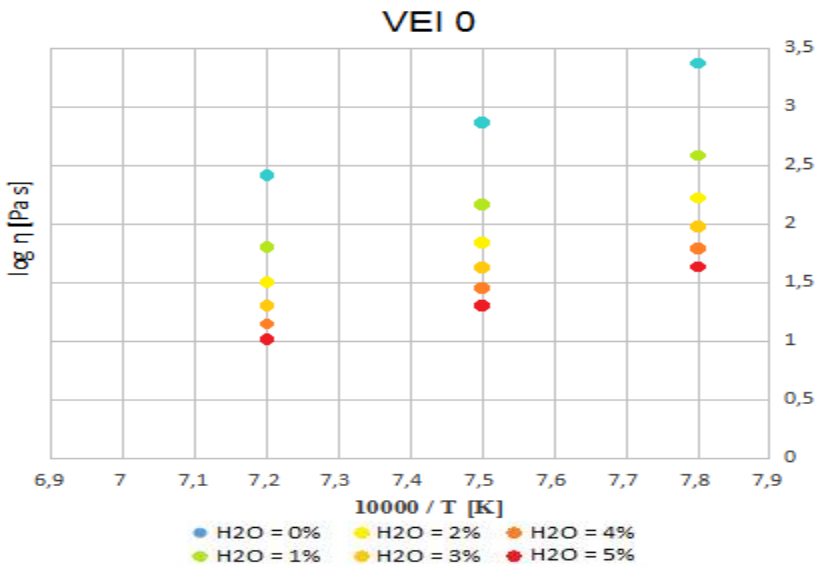


Fig. 4.20 – Viscosity vs. temperature plot showing how the viscosity is influenced by the $H_2O$ wt % in VEI 0 sample (PA-19).

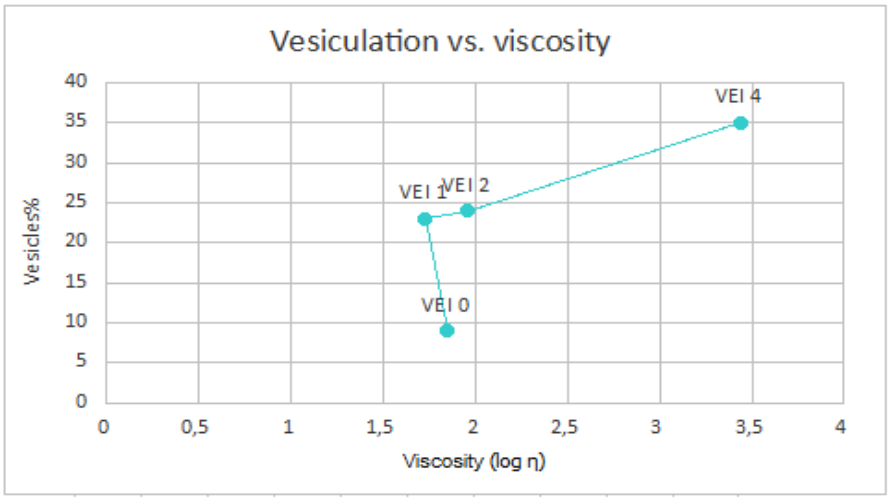


Fig. 4.21 – Vesiculation vs. viscosity diagram for each VEI.

# 5 – Discussion

## 5.1 – Magma mixing signatures

Magmatic systems at Pacaya and Fuego volcanoes are thought to have shallow magma bodies where mixing could occur (Kozak & Cermak, 2010; Chesner & Rose 1984; Eggers, 1971; Berlo *et al.*, 2012).

For Pacaya volcano, in particular, the Cerro Chiquito cinder cone, the coexistence of two shallow magma chambers was proposed (Bardintzeff & Deniel, 1992). The mantle source of shallow magma bodies is likely the same, and their compositional gas and temperature differences could reflect their different ages and cooling histories before they mixed. There is important evidence for dynamic shallow magma at Pacaya's Mckenney Cone: 1) Gravity data that reveal the location of magma bodies characterized by low-density (0.4 g/cm$^3$), which are located at a depth of 100 to 200 m (Eggers, 1983); 2) Vent position and elevation data, in particular the relationships between vent elevation and volume in flow events that seems to be consistent with magma chambers within the McKenney cone itself (Rose *et al*., 2013); 3) Collapse and exploding magma bodies in the past, evidenced by an edifice collapse event at Pacaya during Holocene; and 4) Variable gas emission data, characterized by a high $SO_2$ emission rate that emphasize the presence of a shallow magma chamber (Eggers, 1971; Andres *et al*., 1993).

At Fuego low-frequency seismic events with singular, long codas that seem to correlate with the timing of tremors could be related to the convective activity and shallow magma chamber dynamics (McNutt & Harlow, 1983), moreover, the $SO_2$

emission rate is consistent with a high level magma body that is crystallizing and degassing (Andres *et al*., 1993). Melt inclusion analyses show a modified $H_2O$ concentration due to diffusive re-equilibration that can occur in a shallow pressure magma body (Berlo *et al*., 2012), besides mixing may involve magma from deeper levels as there is evidence of rapid ascent of magma from 10 km. From trace-element analysis of Fuego volcanic material it was determined that the shallow magma chamber is located at a depth of 8-16 km and reflect evidence of input from olivine tholeiitic melts fractionated from a deeper magmatic source (Chesner & Rose, 1984).

Geochemistry of samples was compared with previous study in Fig. 5.1.

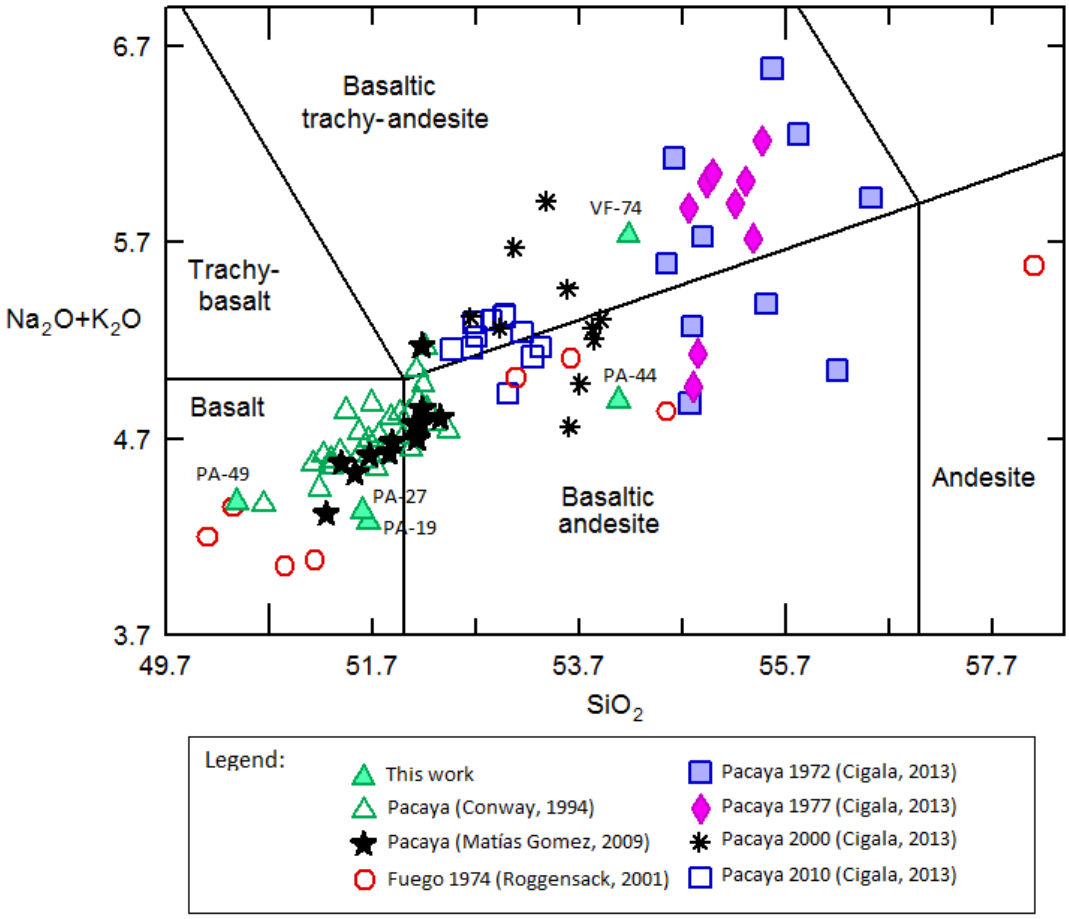


Fig. 5.1 – Geochemical comparison between this work and previous work at Pacaya and Fuego (Conway, 1994; Matías Gomez, 2009; Cigala, 2013; and Roggensack, 2001)

Do petrographic features reflect mixing and mingling variation that could be associated with style and intensity of eruptions.

1) Do they reflect disequilibria caused by magma mixing phenomena? ; 2) decompression processes (Nelson & Montana, 1992); or 3) could they reflect phreatomagmatism as suggested at Pacaya because of groundwater interaction with shallow magma (Cigala, 2013). Examples of fractured olivine crystals support the possibility of a magma-$H_2O$ interction, but the total absence of diktytaxitic textures due to phreatomagmatic events reject this hypothesis. Instead, several pieces of evidence including that there are likely shallow magma chambers beneath the two volcanoes, suggest mixing has occurred. Evidence that supports this idea are: 1) reverse zoning core-to-rim SEM-EDS analyses of Na and Ca composition in plagioclase, that indicate contact within a hotter and cooler liquid, and 2) differences in the crystallinity of the groundmasses that could be connected to a series of mingling episodes. This clearly reflect chemical/thermodynamical disequilibrium in the melt; according to these evidences we can consider these disequilibrium textures as the product of magma mixing (Shcherbakov et al., 2011; Thomber & Huebner, 1985).

The abundance and distribution of mixing textures seems to crudely correlate with VEI. Table 4.4 shows the distribution of each of the disequilibrium textures that we analyzed for each group of samples (Fig. 4.17). Samples from VEI 0 have boxy-cellular plagioclase (~ 50%) and fractured olivine (~ 40%), with some sieve-texture in plagioclase (~ 10%). The VEI 1 group is sieve-plagioclase (~ 80%) and fractured olivine (~ 70%), with minor boxy-cellular plagioclase (~ 20%) and spliced olivine crystals (~ 10%). The group of samples from VEI 2 intensity emphasizes spongy-cellular plagioclase (~ 70%) and fractured olivine (~ 70%) respect to the previous group, and less sieve and boxy textures and spliced crystals of olivine (< 30%). Finally, VEI 4 group shows a type of sieve-texture in olivine that not appear in any other previous group of samples and a relative high quantity of all the previous mixing textures (50-90 %) with large resorped and re-melted rims.

Do these textures evolve during mixing? Fractured olivine, boxy and sieve textures in plagioclase appeared in all samples to different degrees. Spongy-texture in plagioclase is noticeable in the VEI 2 sample group and is less abundant with increasing VEI intensity of the samples. The quantity of all types of textures increases with VEI, except for spongy-cellular plagioclase. The evolution of plagioclase crystals in these groups of samples can be described as a change in disequilibrium texture type. From the VEI 0 to 4 group there is an increase in sieve and spongy-textures and a decrease in boxy-textures. Spongy-plagioclase is present mainly starting from VEI 2 samples (Fig. 5.2). The evolution of olivine textures, from the VEI 0 to 4 group, seems to be a linear increase in the depth and width of the fractures (relative to crystal size), the width of the resorption rim, the quantity of broken crystals, and culminated by the appearance of sieve-olivine in VEI 4 samples (Fig. 5.3).

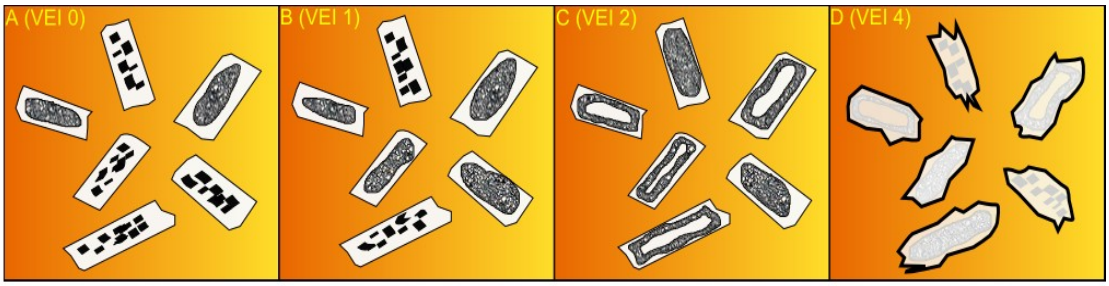


Fig. 5.2 – Evolution of mixing textures in plagioclase crystals with increasing VEI, from observations of thin sections. (A) VEI 0 is characterized mainly by plagioclase in boxy-cellular form, with minor sieve-textures; (B) it is possible to see that VEI 1 have an increase in sieve-textures content with a decrease in the number of boxy-textures; (C) In VEI 2 mixing textures evolve in a spongy-cellular form of plagioclase, with minor sieve-textures; (D) in the highest VEI analyzed plagioclase is characterized by all the mixing textures seen previously but with evidences of re-melted borders and an exaggerate increasing in the width of the reaction rims.

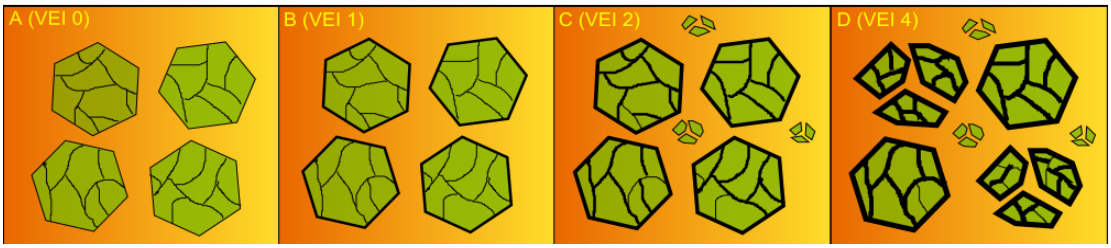


Fig. 5.3 – Evolution of textures in olivine crystals related to the explosive force with increasing VEI, from observations of thin sections. (A) In VEI 0 olivine present no signature of resorpted rims but light fracturation; (B) In VEI 1 there is an increment in the width of the reaction rims; (C) in VEI 2 it is possible to see how the width of both the rims and the fractures increase, and some olivine exists as broken crystals; (D) In VEI 4 olivine evolve with very deep fractures and reaction rims, with an high increasing in content of broken crystals.

Do these mixing textures truly correlate with the degree of explosivity? Is it possible to infer the intensity of the eruption from these textural observations? Other studies suggest that these mixing processes may be related to degree of explosivity as we outline below. In an episode of magma mixing during the 2001 eruption of a trachybasaltic lava at Etna volcano, characterized by a VEI 0 intensity, Viccaro *et al*., 2006 observed the same distribution of mixing textures found in Pacaya VEI 0 eruption. Focusing on the VEI 1 intensity samples of Pacaya, an equal frequency of sieve-textures and the same morphology of the fractures in olivine crystals is clearly noticeable during a mixing phase at Stromboli volcano in 2009 (La Felice & Landi, 2011), characterized by an intensity around VEI 1.5, and other two eruptions, energetically comparables, at Tatara-San Pedro volcanic complex (Singer *et al*., 1995), affected by mixing due to a shallow magma chamber close to input of basic magma, and during the mixing in the effusive VEI 1 pre-2010 eruption at Eyjafjallajökull volcano (Mari, 2013). The high quantity of spongy-cellular textures in plagioclase and fractured olivine in VEI 2 samples

of Pacaya are quite similar to three cases of magma mixing and eruptive intensity at Barren-Island volcano in 1994-1995 (Renjith, 2013), at Chimpa volcano (Arnosio, 2010), and at Maipo volcano (Sruoga *et al.*, 2012). Mixing events of VEI 4 intensity showing the same textures found in the sub-plinian eruption at Fuego, with large re-melted and resorpted rims, can be found during the pre-eruptive condition in 2010 of Merapi volcano, characterized by very deep fractures in olivine and highly re-melted plagioclase borders (Innocent *et al*., 2013), as also in an energetically similar event at Payùn Matrù volcano (Hernando *et al*., 2012).

# 5.2 – Interpretation of Crystal Size Distributions data

The size distribution of plagioclase crystals have been shown to be sensitive to the various physical-chemical conditions (temperature, pressure, $H_2O$ pressure, $fO_2$, melt composition) of the magmatic system (Humphreys *et al*., 2006; Ginibre & Worner, 2007; Smith *et al*., 2009; Viccaro *et al*., 2010).

Renjith (2013) interprets the physical-chemical micro-textures of plagioclase as due to mixing. Intense and prolonged dissolution to generate a sieve-plagioclase (resorption surface) occurs when plagioclase comes into contact with a more primitive magma. The explanation for plagioclase having a boxy-cellular texture (coarse-sieve) is the dissolution due to the variable rate of adiabatic decompression of a $H_2O$-undersaturated magma. Spongy-cellular texture (fine-sieve) in plagioclase is seen by Renjith (2013) as the result of partial dissolution due to reaction with more Ca-rich melt. Broken crystals, as found in olivine of VEI 2-4, may result from decompression caused by energetic eruptions. In Table 5.1, interpretations for mixing textures are listed, leaving out the more obvious and known embayed textures in olivine and zonation in plagioclase.

Table 5.1 – Descriptions of the physicochemical interpretations for each of the mixing textures, basing on Renjith (2013).

| Texture | Physicochemical interpretation |
|---|---|
| Sieve plagioclase | Prolonged and intense dissolution for the contact with a more primitive magma |
| Boxy-cellular plagioclase | Dissolution due to the variation rate of decompression (adiabatic) of a $H_2O$-undersaturated magma |
| Spongy-cellular plagioclase | Partial dissolution due to the reaction with more Ca-rich melt |
| Broken olivine crystals | Decompression caused by strong aerial eruptions |

For intensity of VEI 0 we made interpretations on CSDs derived from PA-3 and PA-19 samples. The CSD of PA-3 has a very high micro-phenocryst content and a level of nucleation density similar to the average of the other CSDs. This is interpreted to be the result of a higher degree of undercooling relative to the PA-19. The shape of the CSD seems to be related to mixing with a more mafic magma (Fig. 5.4a). Neglecting the abundant microlites that formed due to final decompression crystallization, it is possible to see that during mixing the normal cycle is likely interrupted; this event caused dissolution of the smaller crystals and growth of the bigger crystals (textural coarsening). However, by looking at the curve, mixing here is slight and relatively rapid. This event was followed by a process of buffering characterized first by the dissolution of small crystals of plagioclase, creating the coarse textures observed using polarized light microscopy (boxy-cellular and sieve plagioclase) and later by a crystallization phase of the same crystal type. In other words, the slope reflects the conditions about the cooler evolved magma during mixing, explaining as the normal curve is influenced by the entrance of a hotter less-evolved magma in the system. PA-19 CSD have the highest content in microlites, mainly due to initial decompression, and the remaining shape of the curve that remarks the same process of the previous curve, but with a steeper and rapid event of mixing (Fig. 5.4b)

For VEI 1 samples we made interpretations on CSDs of PA-44 and PA-45. PA-44 CSD have a medium-low micro-phenocryst content and higher level of nucleation density relative to VEI 0 samples. By looking at the shape of the curve it is possible to see the final decompression crystallization underlined by microlites, successively the curve is perturbed by a mixing event (Fig. 5.4c) which changed the linear cycle into a series of small steps of dissolution and crystallization of plagioclase, well visible in sieve textures. The number of steps indicate that input of a more basic magma occur more than once. PA-45 is very similar, presenting these various steps in the shape of the curve that could indicate plagioclase dissolution (sieve and boxy-cellular textures) and successive crystal nucleation. The CSD is also very close to the previous one both regarding nucleation density and crystallinity.

For VEI 2 we determined CSDs for samples PA-27 and PA-14. The PA-27 CSD shows a final decompression state followed by an almost linear crystallization process. Since that we detected mixing textures in this eruption and that the content in micro-phenocrysts is lower than the previous CSDs (with lower intensities), it is possible to interpret this curve according to a dynamic model on a CSD development in a study (Higgins & Roberge, 2003) of Soufrière Hills volcano. This study also related the development of the observed disequilibrium textures in this eruption to VEI. The shape of the CSD shows how after the initial texture development by nucleation and growth a mixing event occur due to the input of a more primitive magma, this event caused dissolution and textural coarsening (as seen in sieve and spongy-cellular textures). Consequently, a phase of buffering characterize further nucleation and growth of

plagioclase. Successively, a new input of mafic magma generated a further period of textural coarsening (and dissolution of microcrysts) followed by another period of buffering (nucleation and growth) in order to create the final CSD shape (Fig. 5.5). An almost similar CSD curve could characterize sample PA-14, with the difference in the higher level of nucleation density and undercooling.

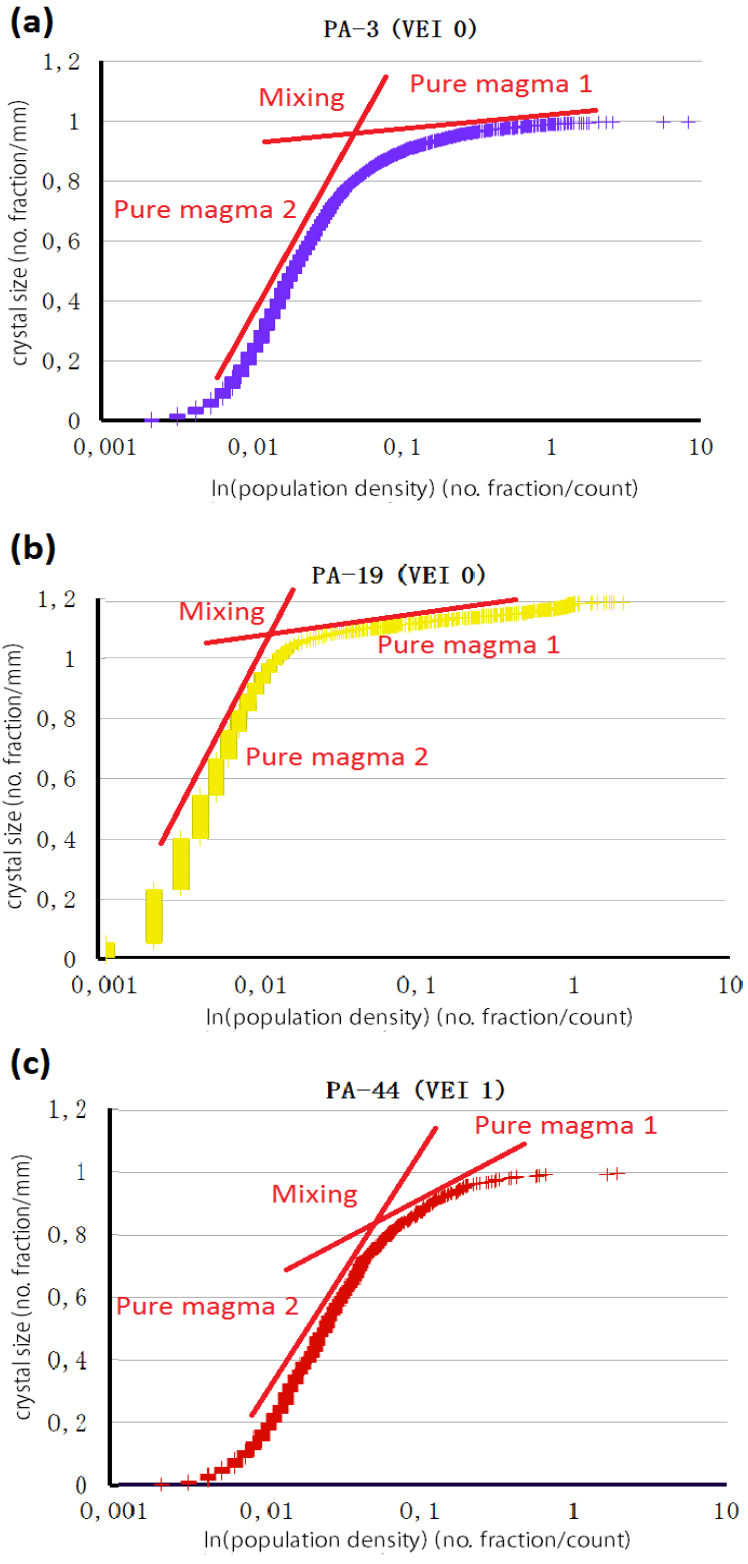
(a)
PA-3 (VEI 0)
Mixing
Pure magma 1
Pure magma 2
crystal size (no. fraction/mm)
1, 2
1
0, 8
0, 6
0, 4
0, 2
0
0, 001
0, 01
0, 1
1
10
ln(population density) (no. fraction/count)
(b)
PA-19 (VEI 0)
Mixing
Pure magma 1
Pure magma 2
crystal size (no. fraction/mm)
ln(population density) (no. fraction/count)
(c)
PA-44 (VEI 1)
Pure magma 1
Mixing
Pure magma 2
crystal size (no. fraction/mm)
ln(population density) (no. fraction/count)

Fig. 5.4 - Mixing interpretation on CSDs. (a) PA-3; (b) PA-19; (c) PA-44. Although these shapes could be related with two different cooling or depressurization events, we chose the mixing hypothesis by considering the mixing indicators described in Chapter 5.1.

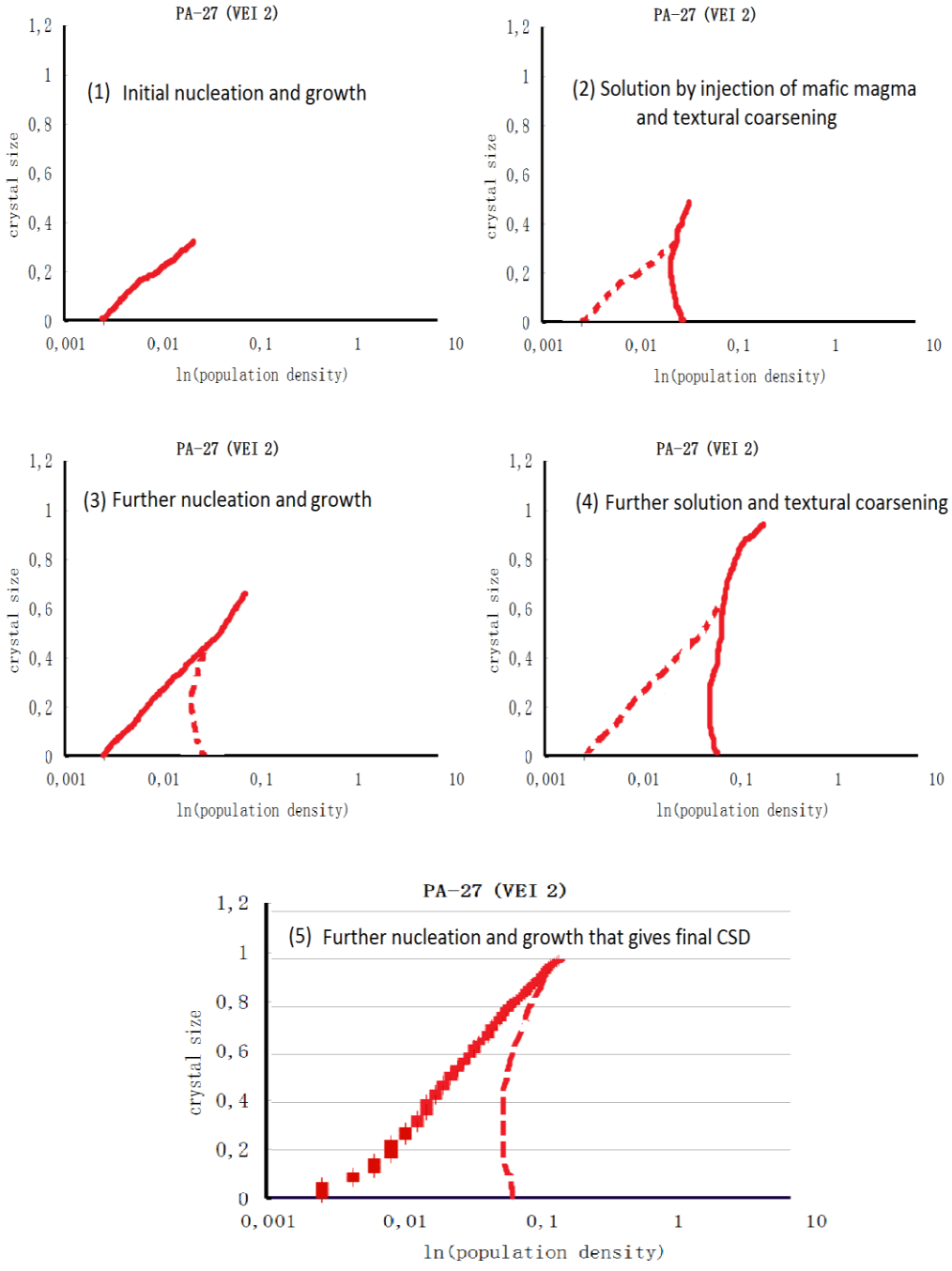


Fig. 5.5 - Alternate cycles of nucleation/growth and dissolution/buffering in order to generate coarse textures and the final CSD shape on sample PA-27. (1) Initial nucleation and growth with the solid phases

(plagioclase) that increases almost linearly; (2) interruption of the cycle by injection of mafic magma into the magma chamber, the smaller plagioclase crystals will dissolve while bigger crystals continue to grow with textural coarsening due to a period of buffering of the magma temperature; (3) restarting of the cycle with renewed nucleation and crystal growth; (4) new injection of mafic magma that induce the same process of panel (2), extending the CSD to larger crystal sizes; (5) Further nucleation and growth that gives the final CSD seen in erupted samples. These considerations are based on Higgins & Roberge (2003).

Mixing events trigger a period of dissolution of plagioclase crystals and flat CSDs representing high nucleation and growth periods and higher crystallinity of the magma. A model (Fig. 5.6) that relates mixing and VEI is proposed, where mixing occurs only once dissolution of microcrystals slows convection of the magmatic system and the eruption is less explosive. Thus, VEI=0 have steeper CSDs; on the other hand, where CSDs are flatter (PA-44, PA-45, PA-14, and PA-27) more than one period of mixing has possibly occurred, consistent with the observation and analysis of disequilibrium textures in these samples. In this case convection is inhibited by the great abundance of phenocrysts resulting from mixing induced nucleation and growth. This leads to more explosive eruptions. This model seems to be in accord with textural analysis, viscosity, and eruptive temperature of the samples.

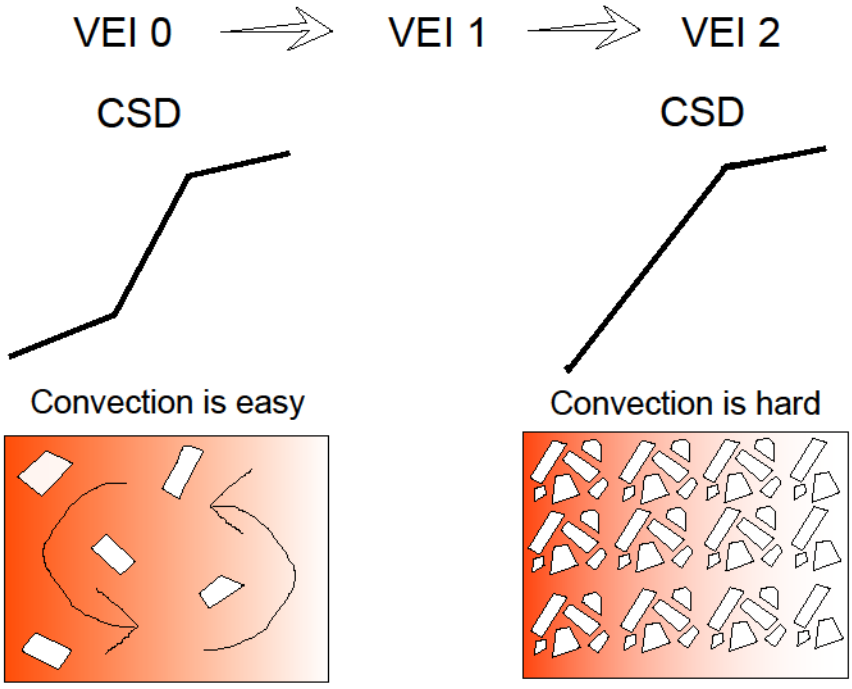


Fig. 5.6 - Proposed model for the correlation between the increase in explosivity and an increase in VEI, according to the shape of the CSDs. Where a single episode of mixing occurs convection is easy and the eruption will result less explosive, where many phases of mixing occurs convection is not easy (because of the abundance of phenocrysts) and the eruption will result more explosive. Indeed, phenocryst contents is higher in VEI=2 samples as well as viscosity. According to Ruprecht & Bachmann (2010), here we present

how is the higher content in phenocrysts that obstaculate the extent of mixing and heat exchange (increasing pressure and viscosity) resulting in more explosive eruptions.

## 5.3 – Timing effect

Magma mixing could trigger explosive eruptions, or in general for changes in eruptive style (Sparks & Sigurdsson, 1977; Kremers *et al*., 2012; Ruprecht & Bachmann, 2010; Murphy *et al*., 1998).

Based on the CSD data we consider, intrinsically, also the timing of the mixing processes that caused an increase in eruptive intensity and changes in eruptive style. Figure 5.7 shows how crystal residence, derived from the CSDs and considering a constant growth rates (Higgins, 2000; Higgins, 2006), increases with the intensity of eruption (VEI 0 to 2).

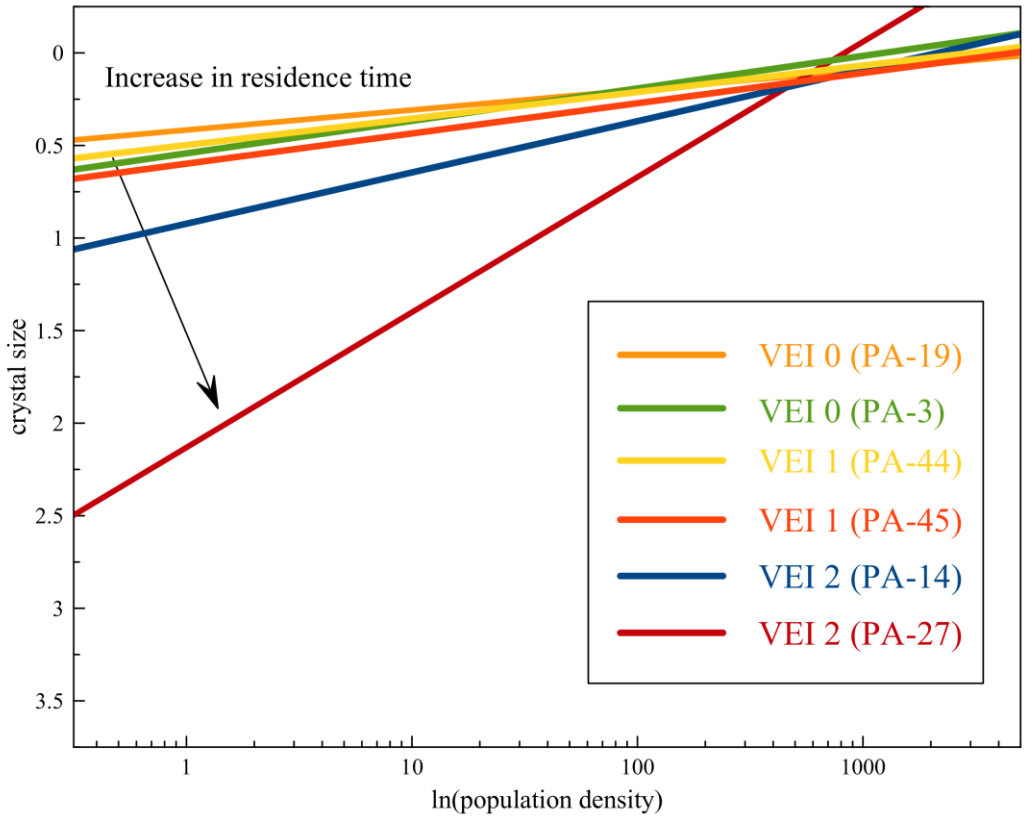


Fig. 5.7 – Crystal size vs. ln(population density) showing the increasing in residence time from VEI 0 to VEI 2 samples. We used the main slope for each CSDs for illustration.

What is the relationship between VEI and the crystal residence time?

According to Sparks and Sigurdsson (1977), the intrusion of a mafic magma (1,100-1,300°C) into a felsic magma (750-950°C) chamber would perturb the normal cooling and crystallization, creating a metastable environment. Studies of vein intrusions

(Blake *et al*., 1965) show how a mafic magma intrudes into the system forming pillow-like morphologies that increase the rate of heat transfer. A thermal wave passes through a substance, with radius *R,* in a time *t* given by

$$t = R^2/8K$$ (Sparks & Sigurdsson, 1977)

where *K* is the thermal diffusivity. For a normal pillow with 1 m in diameter and $K = 3 \times 10^{-7} m^2 s^{-1}$, *t* is ~ 29 hours. Because of the low time that the mafic magma needs to be thermodynamically equilibrated with the system (hours/days), the felsic magma is rapidly superheated. In this way, magma mixing leads to a very energetic convection in the felsic magma leading to a decrease in density from the base to the top of the magma chamber. For the formation of a convective cell the Rayleigh number (*Ra*) needs to exceed 660 (Lighthill, 1953) in the equation

$$Ra = \alpha (\Delta T) d^3 g\rho / Kv$$

where  is the coefficient of thermal expansion ($= 5 \times 10^{-5}$ deg$^{-1}$), *v* the viscosity, *d* the length scale of the chamber, *K* is the thermal diffusivity,  is the density of the acid magma, *g* is the acceleration due to gravity, and  is the difference in temperature of the two magmas. For the occurrence of a typical magma mixing event the value of viscosity can be substituted with $10^6$ P, while *d* will be as 10-1000 m, and is 10-300°C. Thus, by using these substitution the Rayleigh equation result in $4 \times 10^5$ to $10^{13}$: largely above the critical value.

By modeling of a 2D convection cell the vertical velocity is given by

$$V = (0.25\left(Ra^{\frac{2}{3}}\right)K)/d$$ (Sparks & Sigurdsson, 1977)

By substituting the results of the Rayleigh equation in a case of mixing (described above), the vertical velocity *V* will be in a range within 3.5 m d$^{-1}$ and 3,000 m d$^{-1}$. The meaning of this result demonstrate how magma mixing would generate vigorous and fast stirring of the felsic magma increasing the likelihood of an eruption in a time of only weeks or days. If the magma at the base is saturated in volatiles it became extreme supersaturated as it rises and, consequently, gas pressures are affected. This would also occur because of the high temperature of the acid magma that reduces the solubility of volatiles. Besides, the increase in volume of the magma chamber due to the input of mafic magma would increase the fluid pressure, arriving to generate fractures providing an explosive eruption.

# 6 – Conclusion

The goal of this work was to investigate whether  magma mixing phenomena influence the explosivity of mafic volcanic eruptions. Basaltic andesite samples which are

very similar in bulk composition and mode, but with a variety of eruption energy were examined petrographically.

12 samples from two subduction zone volcanoes located adjacent to one another were studied. All samples had $SiO_2$ of 49.27-53.65% and very similar contents of all major elements (near the boundary between hi-Al basalt and basaltic andesite). They were also texturally very similar with a high content of plagioclase (34-45% average, ~ 0.5 mm average diameter) and olivine (4-7% average and 0.2 mm diameters). Eruption intensities ranged from VEI 0 to 4.The samples selected are very similar to those that others have studied from the same volcanoes.

Our observations focused on mixing indications that perturb and influence crystal growth, affecting the advanced crystallization rates and styles in the rocks. By textural and chemical analyses a great variability of mixing textures were detected: sieve-plagioclase, boxy-cellular plagioclase, spongy-cellular plagioclase, fractured olivine, sieve-olivine, resorption rims. We used observed VEI as an indicator of eruption intensity for studies samples to compare each mixing texture with its degree of explosivity.

From these data we reconstruct an evolving stage of mixing, with an increase in eruptive intensity, for textures in plagioclase and olivine crystals. Plagioclase disequilibrium textures change with increasing explosivity from boxy to sieve and spongy texture, while olivine show a linear increase in the depth and width of the fractures, the width of the resorption rims, and the quantity of broken crystals. Some of these textures/explosivity relationships are comparable with other volcanoes, during mixing episodes.

Crystal size distributions in studied samples show more complex patterns and more crystals in samples erupted explosively. Crystal size distributions that derive from a single mixing event (with an obvious visible step in the curve) correlate with low intensity eruptions (VEI 0 and 1) because of the dissolution of the microcrysts and there is not enough remnant plagioclase growth in order to hinder convection. Multiple or prolonged events of mixing with several cycles of growth and dissolution that results in a high content of phenocrysts that make convection difficult, and the explosive potential increases because of overpressure in the magmatic system (VEI 2).

The number of mixing events reflected in CSD, and the magma mixing-to-eruption duration is apparently proportional to the explosivity of the volcanic event. The application of this method to determine the relationship between mixing duration and style and explosivity is restricted to volcanic products characterized by an intensity of VEI 0-4, where mixing processes are well documented and crystals are fully intact so that accurate CSDs can be measured. Likewise this relationship won't apply to crystal poor samples.

# 7 – References

Anderson A.T., 1984. Probable relations between plagioclase zoning and magma dynamics, Fuego volcano, Guatemala. American Mineralogist, v. 69, p. 660–676.

Andersson UB and Eklund O, 1994. Cellular plagioclase intergrowths as a result of crystal-magma mixing in the Proterozoic Aland rapakivi batholith, SW Finland. Contributions to Mineralogy and Petrology, 117, 124–136.

Andres RJ, Rose WI, Stoiber RE, Williams SN, Matias O and Morales R, 1993. A summary of sulfur dioxide emission rate measurements from Guatemalan volcanoes. Bull. Volcanol., 55, 379-388.

Anonymous, 1990. Metamorphic olivine in picritic metavolcanics from southern Finland. Bull. Geol. Soc. Finland, 62, Part 2, 99-114.

Arnosio M, 2010. Evidencia textural y geoquímica de mezcla de magmas en el volcán Chimpa, Puna Salteña. Revista de la Asociación Geológica Argentina, 66 (1), 251- 268.

Bardintzeff JM and Deniel C, 1992. Magmatic evolution of Pacaya and Cerro Chiquito volcanological complex, Guatemala. Bull Volcanol, 54, 267-279.

Bardintzeff JM, 1992. Magma mixing processes in volcanic contexts, a thermodynamic approach with the examples of St Vincent Soufrire volcano, West lndies and Cerro Chiquito, Guatemala. In Journal: Terra Nova, vol. 4, issue 5, pp. 553-556.

Berg JH, 1980. Snowflake troctolite in the Hettasch Intrusion, Labrador: Evidence for magma mixing and supercooling in a plutonic environment. Contributions to Mineralogy and Petrology, 72, 339-351.

Berlo K., Stix J., Roggensack K. and Ghaleb B., 2012. A Tale of Two Magmas, Fuego, Guatemala. Bulletin of Volcanology, 74 (2), 377-390.

Blake DH, Elwell RWD, Skelhorn RR and Walker GPL, 1965. Some relationships resulting from the intimate association of acid and basic magmas. Quarterly Journal of the Geological Society, London, 121, 31–49.

Bollasina A.J., Sehlke A., Gurioli L., Harris A.J.L. and Whittington A.G., 2013. Subliquidus rheology of arc magmas: A comparison of Pacaya, Guatemala, and Stromboli, Italy. GSA Annual Meeting, Denver, CO.

Brugger CR and Hammer JE, 2010. Crystal size distribution analysis of plagioclase in experimentally decompressed hydrous rhyodacite magma. Earth Planet. Sci. Lett., 300, 246–254.

Carr MJ, 1984. Symmetrical and segmented variation of physical and geochemical characteristics of the Central American volcanic front. Journal of Volcanology and Geothermal Research, 20, 231-252.

Carr MJ, Patino LC and Feigenson MD, 2002. Petrology and geochemistry of lavas. In: Bundschuh J, Alvarado GE (eds) Central America: geology, resources, and hazards. Taylor and Francis, London, pp 565–590.

Carr MJ, Rose WI and Stoiber RE, 1982. Central America. In: Thorpe RS (ed) Andesites, Wiley & Sons, pp 149-166.

Chesner CA and Rose WI Jr, 1984. Geochemistry and evolution of the Fuego volcanic complex, Guatemala. J Volcanol Geotherm Res, 21, 25–44.

Cigala V., 2013. Fossil bubble in porphyritic basaltic pyroclasts produced by small and large strombolian eruption at Pacaya, Guatemala. Master's Thesis, Michigan Technological University, 122 pp.

Claeson DT, 1998. Coronas, reaction rims, symplectites and emplacement depth of the Rymmen gabbro, Transscandinavian Igneous Belt, southern Sweden. Mineral. Mag., 62, 743-757.

Conway FM, 1994. Construction Patterns and timing of volcanism at the Cerro Quemado, Santa María and Pacaya Volcanoes, Guatemala. PhD Thesis, Michigan Technological University.

Coombs ML and Gardner JE, 2004. Reaction rim growth on olivine in silicic melts: implications for magma mixing. American Mineralogist, 89, 748-758.

Eggers AA, 1983. Temporal gravity and elevation changes at Pacaya Volcano, Guatemala. Journal of Volcanology and Geothermal Research, 19(3-4), 223-237.

Eggers AA, 1972. The geology and petrology of the Amatitlàn quadrangle, Guatemala. PhD Dissertation. Dartmouth College, Hanover, New Hampshire. 221 pp.

Eggers AA, 1971. The geology and petrology of the Amatitlan quadrangle, Guatemala. Unpublished PhD thesis. Darthmouth College, Hannover, New Hampshire. 221p.

Gibson D., Lux D.R. and Choate M. A., 2003. Petrography of a "cryptic" mixed magma system - the Mount Waldo granite, coastal Maine. Atlantic Geology, v. 39, p. 163-173.

Ginibre C and Wörner G, 2007. Variable parent magmas and recharge regimes of the Parinacota magma system (N. Chile) revealed by Fe, Mg and Sr zoning in plagioclase. Lithos, 98, 118-140.

Giordano D, Russell JK and Dingwell DB, 2008. Viscosity of Magmatic Liquids: A Model. Earth & Planetary Science Letters, 271, 123-134.

Hernando I.R., Llambías E.J, González P.D. and Sato K., 2012. Volcanic stratigraphy and evidence of magma mixing in the Quaternary Payún Matrú volcano, Andean backarc in western Argentina. Andean Geology, 39, 158-179.

Higgins M.D., 2000. Measurement of crystal size distributions. American Mineralogist, 85, 1105–1116.

Higgins M.D. and Roberge J., 2003. Crystal Size Distribution of Plagioclase and Amphibole from Soufriere Hills Volcano, Montserrat: Evidence for Dynamic Crystallization-Textural Coarsening Cycles. J. Petrol., 44, 1401-1411.

Higgins MD, 2006. Quantitative textural measurements in igneous and metamorphic petrology. Book, Cambridge University Press, 270 pp.

Humphreys M.C.S., Blundy J.D. and Sparks S.J., 2006. Magma evolution and open system processes at shiveluch volcano: insights from phenocryst zoning. Journal of Petrology, 47 (12), 2303-2334.

Innocenti S., Andreastuti S., Furman T., Del Marmol M. and Voight B., 2013. The pre-eruption conditions for explosive eruptions at Merapi volcano as revealed by crystal texture and mineralogy. Journal of Volcanology and Geothermal Research, 261, 69-86.

Kitamura S. and Matías O., 1995. Tephra stratigraphic approach to the eruptive history of Pacaya volcano, Guatemala. Science Reports, Tohoku University, Seventh Series: Geography, 45 (1), 1-41.

Kozak J and Cermak V, 2010. The Illustrated Hystory of Natural Disasters. Pacaya Volcano, pp. 93-94.

Kremers S., Hanson J., Lavallee Y., Hess K.U., Chevrel O., Wassermann J. and Dingwell D. B., 2012. Shallow magma-mingling-driven Strombolian eruptions at Mt. Yasur volcano, Vanuatu. Submitted to GRL.

La Felice S and Landi P, 2011. The 2009 paroxysmal explosions at Stromboli (Italy): magma mixing and eruption dynamics. Bull. Volcanol., 73, 1147-1154.

Laumonier M., Scaillet B., Arbaret L. and Champallier R., 2014. Experimental simulation of magma mixing at high pressure. Lithos, Vol. 196, p. 281-300.

LeBas MJ, LeMaitre RW, Streckeisen A and Zanettin B, 1986. A chemical classification of volcanic rocks based on the total alkali-silica diagram. Journal of Petrology, v. 27, p. 745- 750.

Lighthill MJ, 1953. Theoretical Considerations on Free Convection in Tubes. Journal of Mechanics and Applied Mathematics, vol. 6, 398-439.

Lloyd AS, Plank T, Ruprecht P, Hauri E, Rose W and Gonnermann H, 2014. NanoSIMS results from olivine-hosted melt embayments: Magma ascent rate during explosive basaltic eruptions. J Volcanol Geoth Res, 283, 1-18.

Lloyd AS, Plank T, Ruprecht P, Hauri EH and Rose WI, 2013. Volatile loss from melt inclusions in pyroclasts of differing sizes. Contributions to Mineralogy and Petrology, Volume 165, Issue 1, pp 129-153.

Lyons JJ, Waite GP, Rose WI and Chigna G, 2010. Patterns in open vent, Strombolian behavior at Fuego volcano, Guatemala, 2005–2007. Bull. Volcanol., 72, 1–15.

Mari N., 2013. Studio dei prodotti iniziali dell'eruzione 2010 del vulcano Eyjafjallajökull (Islanda). Unpublished Bachelor's Thesis, University of Urbino, 100 pp.

Marsh BD, 1998. On the interpretation of Crystal Size Distributions in Magmatic Systems. J. Petrol., v. 39, 553-599.

Marsh BD, 1981. On the crystallinity, probability of occurrence, and rheology of lava and magma. Contrib Mineral Petrol., 78, 85–98.

Martin DP and Rose WI, 1981. Behavioral patterns of Fuego volcano, Guatemala. J. Volcanol. Geotherm. Res., 10, 67-81.

Matías Gomez RO, 2009. Volcanological map of the 1961 - 2009 eruption of Volcan de Pacaya, Guatemala. MS Thesis, Michigan Technological University.

McNutt SR and Harlow DH, 1983. Seismicity at Fuego, Pacaya, Izalco, and San Cristobal Volcanoes, Central America, 1973–1974. Bull. Volc., 46 (3), 283-297.

Morgan H.A., Harris A.J.L. and Gurioli L., 2013. Lava discharge rate estimates from thermal infrared satellite data for Pacaya Volcano during 2004 – 2010. Journal of Volcanology and Geothermal Research, 264, 1-11.

Murphy MD, Sparks RSJ, Barclay J, Carroll MR, Lejeune AM, Brewer TS, Macdonald R, Black S and Young S, 1998. The role of magma mixing in triggering the current eruption at the Soufriere Hills volcano, Montserrat, West Indies. Geophysical Research Letters, vol. 25, n.18, 3433-3436.

Nelson ST and Montana A, 1992. Sieve-textured plagioclase in volcanic rocks produced by rapid decompression. American Mineralogist, v. 77, p. 1242-1249.

Newhall CG and Self S, 1982. The volcanic explosivity index (VEI): An estimate of explosive magnitude for historical volcanism. J. Geophys. Res., 87, 1231–1238.

Newhall CG, 2000. Volcano Warnings. In: Encyclopaedia of Volcanoes (Chief Editor H. Sigurdsson) Academic Press, San Diego, 1185-1197.

Rasband WS, 1997. ImageJ. U. S. National Institutes of Health, Bethesda, Maryland, USA, http://imagej.nih.gov/ij/, 1997-2012.

Renjith M.L., 2013. Micro-textures in Plagioclase from 1994-1995 Eruption, Barren Island Volcano: Evidence of Dynamic Magma Plumbing System in The Andaman Subduction Zone. Geoscience Frontiers, vol. 5, issue 1, 113-126.

Rodriguez LA, Watson MW, Rose WI, Branan YK, Bluth GJS, Chigna G, Matias O, Escobar D, Carn SA and Fischer TP, 2004. $SO_2$ emissions to the atmosphere from active volcanoes in Guatemala and El Salvador, 1999-2002. Journal of Volcanology and Geothermal Research, v. 138, p. 325-344.

Roggensack K., 2001. Unraveling the 1974 eruption of Fuego volcano (Guatemala) with small crystals and their young melt inclusions. Geology, 29, 911-914.

Rose W.I., Anderson A.T. Jr., Bonis S. and Woodruff L.G., 1978. The October 1974 basaltic tephra from Fuego Volcano, Guatemala: Description and history of the magma body. J. Volcanol. Geotherm. Res., 4, 3-53.

Rose WI, Newhall CG, Bornhorst TJ and Self S, 1987. Quaternary silicic pyroclastic deposits of Atitlán Caldera, Guatemala. J Volcanol Geotherm Res, 33, 57-80.

Rose WI, Self S, Murrow PJ, Ernst GGJ, Bonadonna C and Durant AJ, 2007. Pyroclastic fall deposit from the October 14, 1974 eruption of Fuego Volcano, Guatemala. Bull. Volcanol., vol. 70(9), 1043-1067.

Rose WI, Palma JL, Escobar Wolf R and Matias RO, 2013. 50 years of activity at a basaltic composit cone: Pacaya, Guatemala, 1961-2011. GSA Special Paper 498 “Open Vent Volcanoes”.

Ruprecht P and Bachmann O, 2010. Pre-eruptive reheating during magma mixing at Quizapu volcano and the implications for the explosiveness of silicic arc volcanoes. Geology, 38, 919-922.

Sato H., 2005. Viscosity measurement of subliquidus magmas: 1707 basalt of Fuji volcano. J Mineral Petrol Sci., 100, 133–142.

Shcherbakov V., Plechov P., Izbekov P. and Shipman J., 2011. Plagioclase zoning as an indicator of magma processes at Bezymianny Volcano, Kamchatka. Contributions to Mineralogy and Petrology, 162, 83-99.

Singer BS, Dungan MA and Layne GD, 1995. Textures and Sr, Ba, Mg, Fe, K, and Ti compositional profiles in volcanic plagioclase: clues to the dynamics of calc-alkaline magma chambers. American Mineralogist, 80, 776–798.

Sisson TW and Layne GD, 1993. $H_20$ in basalt and basaltic andesite glass inclusions from four subduction related volcanoes. Earth Planet Sci Lett, 117, 619-635.

Soldati A., Bollasina A., Chigna G., Sehlke A. and Whittington, A. G., 2014. The January 2014 Eruption of Pacaya (Guatemala): Rheology and Morphology through Field Observations and Laboratory Experiments. American Geophysical Union, Fall Meeting 2014.

Smith V.C., Blundy J.D. and Arce J.L., 2009. A temporal record of magma accumulation and evolution beneath Nevado de Toluca, Mexico, preserved in plagioclase phenocrysts. Journal of Petrology, 50 (3), 405-426.

Smithsonian Institute, Global Volcanism Program, http://www.volcano.si.edu.

Sparks RSJ and Aspinall WP, 2004. Volcanic activity: Frontiers and challenges in forecasting, prediction and risk assessment. In The State of the Planet: Frontiers and Challenges in Geophysics, Geophys. Monogr. Ser., vol. 150, edited by R. S. J. Sparks and C. J. Hawkesworth, pp. 359–373, AGU, Washington, D. C..

Sparks S.R.J., Sigurdsson H. and Wilson L, 1997. Magma mixing: a mechanism for triggering acid explosive eruptions. Nature 267, 315–318.

Sruoga P., Etcheverría M. P., Feineman M., Rosas M., Burker C. and Ibañes O., 2012. Complejo Caldera Diamante-Volcán Maipo (34°10´S, 69º50´O): Evolución Volcanológica y Geoquímica e Implicancias en su peligrosidad. Revista de la Asociación Geológica Argentina, 69 (4), 508 – 530.

Swain MW and Atkinson BK, 1978. Fracture surface energy of olivine. Pageoph., 116, 866-872.

Thornber CR and Huebner JS, 1985. Dissolution of olivine in basaltic liquids: experimental observations and applications. Am. Mineral., 70, 934–945.

Tsuchiyama A, 1985. Dissolution kinetics of plagioclase in the melt of the system diopside-albite-anorthite, and origin of dusty plagioclase in andesites. Contributions to Mineralogy and Petrology, 89 (1), 1-16.

Viccaro M., Ferlito C., Cortesogno L., Cristofolini R., Gaggero L., 2006. Magma mixing during the 2001 event at Mount Etna (Italy): effects on the eruptive dynamics. Journal of Volcanology and Geothermal Research, 149, 139-159.

Viccaro M., Giacomoni P.P., Ferlito C. and Cristofolini R., 2010. Dynamics of magma supply at Mt. Etna volcano (Southern Italy) as revealed by textural and compositional features of plagioclase phenocrysts. Lithos 116, 77-91.

Vinet N and Higgins M.D., 2010. Magma solidification processes beneath Kilauea Volcano, Hawaii: A quantitative textural and geochemical study of the 1969-1974 Mauna Ulu lavas. Journal of Petrology, 51 (6), 1297-1332.

Wade JA, Plank T, Hauri EH, Kelley KA, Roggensack K and Zimmer M, 2008. Prediction of magmatic water contents via measurement of $H_2O$ in clinopyroxene phenocrysts. Geology, 36, 799-802.

Walker JA, Roggensack K, Patino LC, Cameron BI and Matias O, 2003. The water and trace element contents of melt inclusions across an active subduction zone. Contrib. Mineral Petrol, 146, 62–77.

Wohletz K, 2002. http://internet.cybermesa.com/~wohletz/KWare/KWare.htm.

Wunderman RL and Rose WI, 1984. Amatitlán, an actively resurging cauldron 10 km south of Guatemala City. J. Geophys. Res., 89, 8525-8539.

# 8 – Appendices

## 8.1 – Appendix A _ Optical Microscopy Sample Preparation procedure

First of all, in the process of preparation of the thin sections, it is made a cut of a small representative slice of the sample to analyze, isolating the superfluous part, from

this slice the thin section will be obtained subsequently. For this operation a diamond abrasive disk is used; during the cutting process the disk is continually wet with a cooling-liquid so that to avoid overheatings and also to remove the deposits that can be formed during the cutting. This phase is very delicate because needs to be careful in order to not create scratches or some type of microfractures in the slice of the sample, in fact this would be able to make the following phases more difficult and tiresome. The cut samples must be as the same size of the thin glass.

In this case, the redoubt granulometry (size distribution of grains) and the high degree of porosity of the scoria and tephra samples made the phase of cutting almost impossible. To prevent this problem the samples were englobed using the EPOXY resin bicomponent, mixing with 12.5 ml of resin + 2.5 ml of hardening liquid. For the englobing phase of the resin in the sample was used a heated oven in order to facilitate the flowing of the EPOXY inside the pore of the samples. After 24 hours can start the phase of cutting, the cut residues were preserved in case of future analyses. After the cutting process, the "little bricks" are heated in oven at 60° C.

Subsequently the samples are smoothed (on one side) through the lapping, using the carborundum (silicon carbide, SiC) as abrasive and a base of glass. In this phase it is important to not leave undulations or microfractures on the meaningful side of the sample, so diamond abrasive of 9, 6, 3, 1, 0.25 μm are used (more and more small size of SiC).

Then the thin glasses are prepared, on which must be glues the "little bricks". The thin glasses were necessarily submitted to a lapping process, the final thickness requested is 1.200 μm. To do this was used an automatic polisher in which the setting has been programmed to 1.235 μm and the lapping time was planned in accord to the initial thickness of the thin glass.

Once that the thin glasses are prepared, the next phase was the gluing of the lapped "little bricks". After at least 24 hours until the gluing phase, the following footstep occurred: the cutting of the "little bricks" glued on the thin glass. In the laboratory has been used a grinder, working through abrasive disks; the use of these disks need a continuous lubrication and cooling with water. At the end of this phase, was obtained a "little slice" of the sample with 2 mm of thickness. Successively, the lapping of the samples occur: the requested thickness is 1.235 μm (1.200 μm of glass + 35 μm of rock-sample).

## 8.2 – Appendix B _ More polarized light microscope images

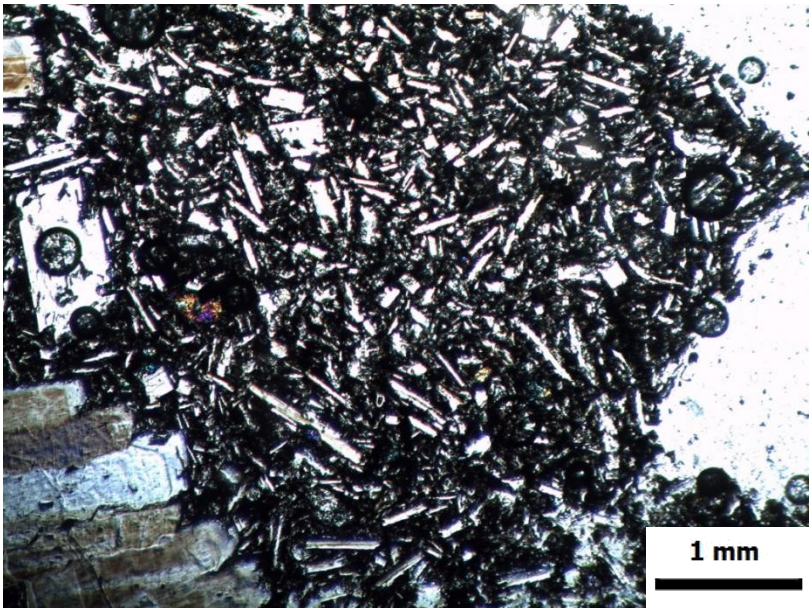


Fig. 8.1 - Microphotograph of sample PA-19 (N//), at 2.5x: panoramic of the thin section where it is possible to see the great quantity of plagioclase crystals.

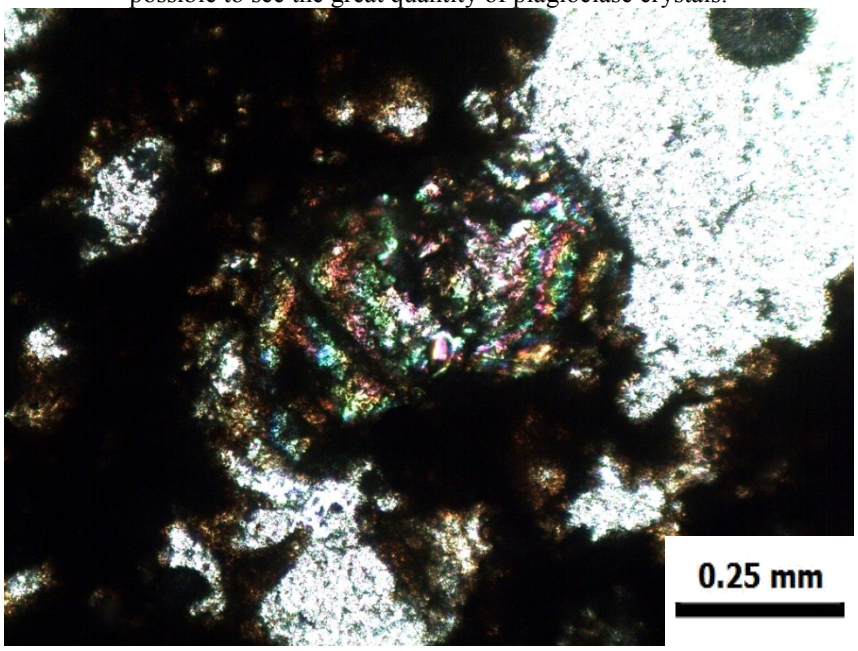


Fig. 8.2 - Microphotograph of sample PA-45 (NX), at 10x: example of olivine with skeletal texture and thin resorption rims.

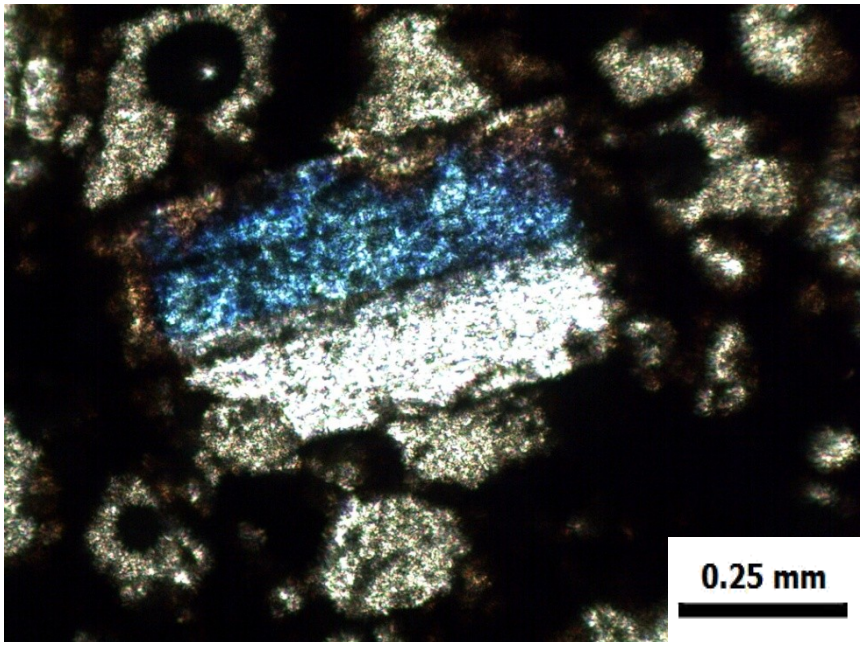


Fig. 8.3 - Microphotograph of sample PA-45 (NX), at 10x: particular of a clear Albite-Carlsbad twinning in a plagioclase crystal.

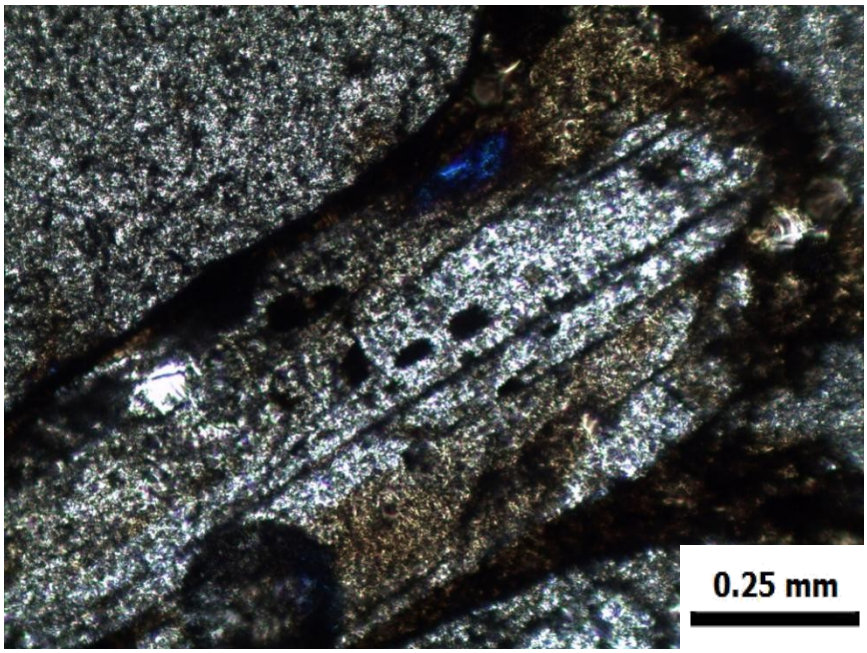


Fig. 8.4 - Microphotograph of sample PA-46 (N//), at 10x: particular of a polysynthetic twinning of a sieve-plagioclase.

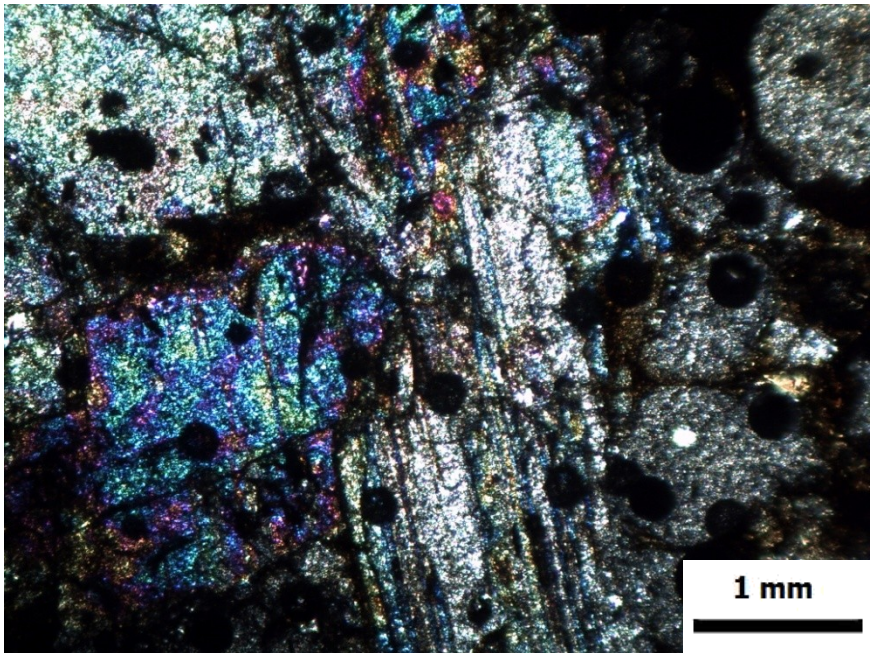


Fig. 8.5 - Microphotograph of sample PA-46 (NX), at 2.5x: fractured olivine crystal twinned with a plagioclase crystal. Both crystals shows disequilibrium textures.

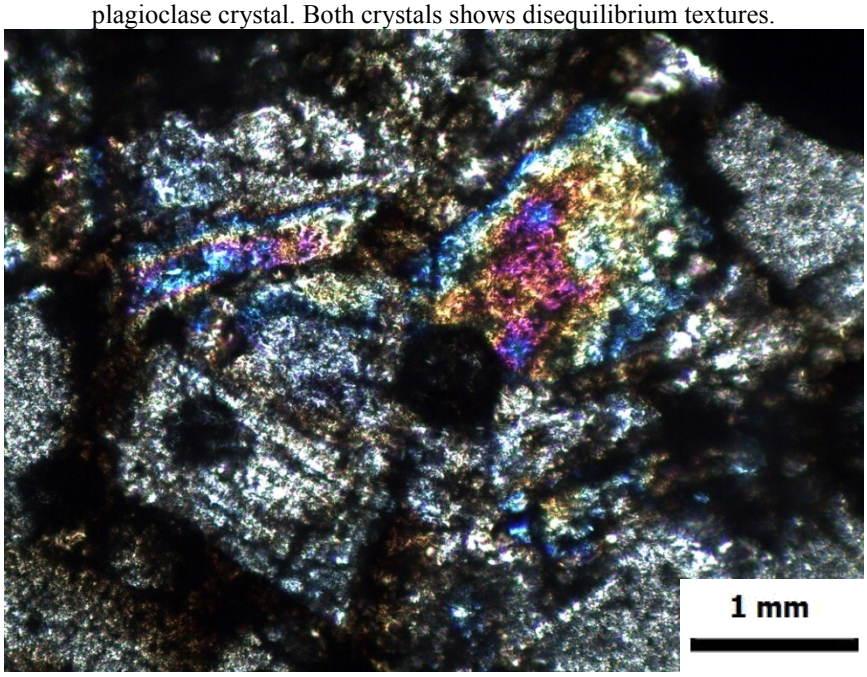


Fig. 8.6 - Microphotograph of sample PA-46 (NX), at 2.5x: particular of fractured olivine crystal.

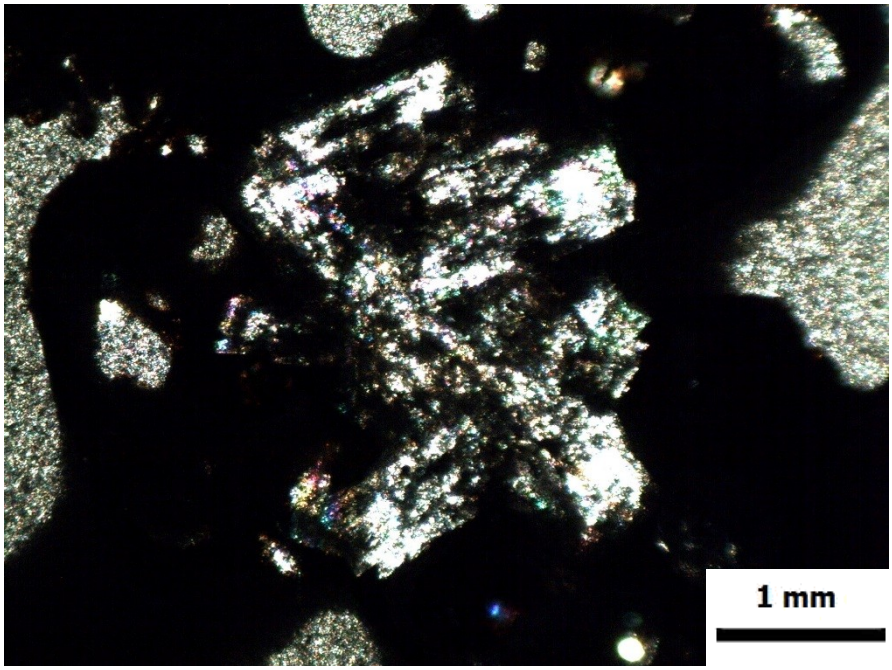


Fig. 8.7 - Microphotograph of sample PA-47 (NX), at 2.5x: panoramic of the sample showing an aggregate of sieve-plagioclase. It is possible to notice the hypocrystalline depth mass.

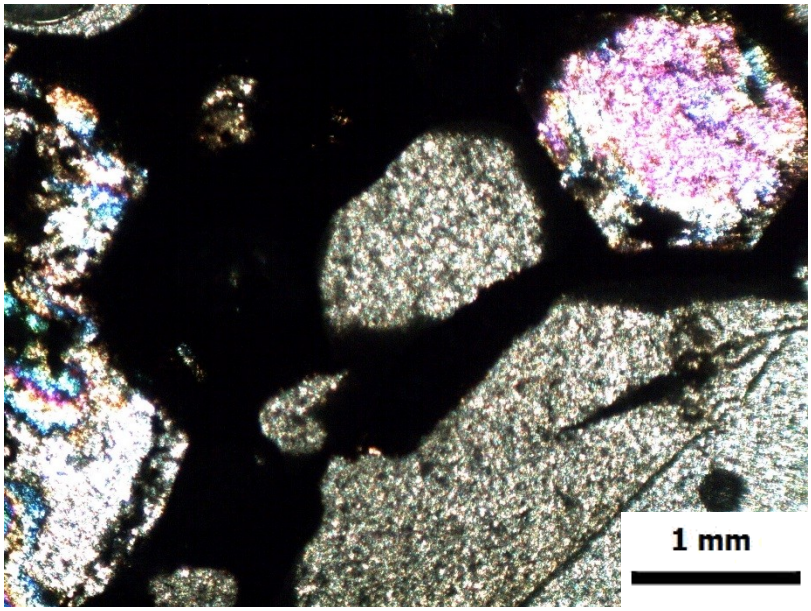


Fig. 8.8 - Microphotograph of sample PA-47 (NX), at 2.5x: image showing a part of another aggregate of sieve-plagioclase (on the left) and an euhedral zonated crystal of olivine (on the upper right).

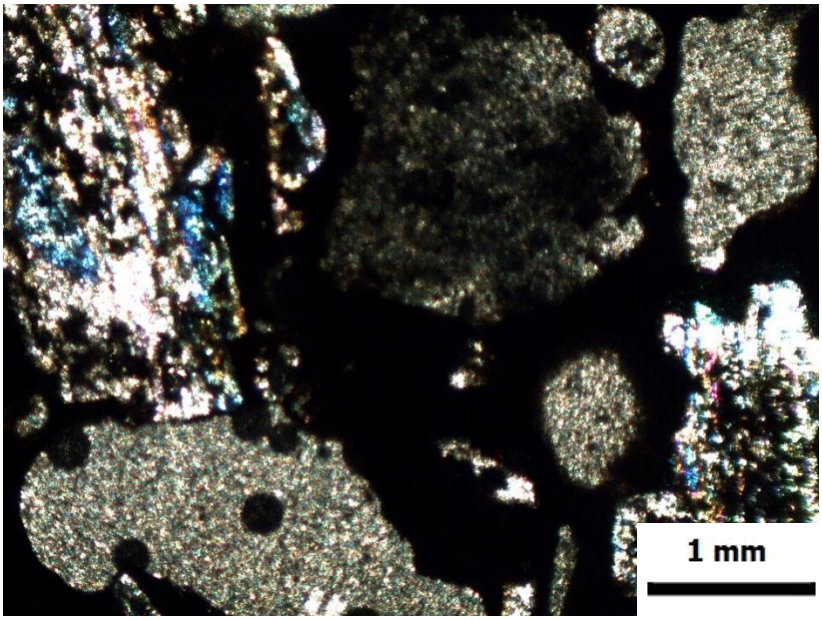


Fig. 8.9 - Microphotograph of sample PA-47 (NX), at 2.5x: it is possible to notice the two type of disequilibrium textures that characterize plagioclase crystals in this sample, sieve-texture (on the upper left) and boxy-cellular texture (on the right part).

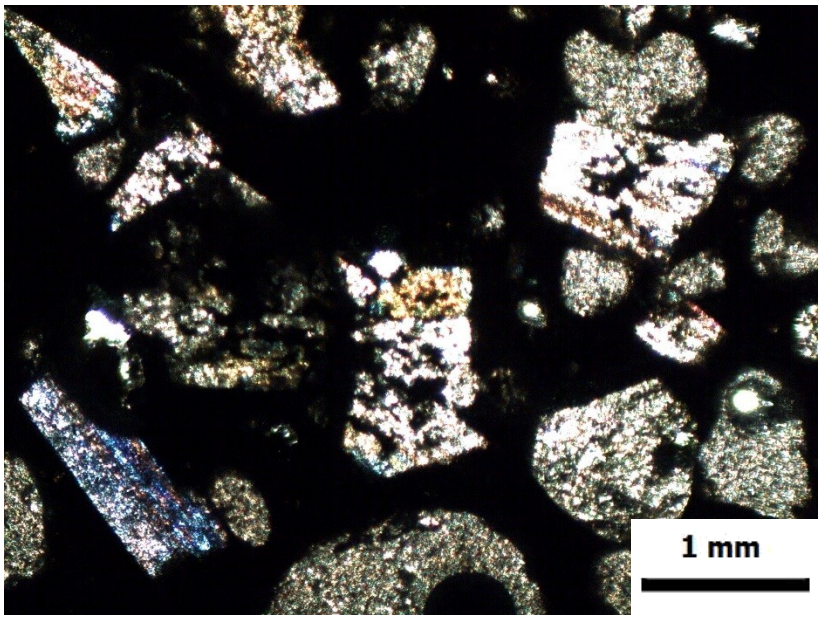


Fig. 8.10 - Microphotograph of sample PA-49 (NX), at 2.5x: panoramic of the sample where it is possible to see both plagioclase and olivine crystals characterized by disequilibrium textures.

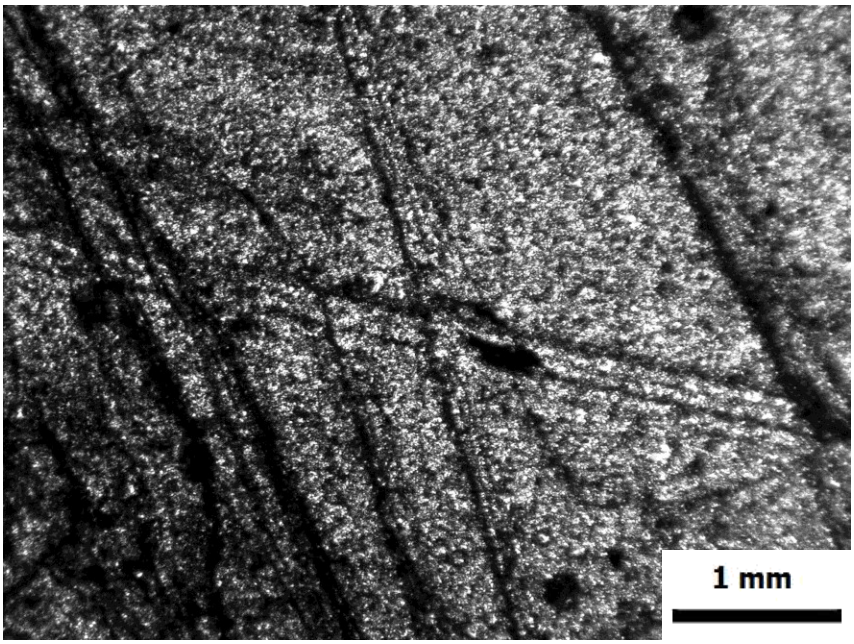

Fig. 8.11 - Microphotograph of sample PA-49 (N//), at 2.5x: centre of a big crystal of plagioclase.

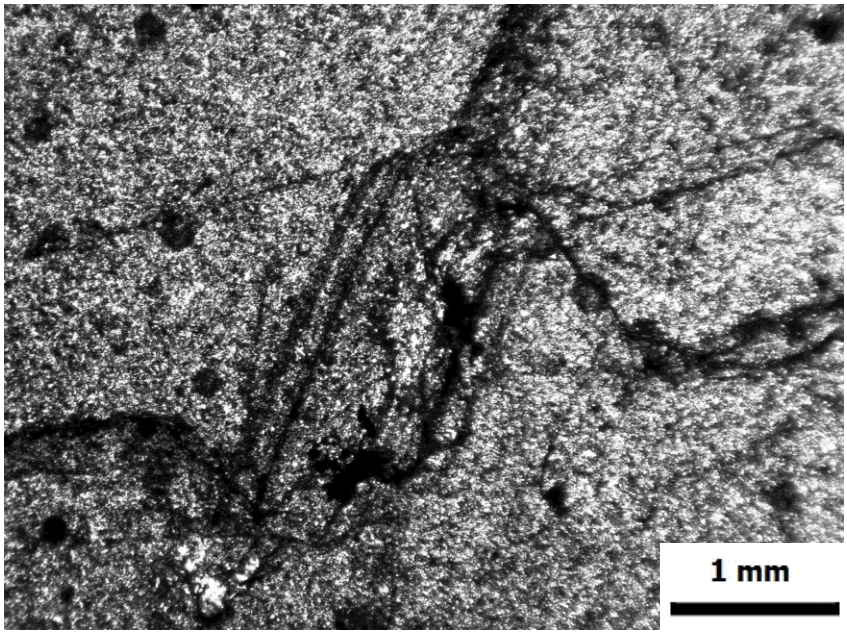

Fig. 8.12 - Microphotograph of sample PA-49 (N//), at 2.5x: crystal of sieve-plagioclase included in the biggest crystal of the same type of Fig. 8.11.

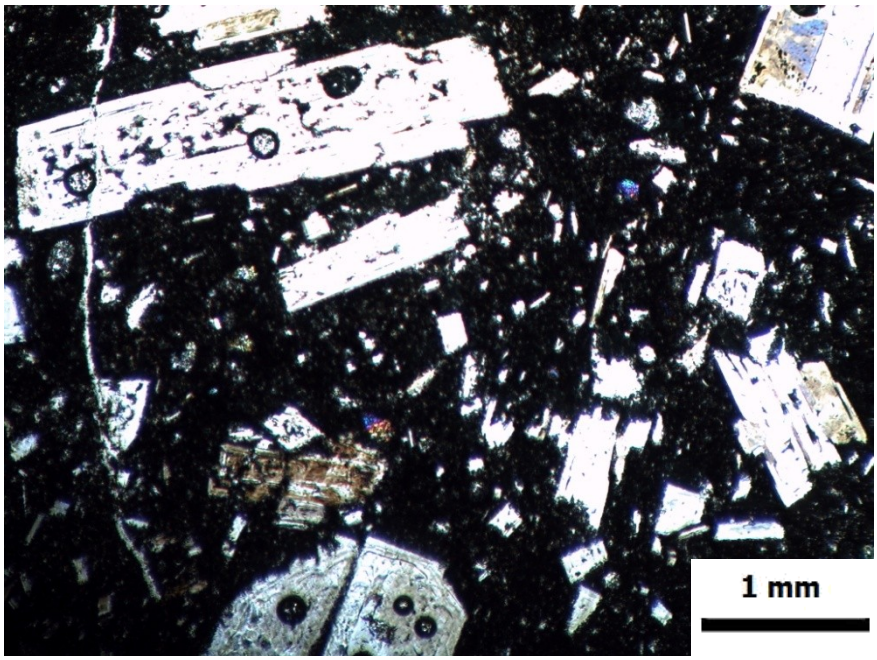


Fig. 8.13 - Microphotograph of sample PA-27 (NX), at 2.5x: panoramic of the thin section, it is possible to see a sieve-plagioclase phenocryst (on the upper left).

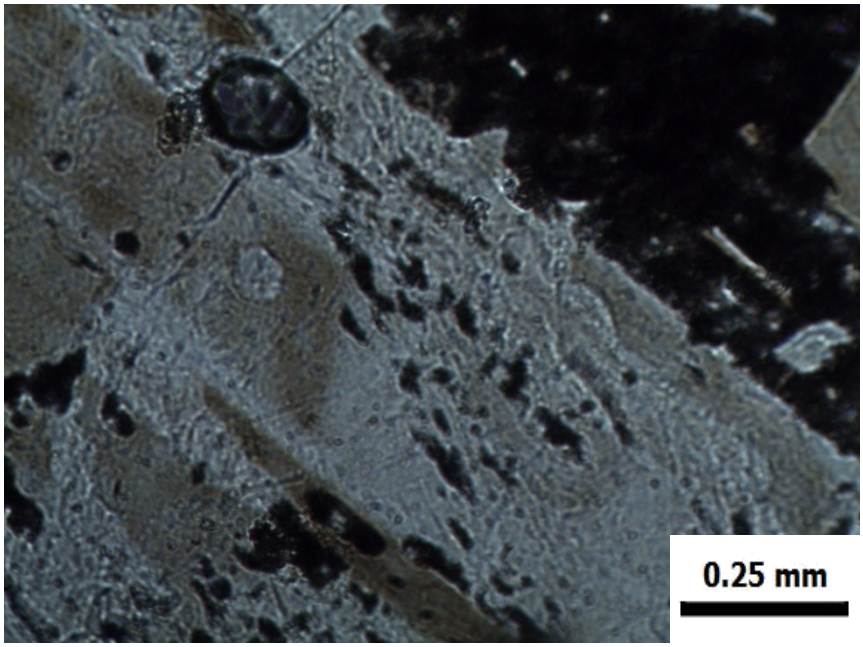


Fig. 8.14 - Microphotograph of sample PA-27 (NX), at 10x: particular of the disequilibrium signatures on the border of a spongy-cellular plagioclase. All these "holes" seems to be glassy inclusions.

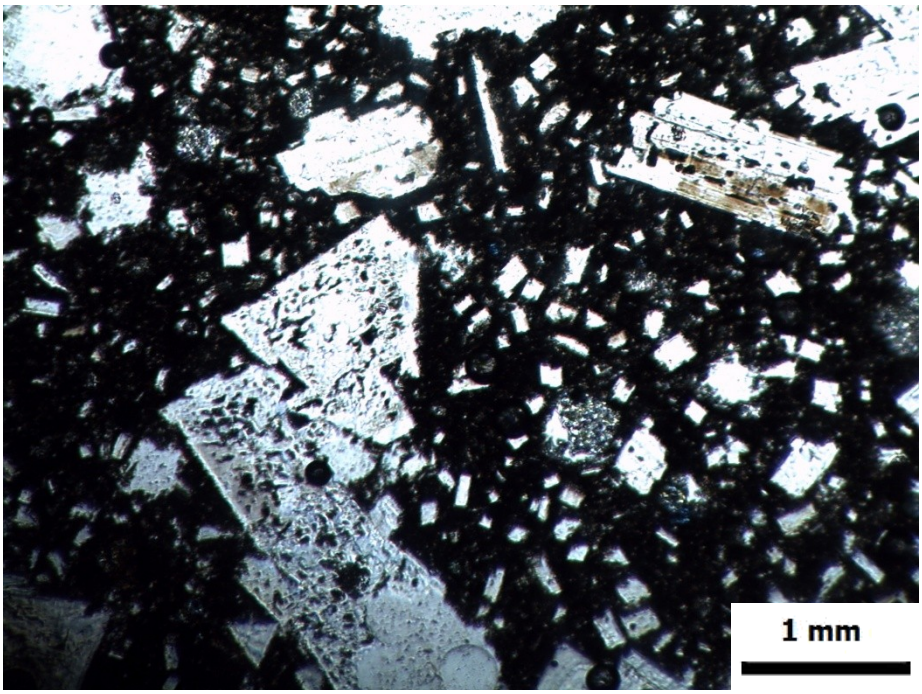


Fig. 8.15 - Microphotograph of sample PA-30 (N//), at 2.5x: panoramic of the thin section, it is possible to see both spongy-cellular and sieve plagioclase crystals.

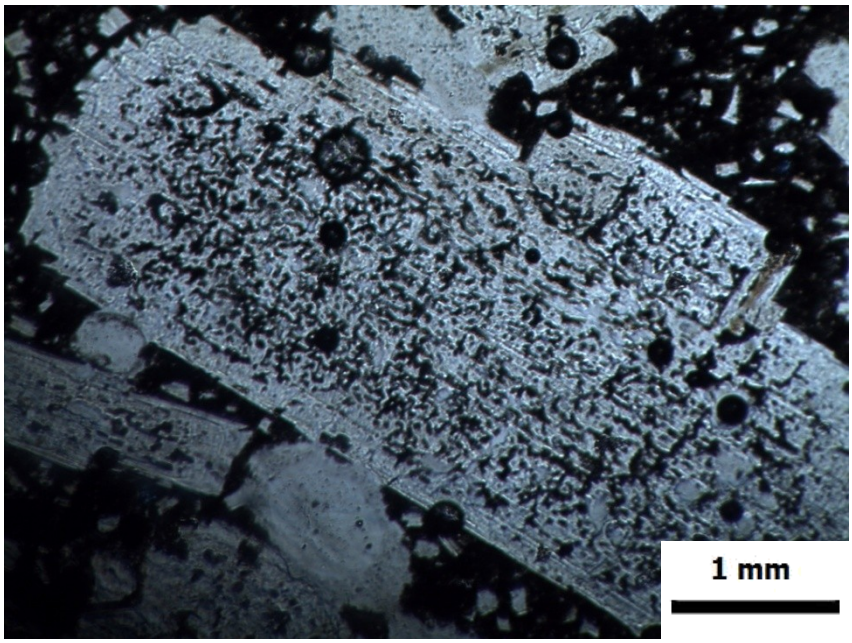


Fig. 8.16 - Microphotograph of sample PA-30 (NX), at 2.5x: large sieve-plagioclase crystal (7 mm) with a high quantity of disequilibrium textures.

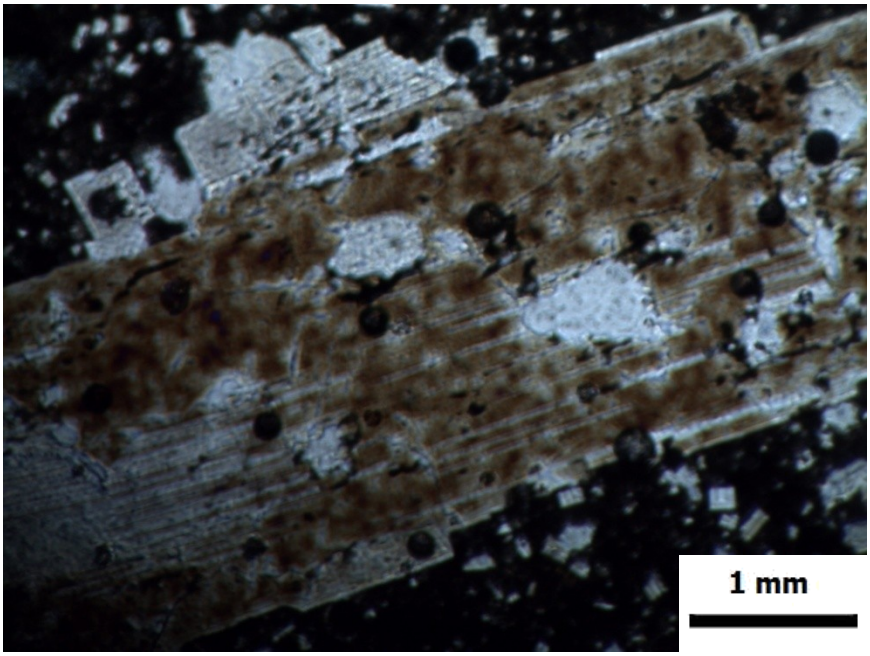


Fig. 8.17 - Microphotograph of sample PA-30 (NX), at 2.5x: other example of plagioclase crystal with disequilibrium textures characterized by many "holes".

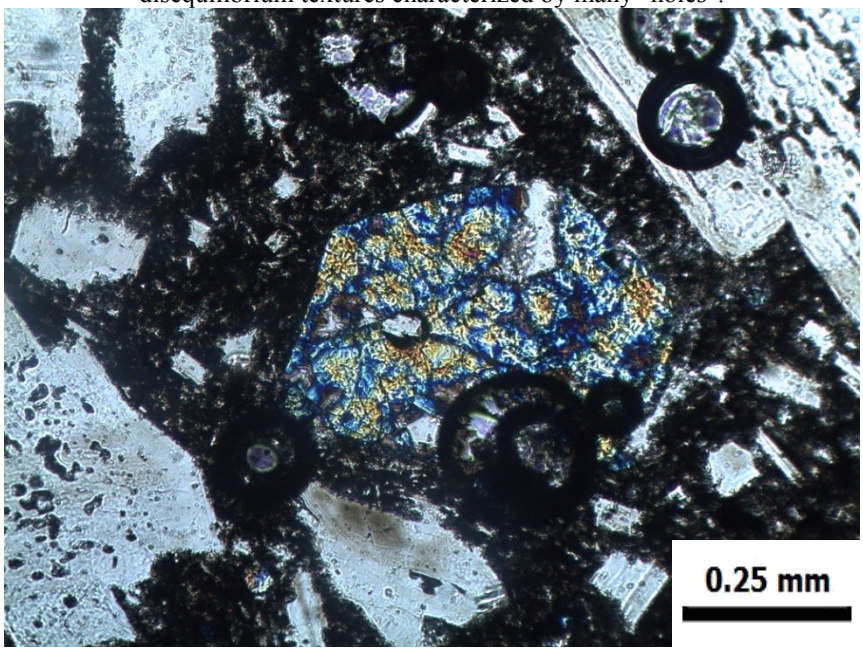


Fig. 8.18 - Microphotograph of sample PA-30 (NX), at 10x: euhedral crystal of olivine with fractures and a silica inclusion. Thermal cracking signatures are also observables.

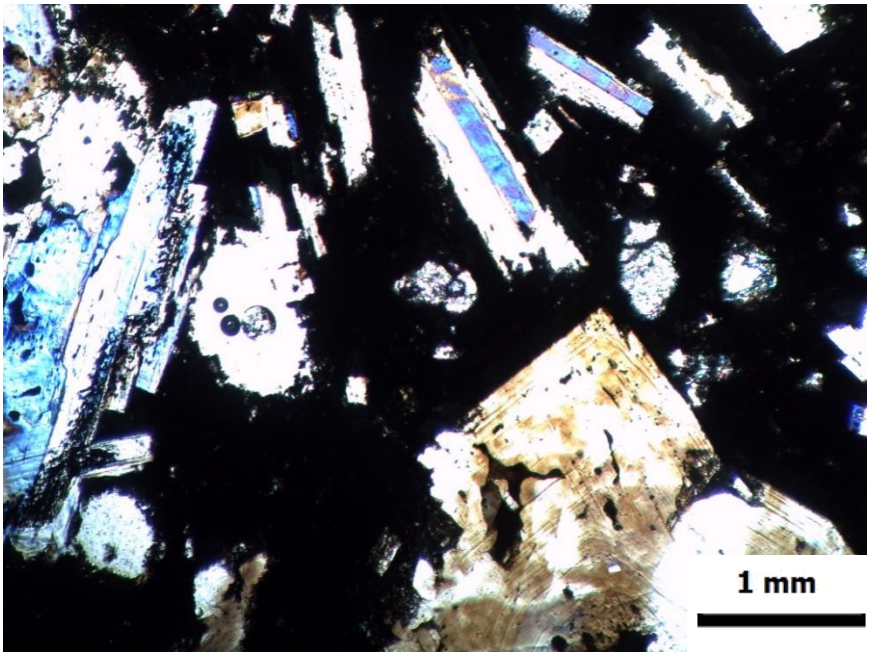


Fig. 8.19 - Microphotograph of sample PA-14 (NX), at 2.5x: panoramic of the thin section, it is possible to see a showy spongy-cellular plagioclase (on the left) and two plagioclase twinned pursuing the Albite-Carlsbad's law (on the upper right).

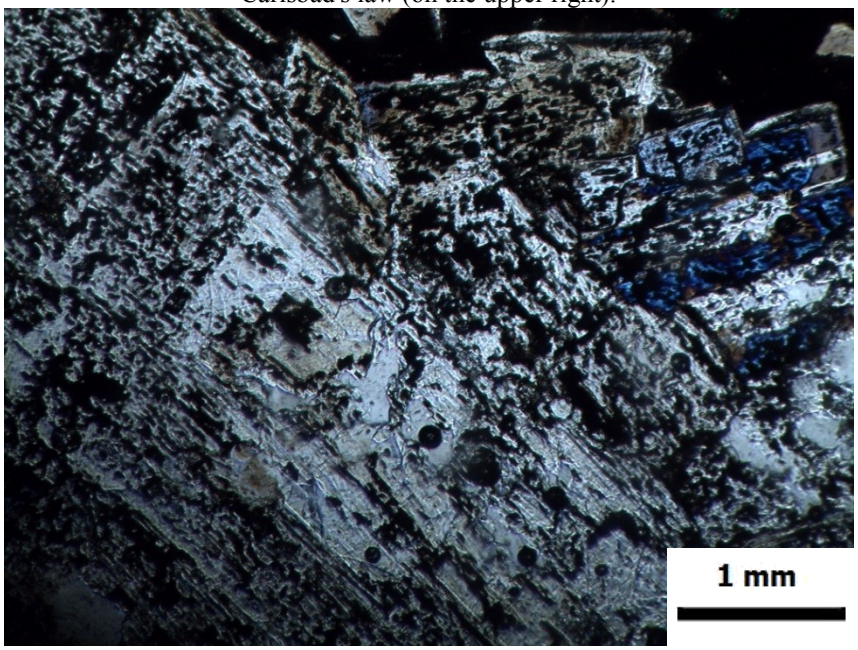


Fig. 8.20 - Microphotograph of sample PA-14 (NX), at 2.5x: heap of plagioclase phenocrysts with prevalent spongy-cellular textures.

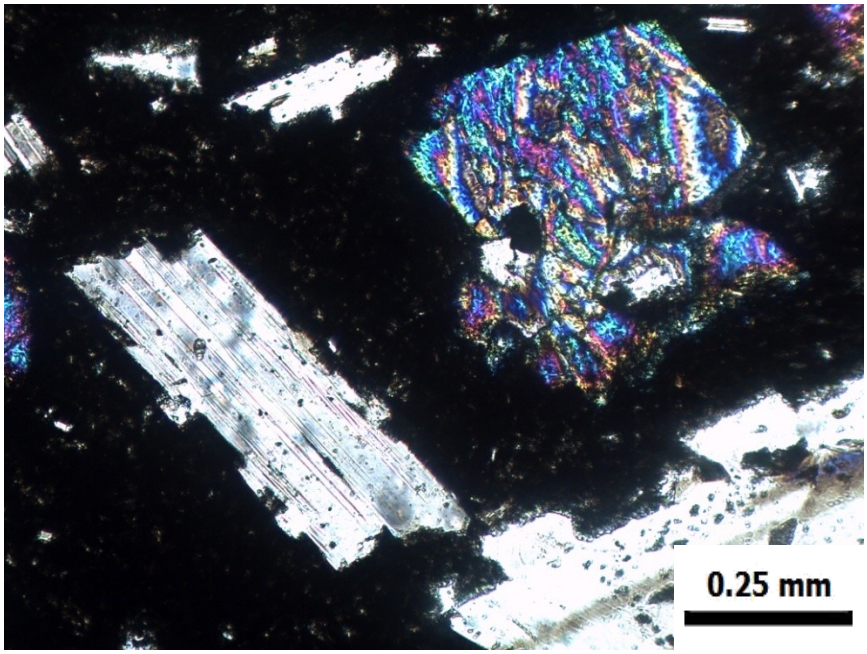


Fig. 8.21 - Microphotograph of sample PA-14 (NX), at 10x: great example of parallel striae in a plagioclase crystal (on the left), and a subhedral olivine crystal (on the upper right).

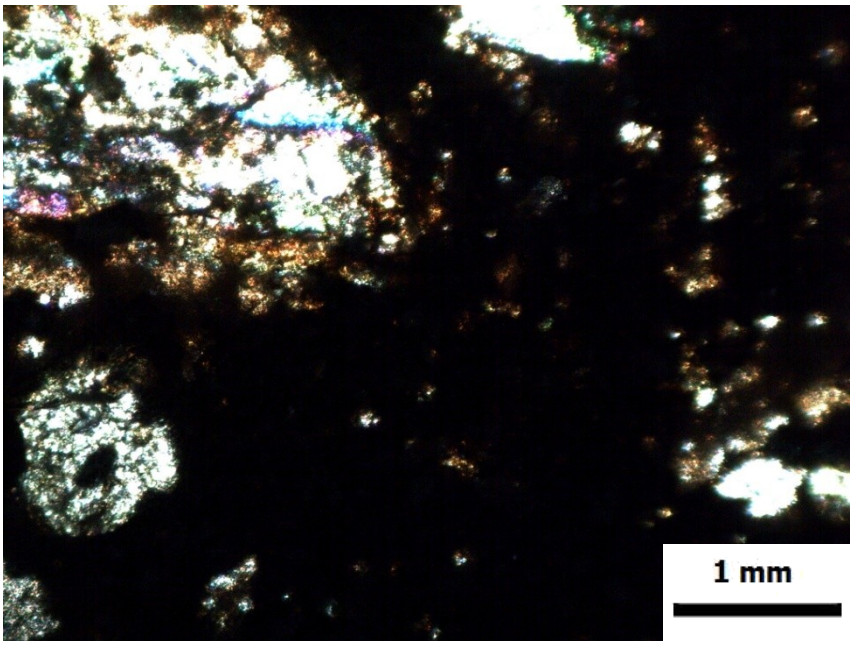


Fig. 8.22 - Microphotograph of sample VF-74-130a (NX), at 2.5x: panoramic of the thin section, it is possible to see the big resorption rims that characterize both plagioclase and olivine minerals.

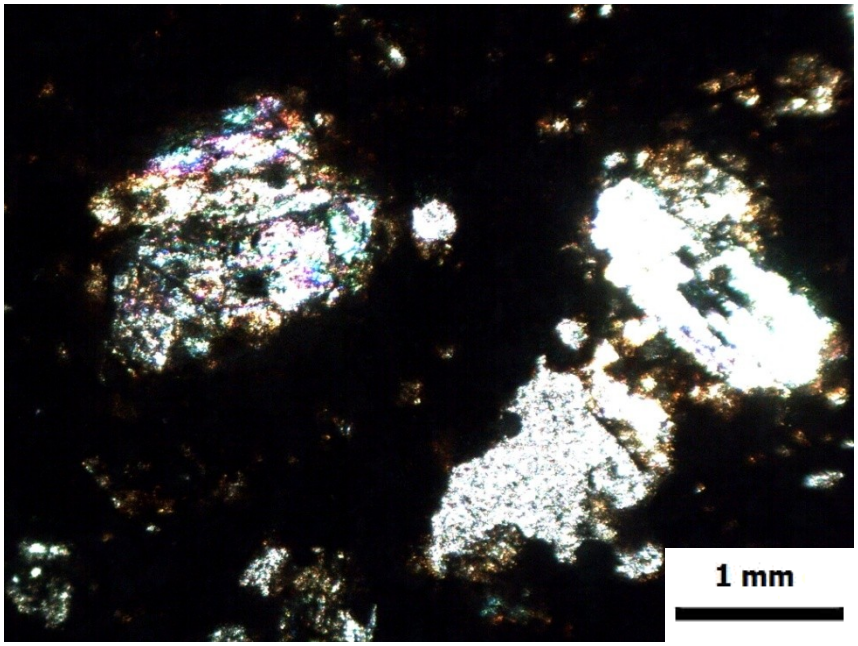


Fig. 8.23 - Microphotograph of sample VF-74-130a (NX), at 2.5x: particular of a sieve-olivine with fractures (on the left) and a skeletal-olivine (on the right). Both minerals have big resorption rims.

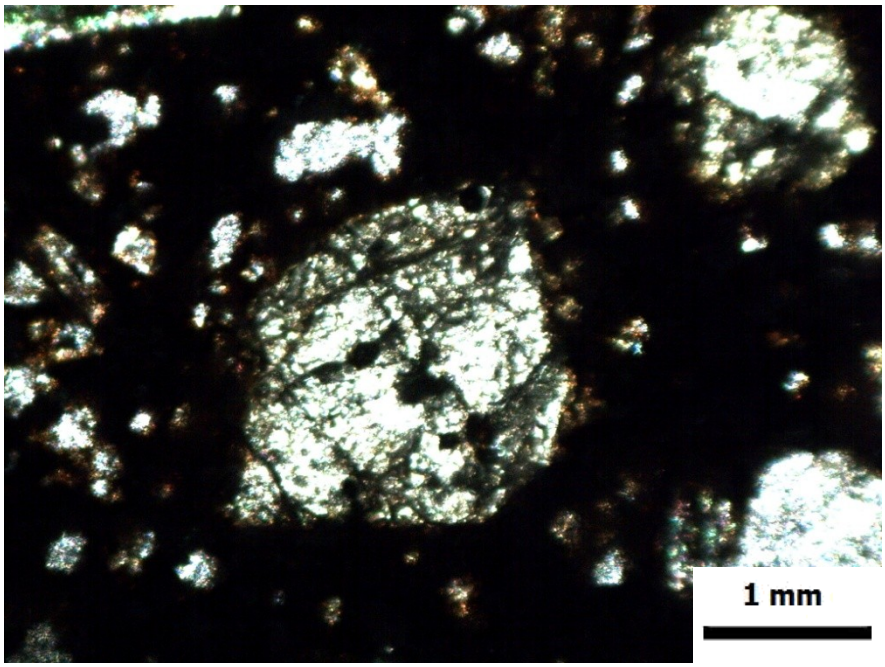


Fig. 8.24 - Microphotograph of sample VF-74-130a (NX), at 2.5x: deep fractures in an euhedral sieve-olivine crystal, a great resorption rim is present.

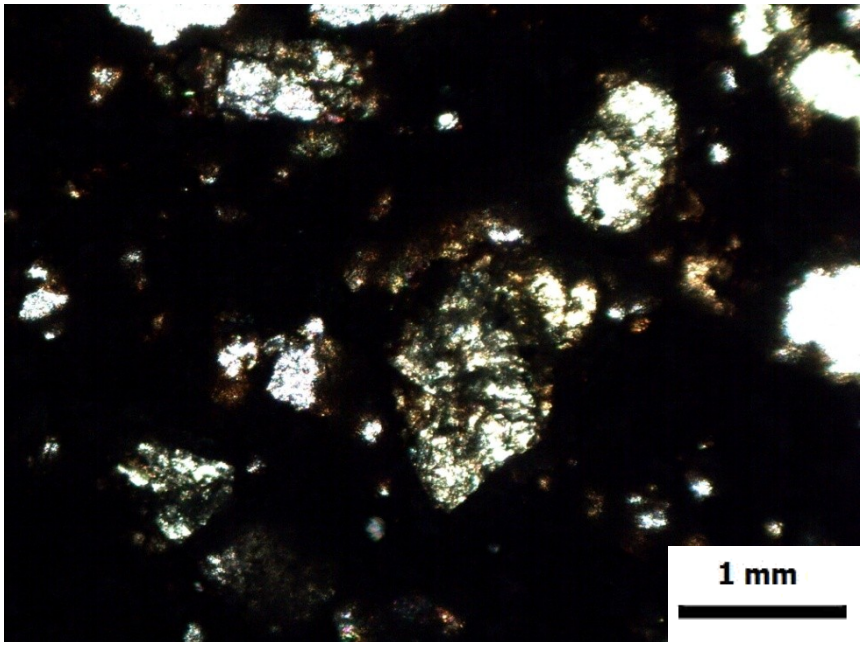

Fig. 8.25 - Microphotograph of sample VF-74-130b (NX), at 2.5x: particular of a spliced olivine.

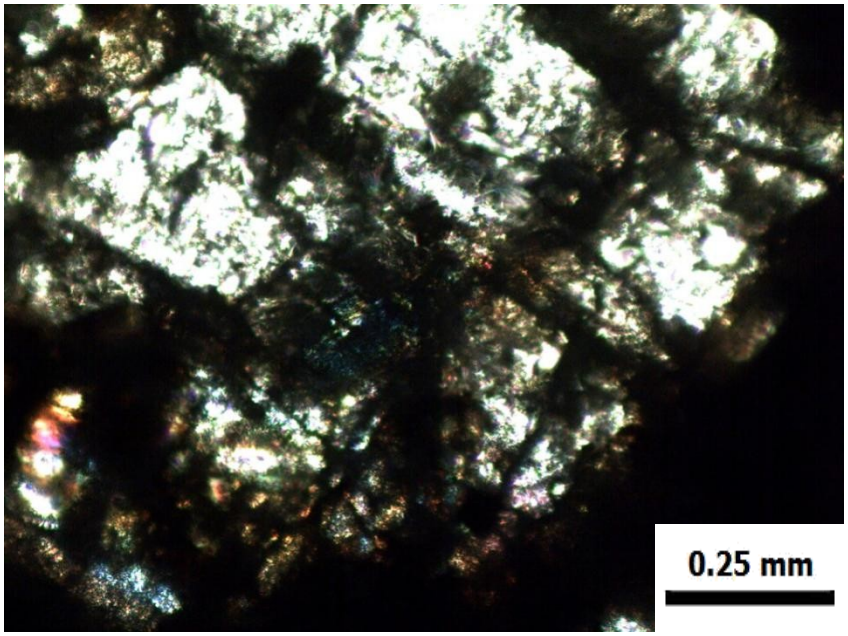

Fig. 8.26 - Microphotograph of sample VF-74-130b (NX), at 10x: very deep and large fractures in an olivine crystal.

# 8.2 – Appendix C _ More SEI images

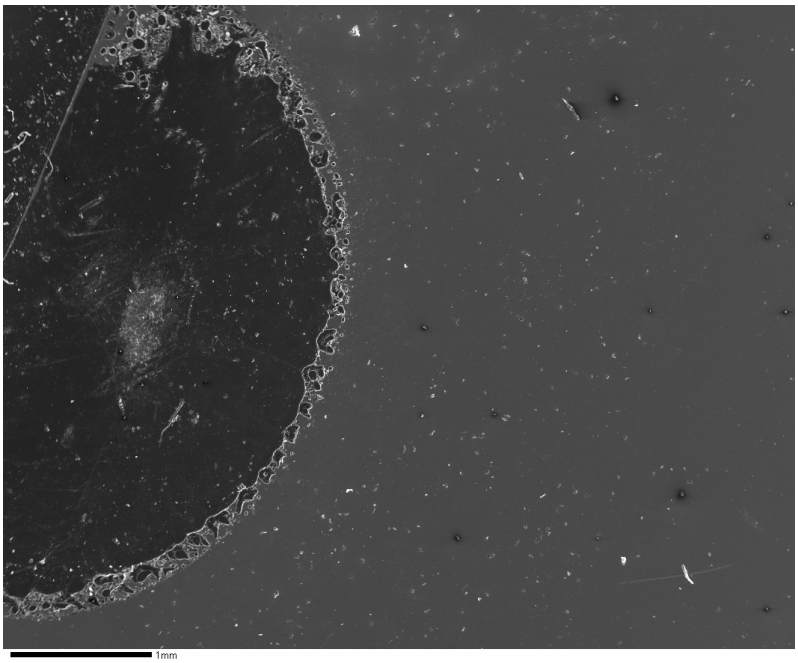


Fig. 8.27 - Panoramic of the sample PA-19: it is possible to notice how the depth mass is microcrystalline, with crystals of plagioclase, olivine, and magnetite (this last characterized by high brightness).

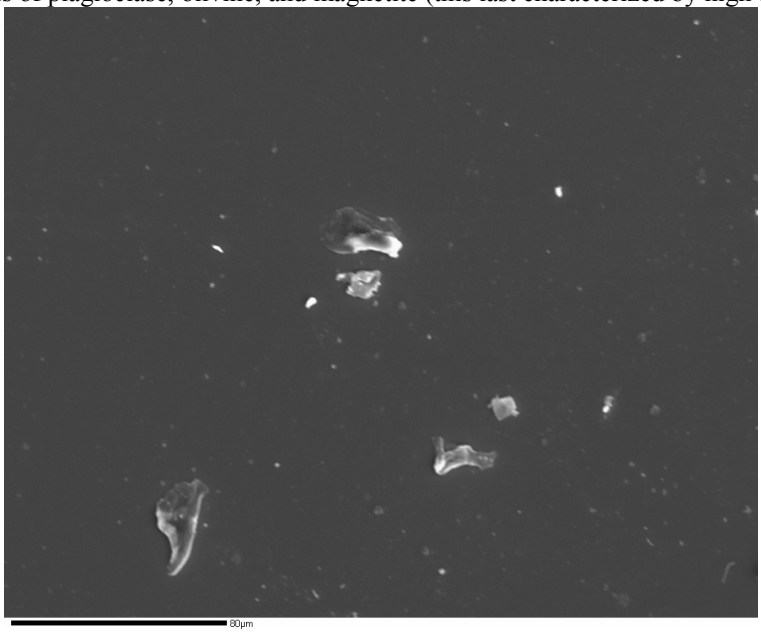


Fig. 8.28 – PA-19: Particular of a portion of the sample with high content in plagioclase microphenocrysts, with a general sharped shape.

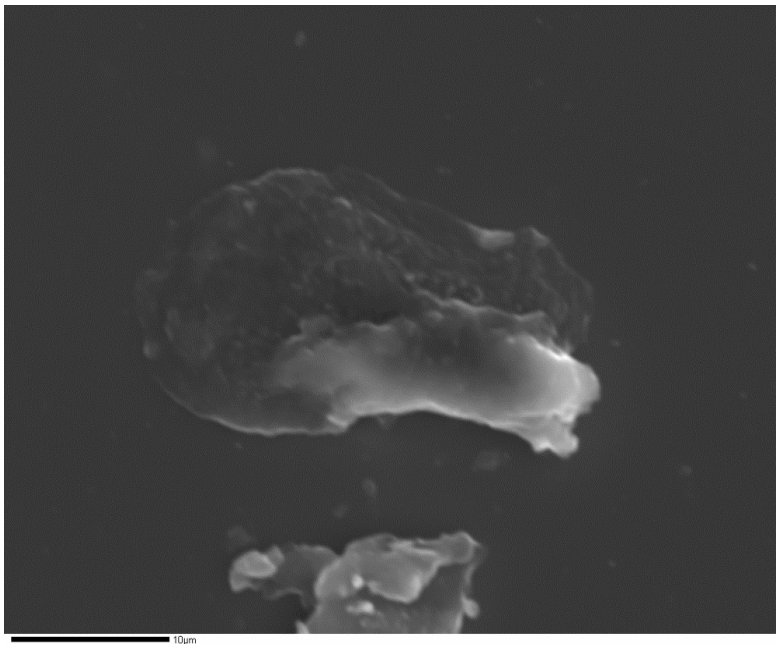

Fig. 8.29 – PA-19: Particular of a microphenocryst of plagioclase.

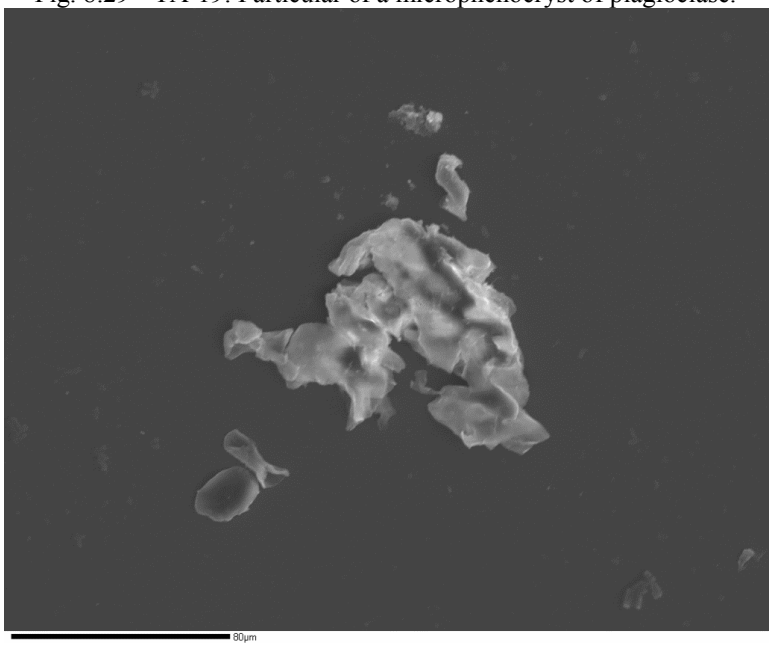

Fig. 8.30 – PA-19: Image that shows a type of plagioclase crystals co-grown.

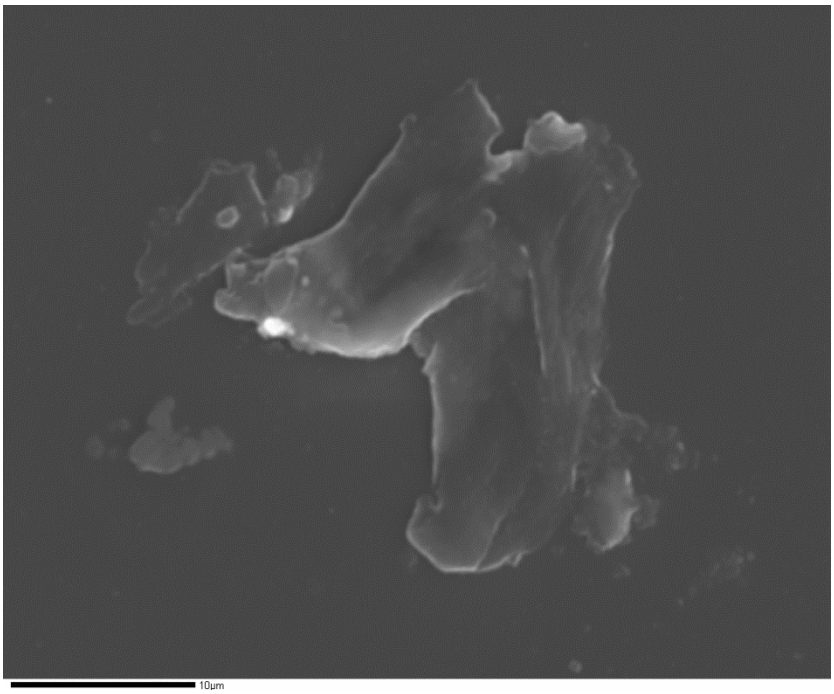


Fig. 8.31 – PA-19: Image that show a co-growth within two plagioclase phenocrysts with sharped border. One of this crystal seems to be euhedral.

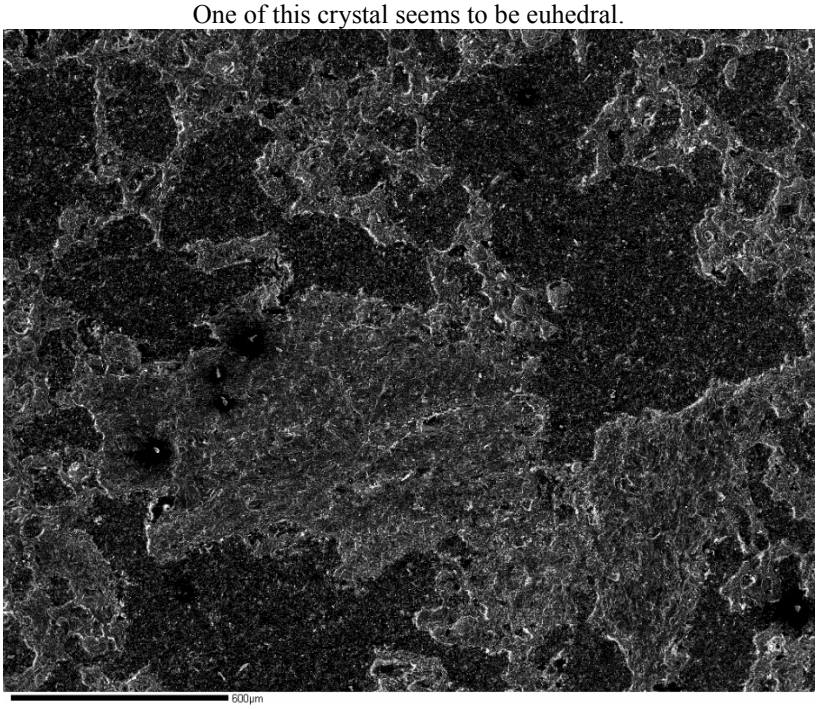


Fig. 8.32 – Panoramic of the sample PA-44 where it is possible to see two different liquids: one more white and one more black in color. The white part is more crystalline.

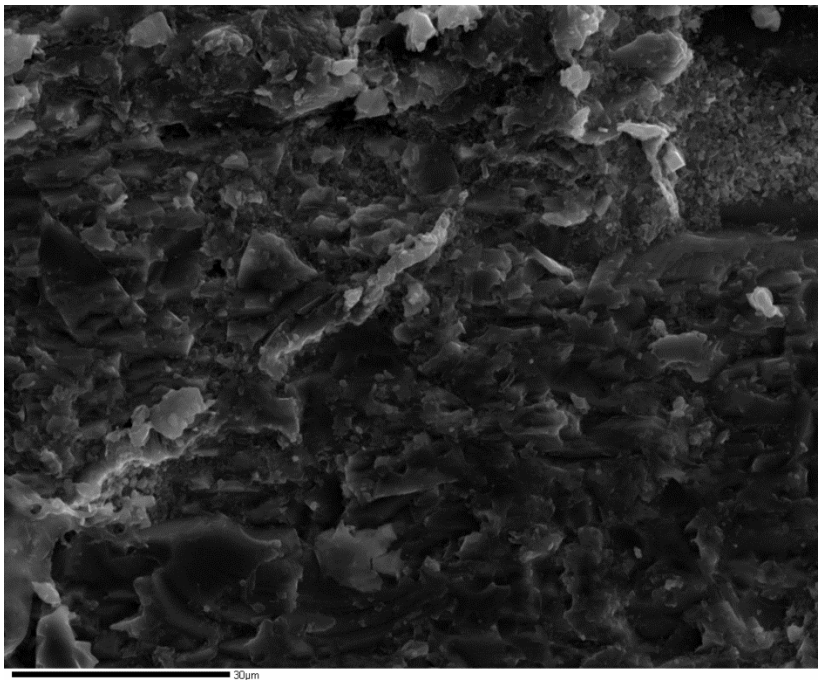


Fig. 8.33 – PA-44: Magnified SEI image of the central white part in Fig. 8.32. Can be noticed how this part is characterized by a high content in crystals of plagioclase, and some olivine and magnetite.

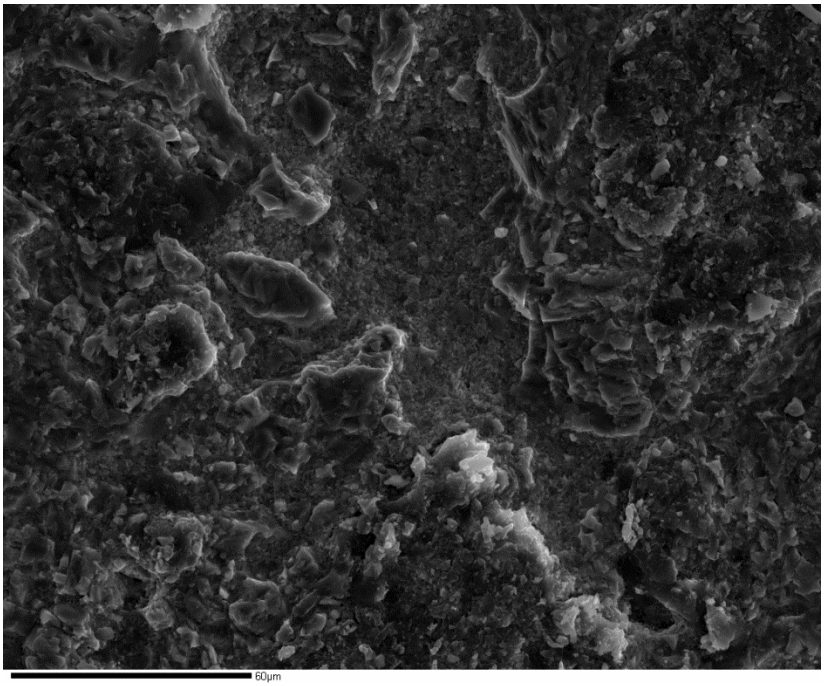


Fig. 8.34 – PA-44: SEI image of the more white part of the sample. It is possible to see many crystals of plagioclase and a depression located at the center.

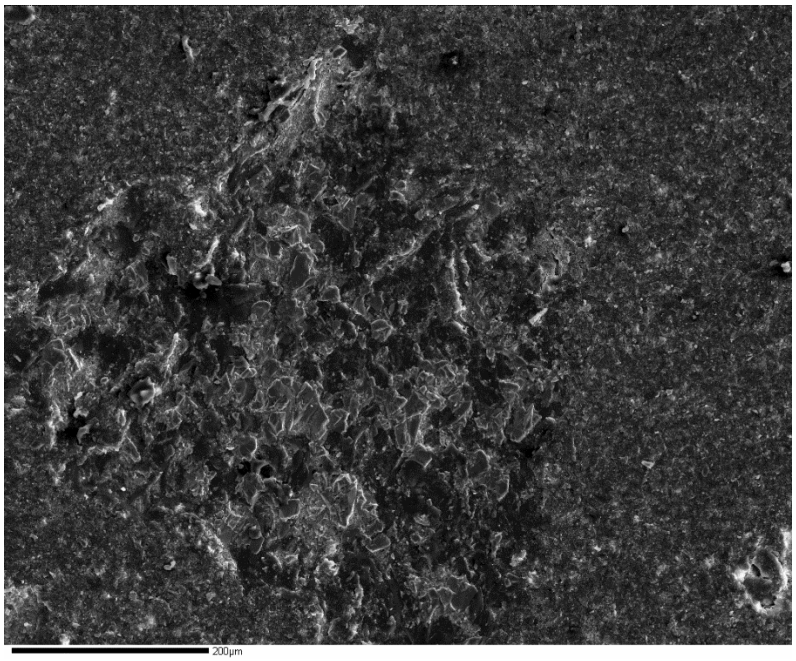


Fig. 8.35 – PA-44: Magnified SEI image on a white part where are present a lot of plagioclase microcrysts with sharped and tabular shapes.

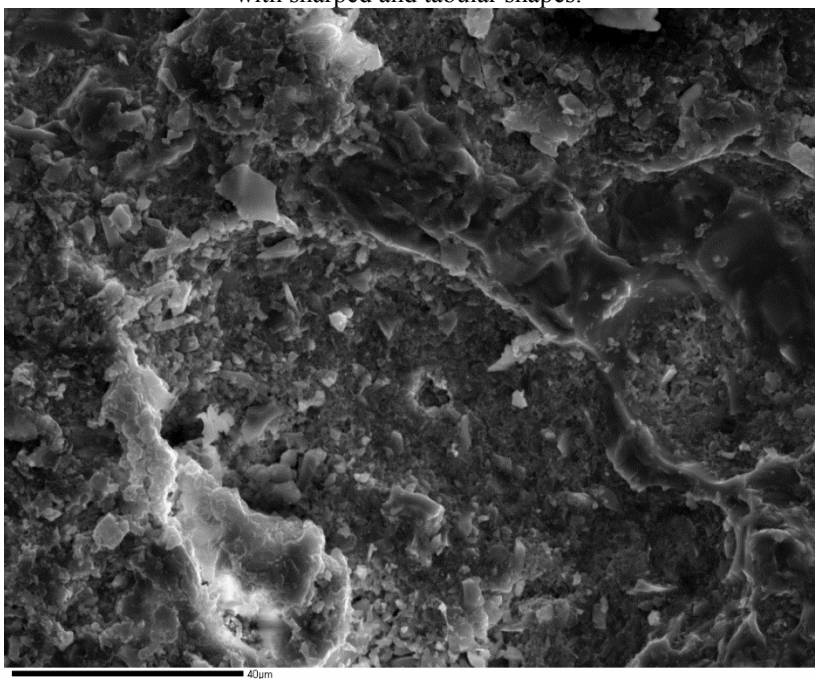


Fig. 8.36 – PA-44: Particular of a phenocrysts of plagioclase, characterized by modified edge, surrounded by the same crystal phase.

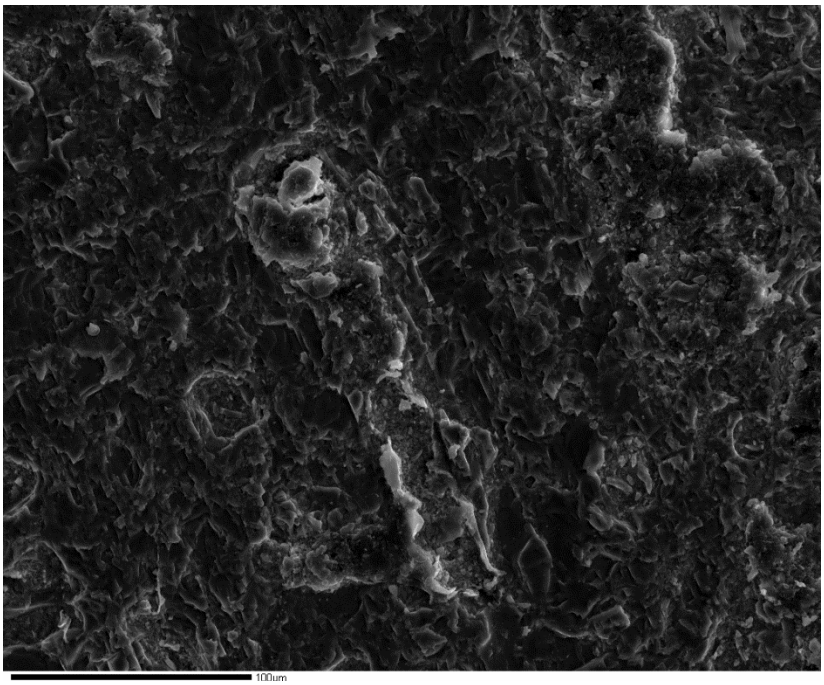

Fig. 8.37 – PA-44: Particular of an euhedral microphenocryst of plagioclase.

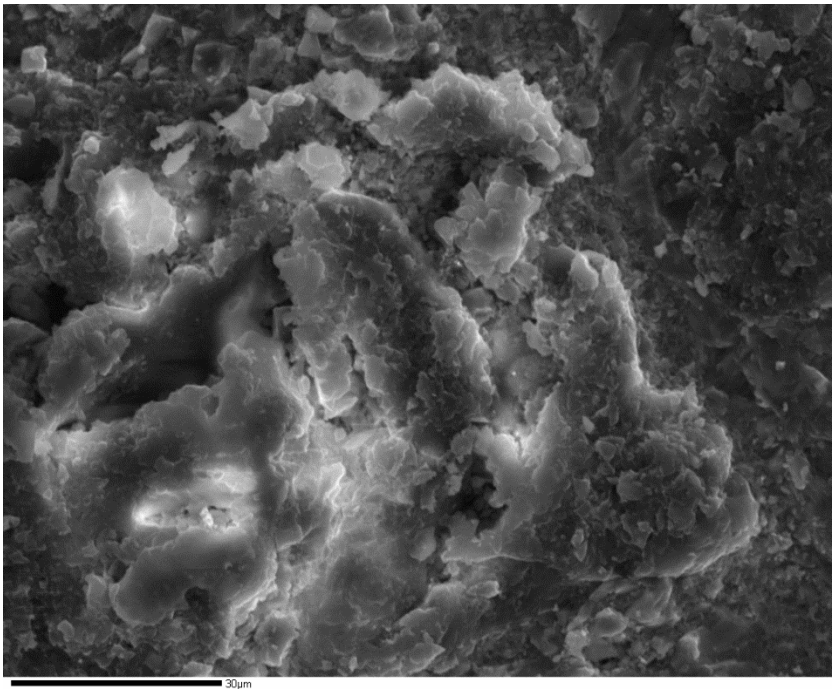

Fig. 8.38 – PA-44: Aggregate of plagioclase crystals.

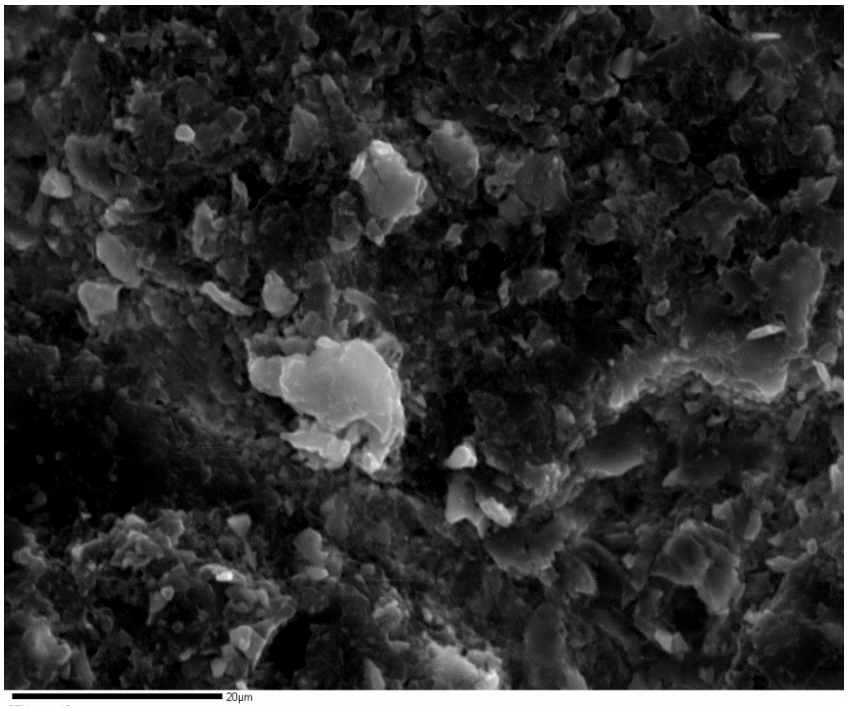


Fig. 8.39 – PA-44: Particular of a bright sharped mineral of plagioclase.

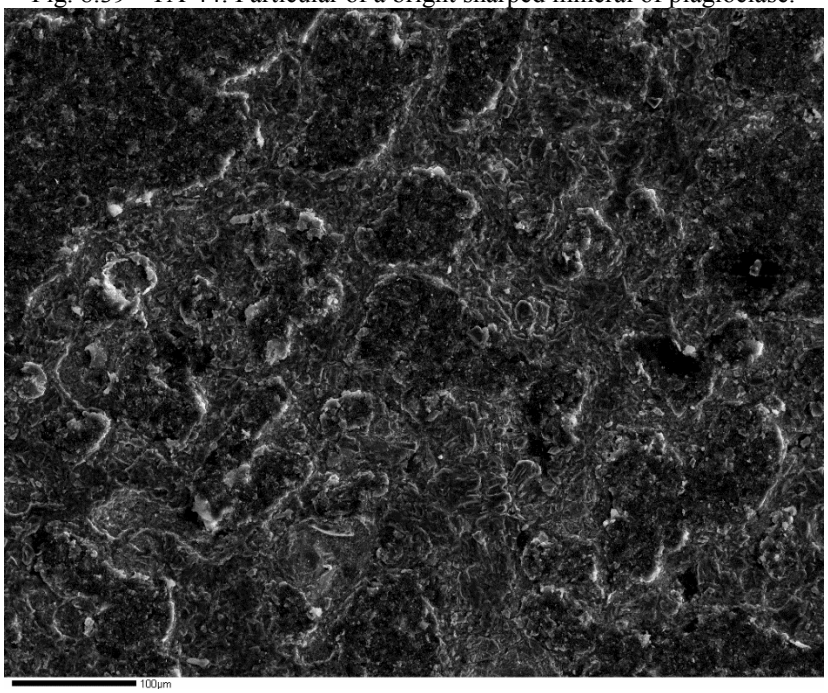


Fig. 8.40 – PA-44: SEI image of another area that contain the two type of liquid (white and black) mingled.

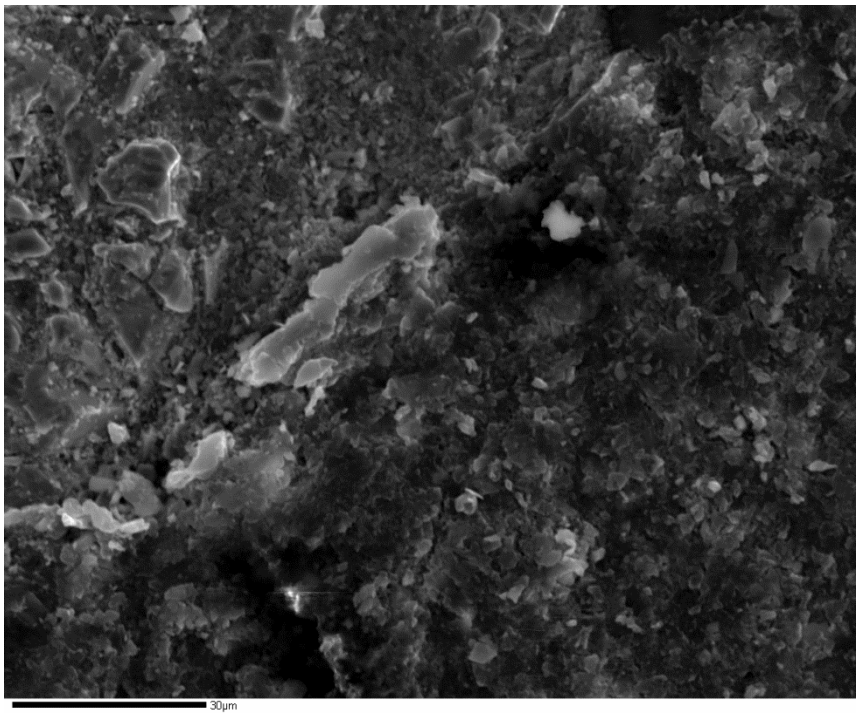

Fig. 8.41 – PA-44: SEI image that show the boundary between the two types of liquids.

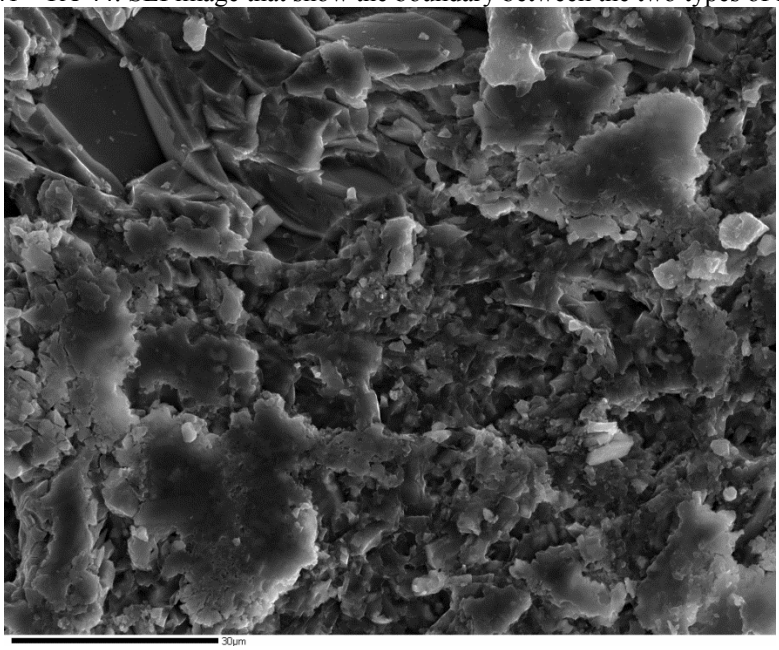

Fig. 8.42 – Panoramic SEI image of sample PA-49. It is possible to see crystals of plagioclase and, in minor content, olivine and magnetite. Crystals are characterized by sharped and reabsorbed edges.

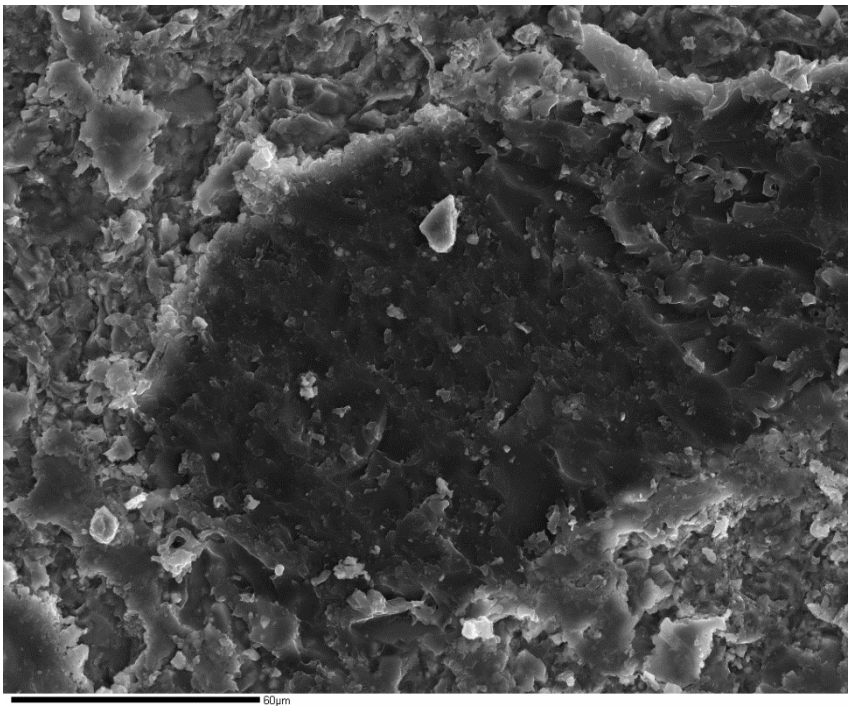

Fig. 8.43 – PA-49: SEI image of a topographical depression filled by glass and some microcrystal.

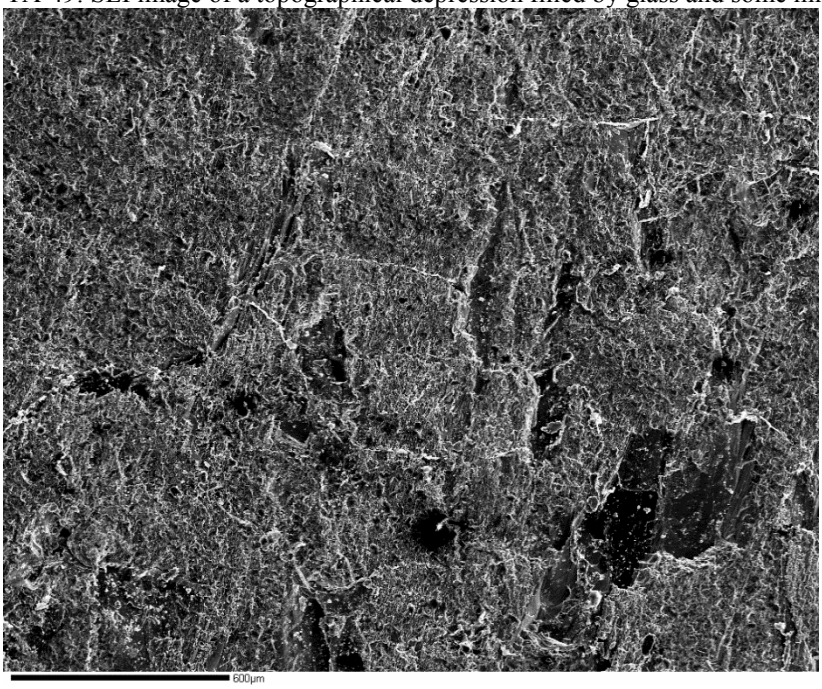

Fig. 8.44 – PA-49: Particular of the center of a big plagioclase crystal characterized by sieve-texture. The parallel striae are well visible.

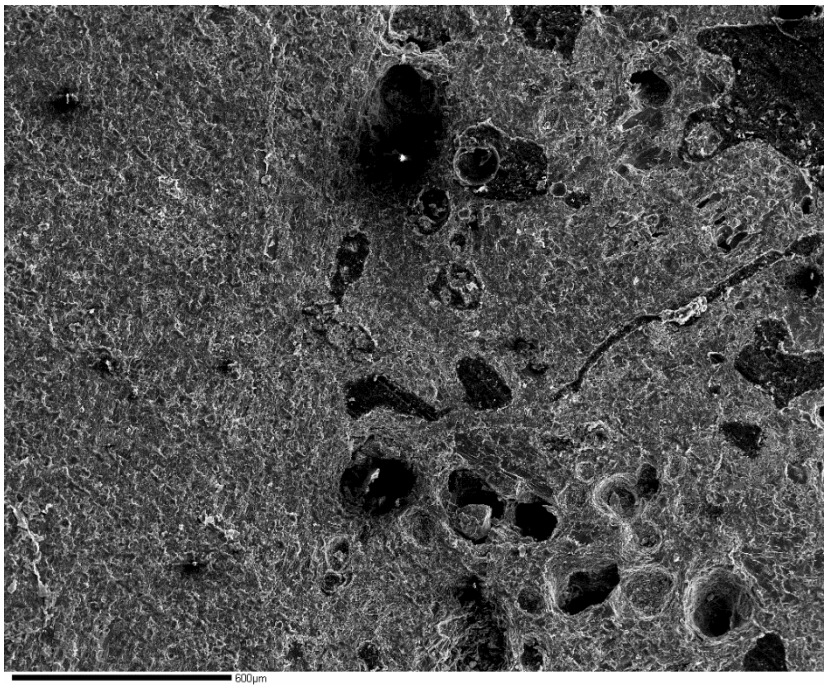


Fig. 8.45 – PA-49: Particular of the boundary between a big crystal of plagioclase (on the left) and the rest of the sample (on the right).

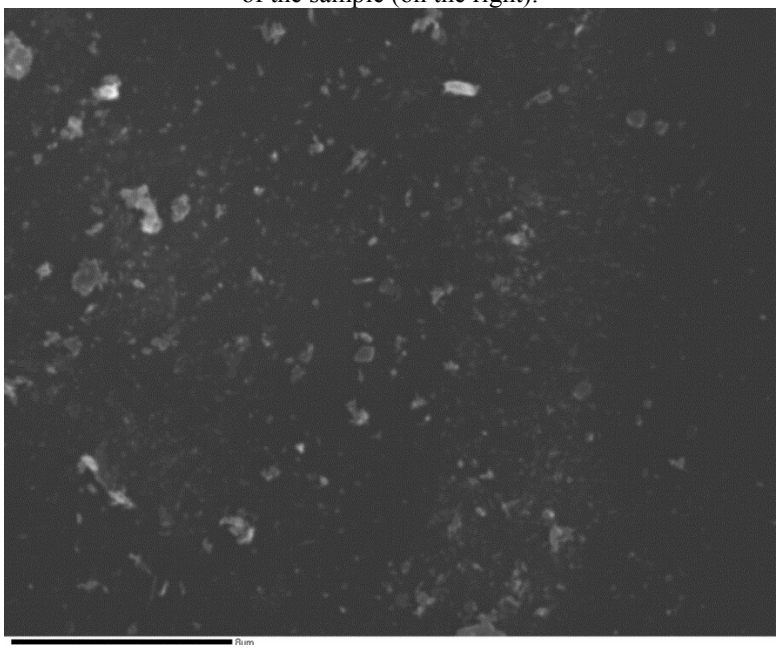

Fig. 8.46 – Panoramic SEI image of sample PA-27. It is possible to see a general abundance of plagioclase with minor content of olivine and a few crystals of magnetite. The groundmass differ from high-concentrated crystal mushes in some parts to cryptocrystalline in other areas.

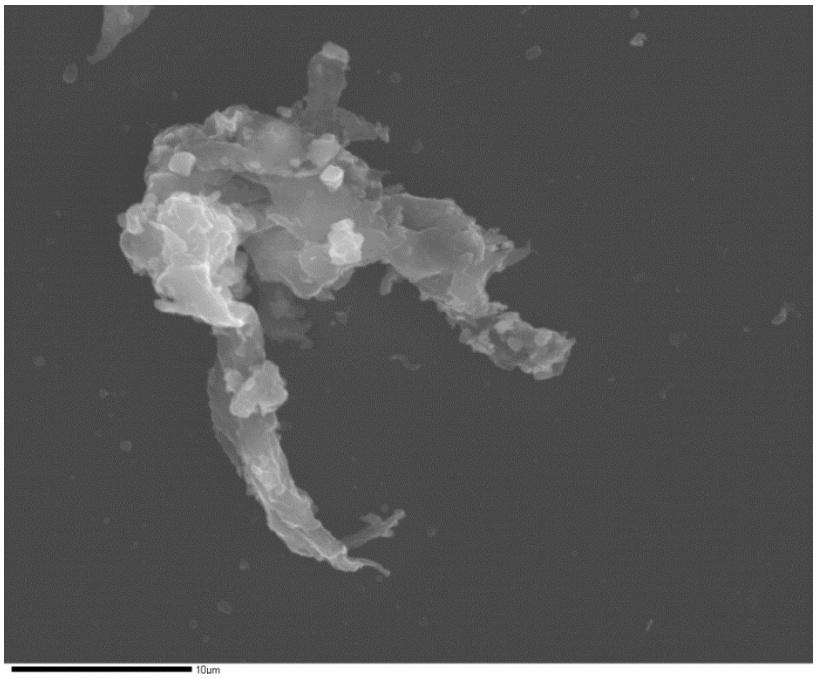

Fig. 8.47 – PA-27: Particular of a phenocryst of plagioclase with a singular shape and two “filaments” with the same composition.

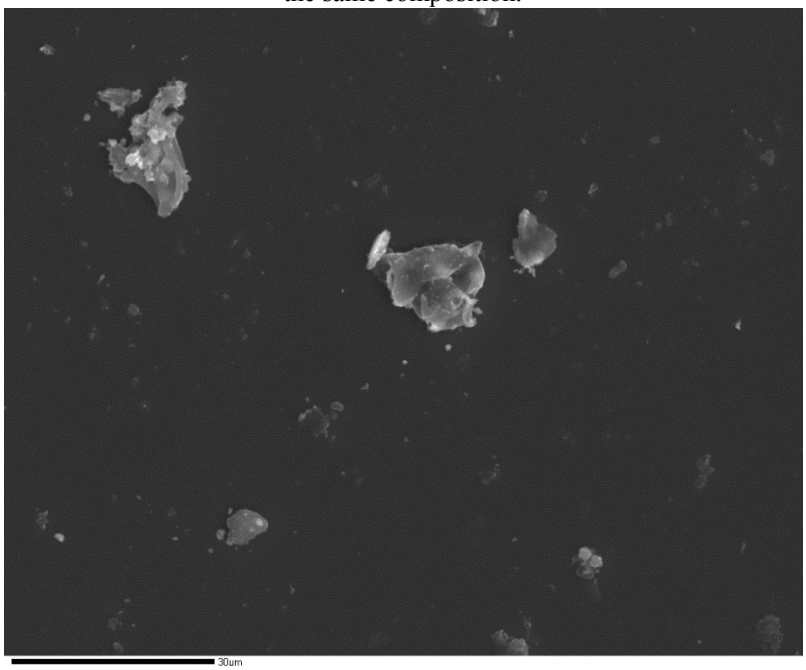

Fig. 8.48 – PA-27: SEI image where it is possible to notice the differences in the pattern of the groundmass and some microphenocrysts of plagioclase with a sharped shape.

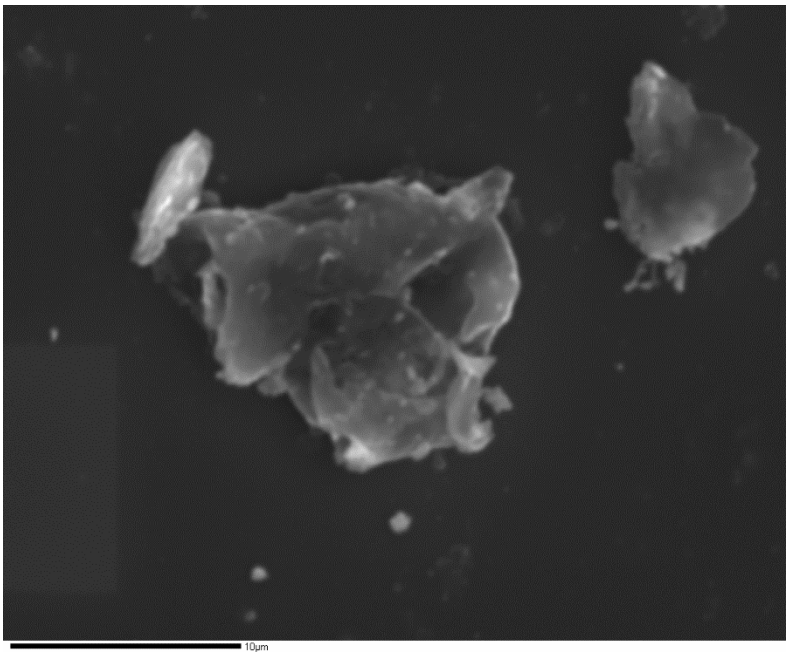


Fig. 8.49 – PA-27: Magnified SEI image of a plagioclase phenocryst in Fig. 8.52. It is possible to see another type of crystal located on the upper part of the main crystal. By basing on the brightness it could be magnetite.

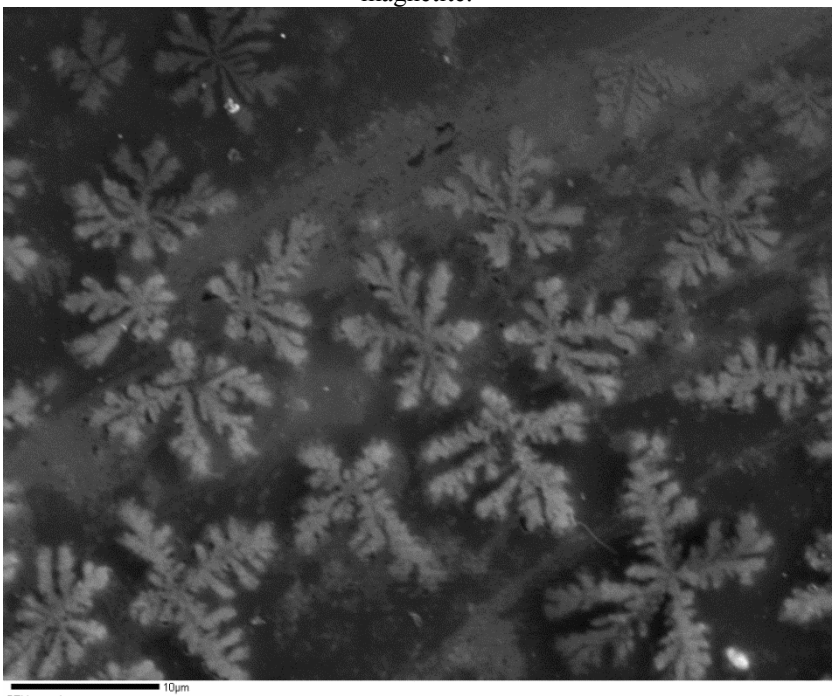


Fig. 8.50 – PA-27: Particular of meaningful disequilibrium textures of snowflake clusters of plagioclase, found on a series of sieve-plagioclase phenocrysts.

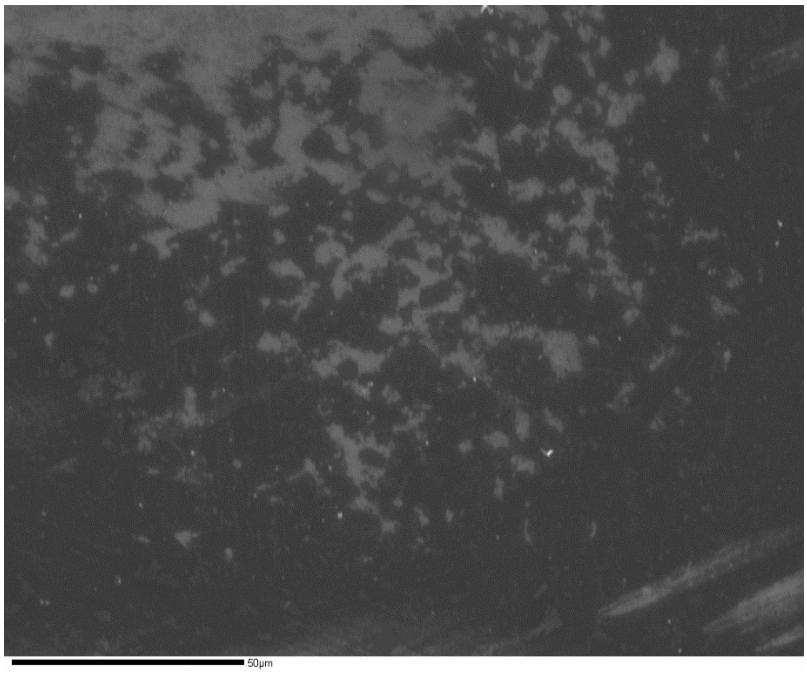


Fig. 8.51 – PA-27: SEI image of an area characterized by the semi-absence of microcrysts in the groundmass.

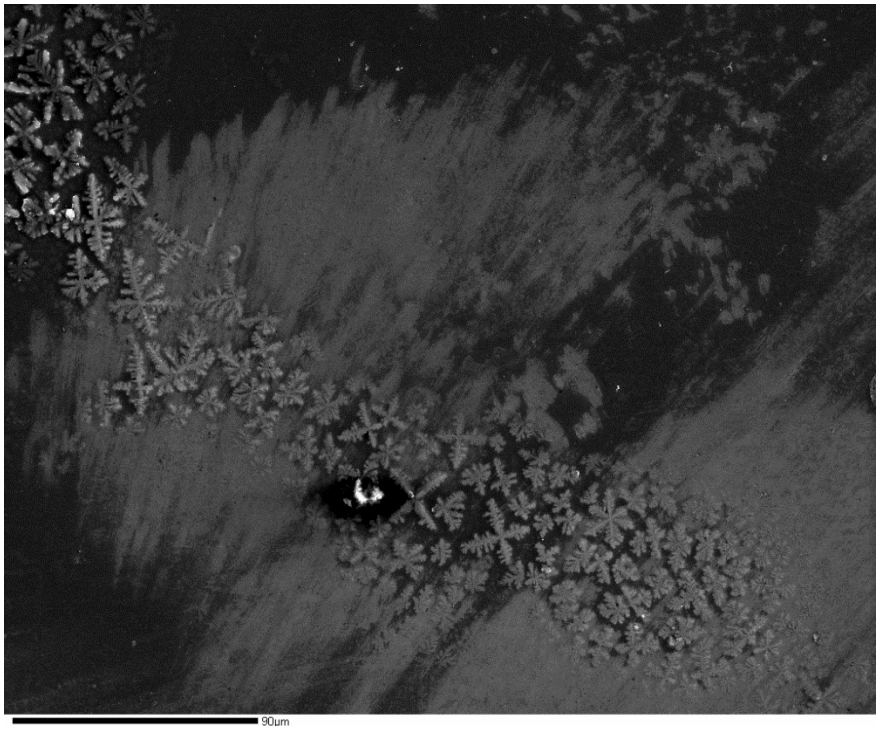


Fig. 8.52 – PA-27: SEI image where it is possible to notice a clear trail of snowflake textures of plagioclase that pass through the main crystal.

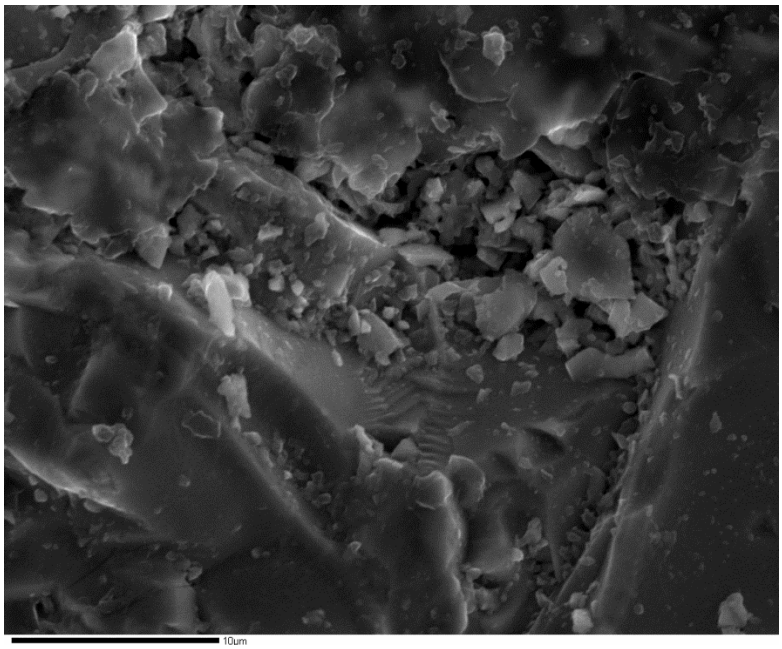

Fig. 8.53 – Panoramic of sample VF-74-130a. Plagioclase, olivine and magnetite crystals are well visible. In general, the size of the minerals varies from large to small microcrysts.

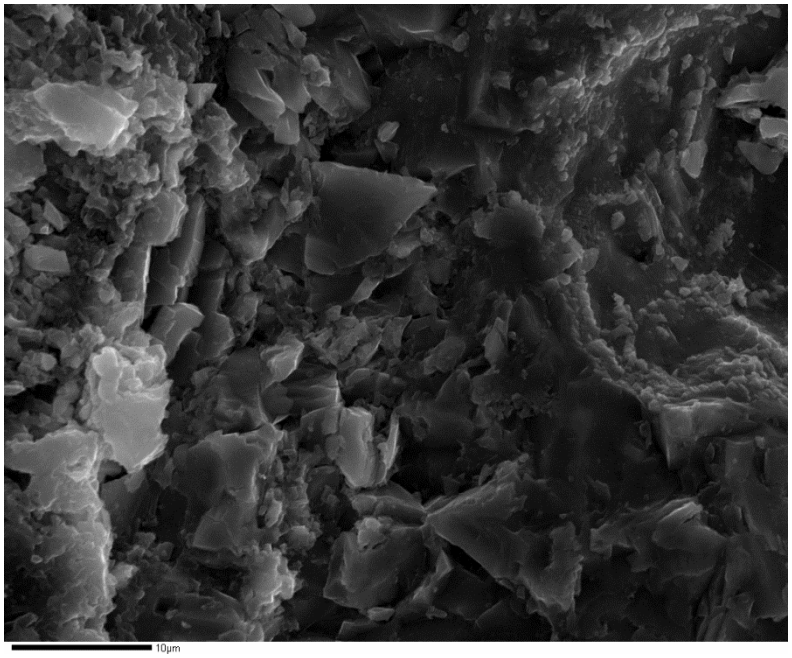

Fig. 8.54 – VF-74-130a: Particular of sharped edge and foil shapes in plagioclase.

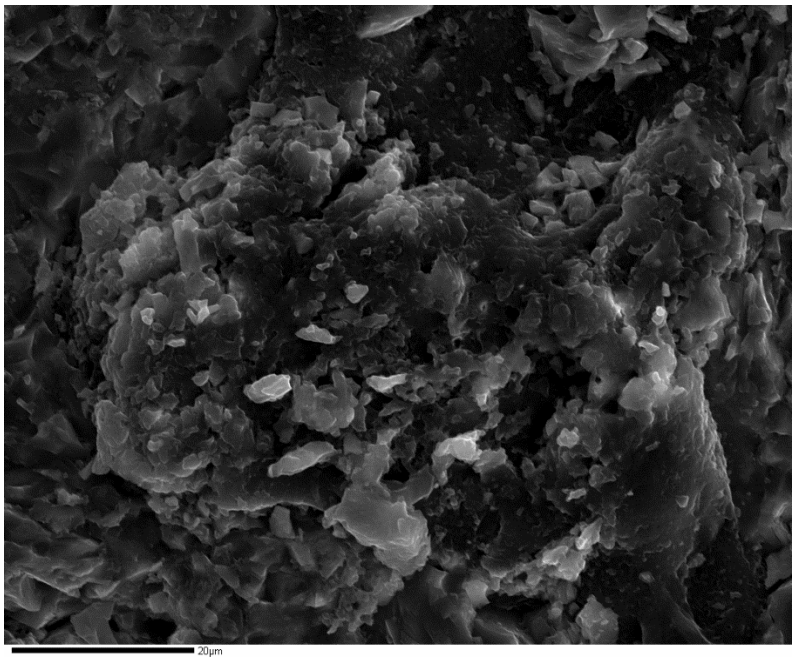


Fig. 8.55 – VF-74-130a: Particular of a subhedral phenocryst of olivine surrounded by microcrysts of magnetite.

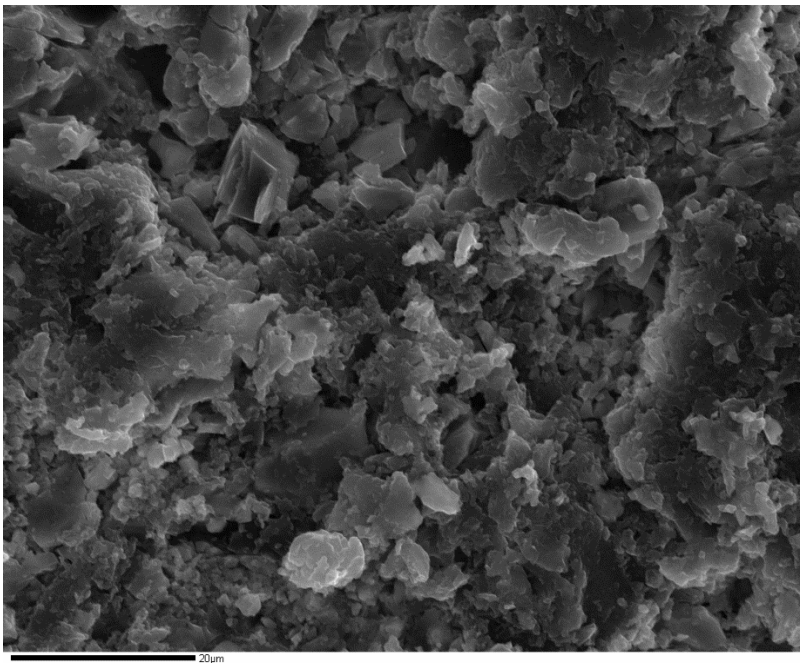


Fig. 8.56 – VF-74-130a: SEI image where it is possible to notice the same mineral phases (plagioclase, olivine, and magnetite) of the previous parts of the sample.

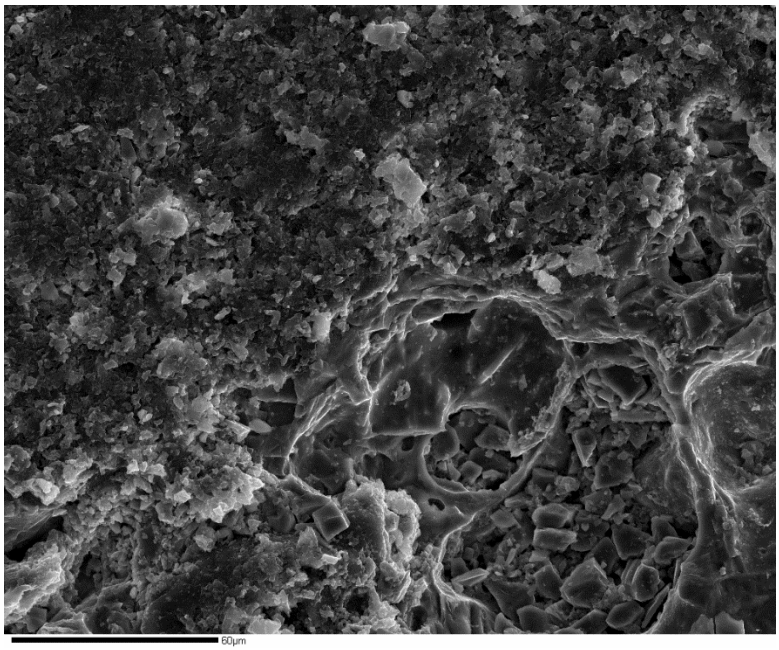


Fig. 8.57 – VF-74-130a: Meaningful SEI image that show two different types of liquids that coexists in the same sample. One more black (on the upper part) and one more white (on the lower part).

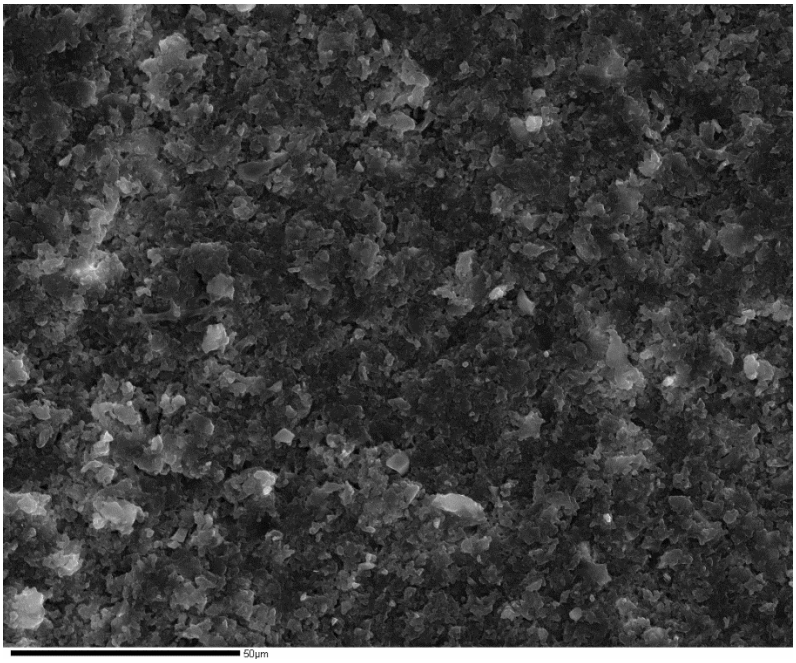


Fig. 8.58 – VF-74-130a: Particular of the black part where it is possible to notice the semi-absence of phenocrysts. The degree of crystallinity is high (holocrystalline).

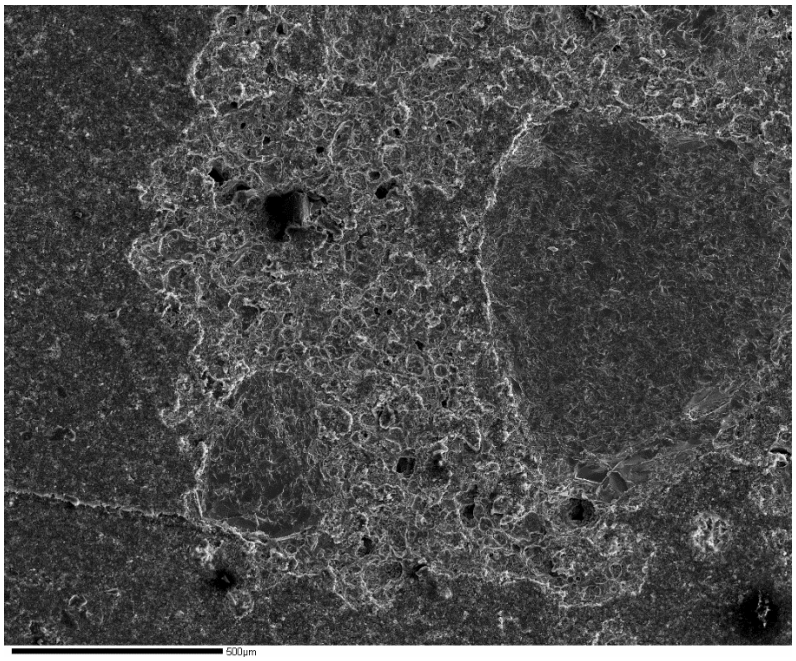

Fig. 8.59 – VF-74-130a: SEI image that shows clearly as the two liquid are mingled. In this case mingling is represented by a convolution within the white and black part.

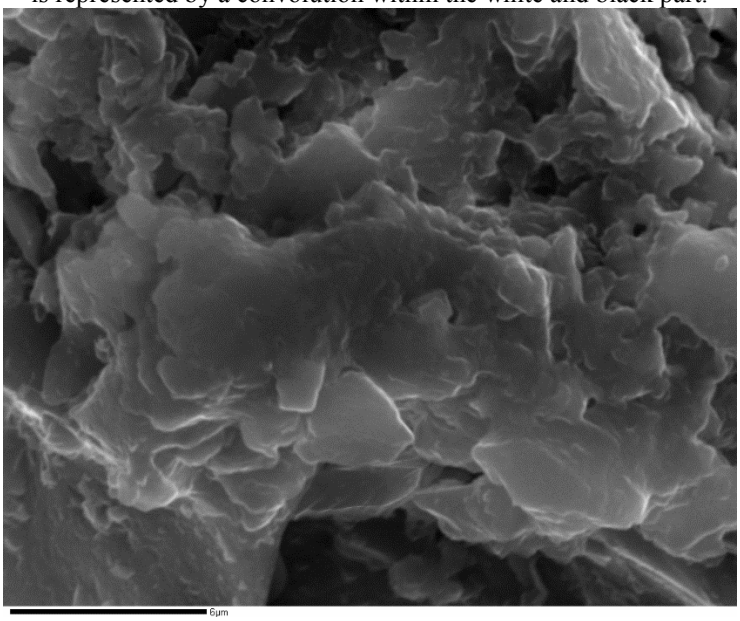

Fig. 8.60 – VF-74-130a: Magnification of the previous Fig. 8.59, on the white part. Phenocryst of plagioclase with a subhedral/anhedral morphology.

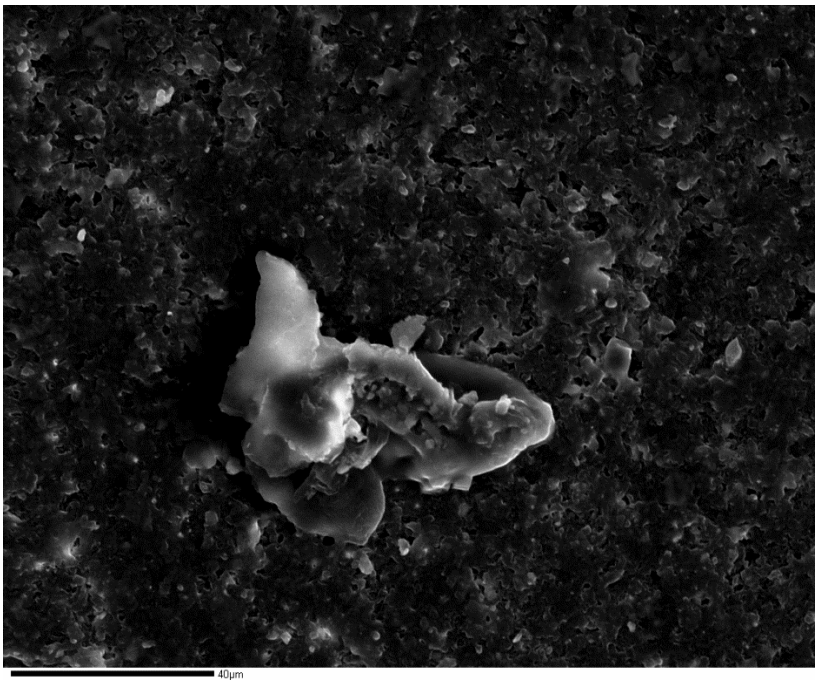

Fig. 8.61 – VF-74-130a: Particular of a sharped plagioclase phenocryst in the black part. It is possible also to notice the great resorption rim on the border.

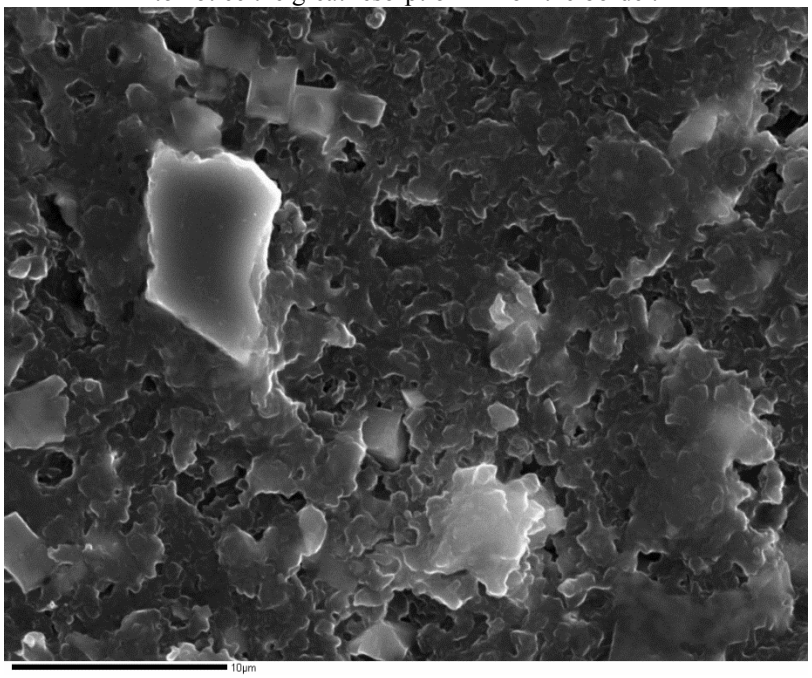

Fig. 8.62 – VF-74-130a: Particular of a xenolith of quartz with a semi-rectangular shape (on the upper left), in the black part.

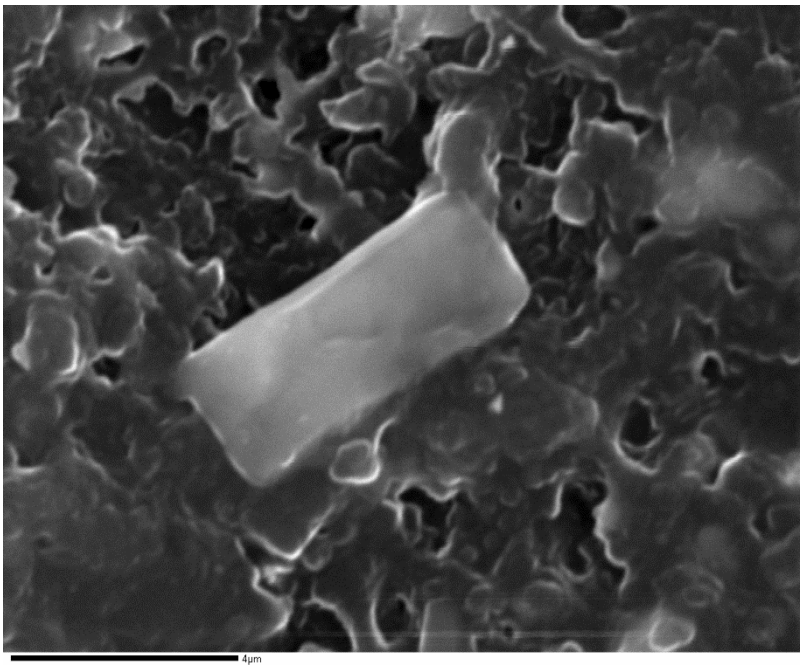


Fig. 8.63 – VF-74-130a: Particular of a xenolith with a rectangular shape that could represent a mica (biotite or muscovite).

# 8.4 – Appendix D _ Modal data from other works

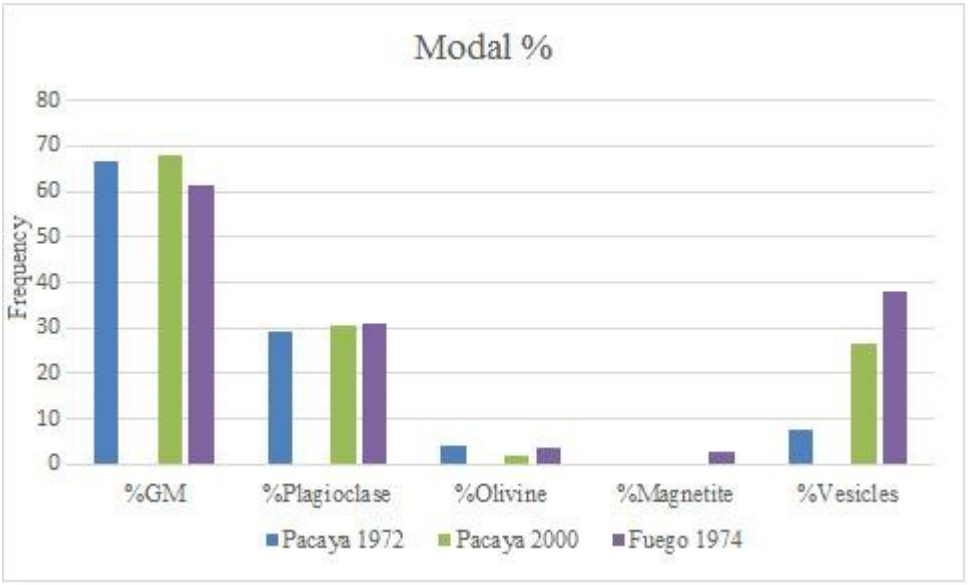


Fig. 8.64 – Modal data derived from other works (Eggers (1972), Bardintzeff & Deniel (1992), Rose *et al*. (2013), Cigala (2013), and Berlo *et a*l. (2012)).

## 8.5 – Appendix E _ SEM characteristics

For this work was used a JEOL JSM-6400 SEM, while for the image and spectra acquisition were used two different software, dPict7 and Revolution. Operational conditions included 20 kV of accelerating voltage and 39 mm of working distance. The acquisitions results in 1060x893 pixel images, with an average size of 928 kb, an horizontal resolution of 120 dpi and a vertical resolution of 120 dpi.

## 8.6 – Appendix F _ More viscosity vs. temperature diagrams

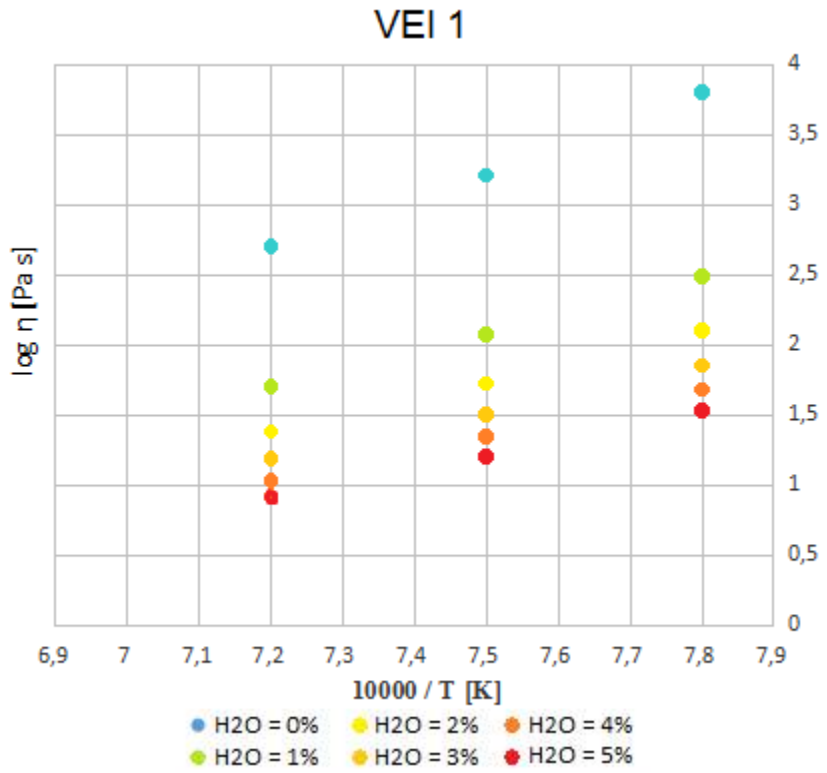


Fig. 8.65 – Viscosity vs. temperature plot showing how the viscosity is influenced by the $H_2O$ wt % in VEI 1 sample (PA-49).

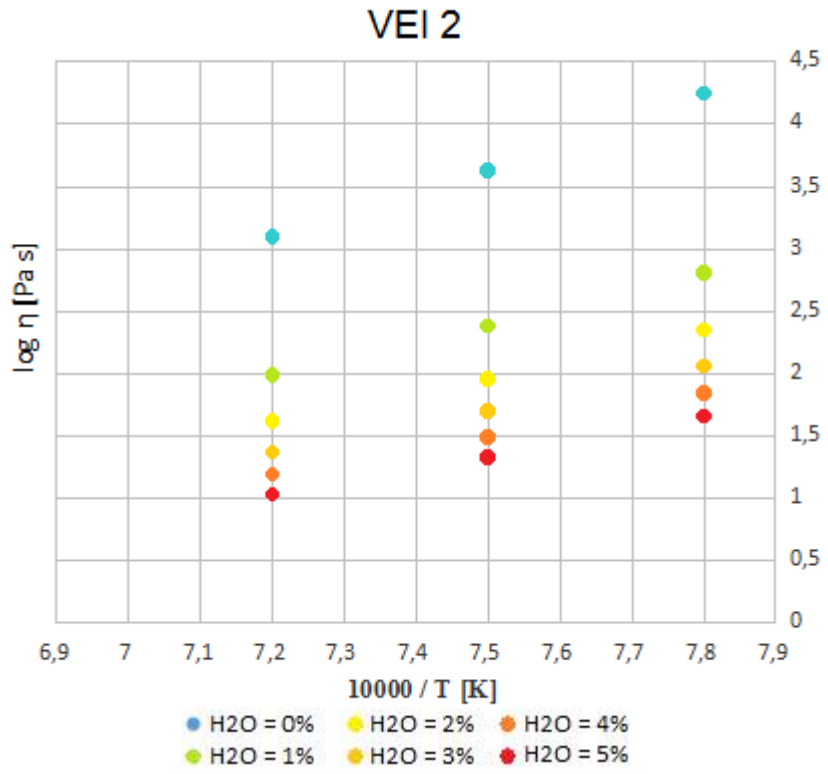


Fig. 8.66 – Viscosity vs. temperature plot showing how the viscosity is influenced by the $H_2O$ wt % in VEI 2 sample (PA-27).

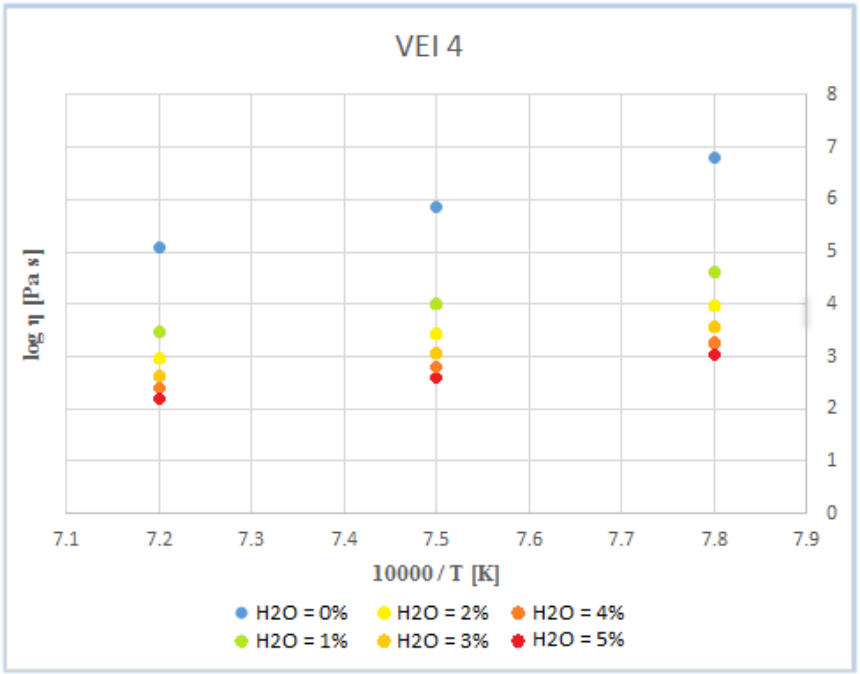


Fig. 8.67 – Viscosity vs. temperature plot showing how the viscosity is influenced by the $H_2O$ wt % in VEI 4 sample (VF-74-130a).